Broken Ergodicity and $1/f$ Noise from Finite, Local Entropy Baths

by

Bryce F. Davis

A Dissertation Presented in Partial Fulfillment
of the Requirement for the Degree
Doctor of Philosophy

Approved November 2018 by the
Graduate Supervisory Committee:

Ralph V. Chamberlin, Chair
Oliver Beckstein
Philip Mauskopf
George Wolf

ARIZONA STATE UNIVERSITY

December 2018

ABSTRACT

Fluctuations with a power spectral density depending on frequency as $1/f^{\alpha}$ ($0 < \alpha < 2$) are found in a wide class of systems. The number of systems exhibiting $1/f$ noise means it has far-reaching practical implications; it also suggests a possibly universal explanation, or at least a set of shared properties. Given this diversity, there are numerous models of $1/f$ noise. In this dissertation, I summarize my research into models based on linking the characteristic times of fluctuations of a quantity to its multiplicity of states. With this condition satisfied, I show that a quantity will undergo $1/f$ fluctuations and exhibit associated properties, such as slow dynamics, divergence of time scales, and ergodicity breaking. I propose that multiplicity-dependent characteristic times come about when a system shares a constant, maximized amount of entropy with a finite bath. This may be the case when systems are imperfectly coupled to their thermal environment and the exchange of conserved quantities is mediated through their local environment. To demonstrate the effects of multiplicity-dependent characteristic times, I present numerical simulations of two models. The first consists of non-interacting spins in 0-field coupled to an explicit finite bath. This model has the advantage of being degenerate, so that its multiplicity alone determines the dynamics. Fluctuations of the alignment of this model will be compared to voltage fluctuations across a mesoscopic metal-insulator-metal junction. The second model consists of classical, interacting Heisenberg spins with a dynamic constraint that slows fluctuations according to the multiplicity of the system's alignment. Fluctuations in one component of the alignment will be compared to the flux noise in superconducting quantum interference devices (SQUIDs). Finally, I will compare both of these models to each other and some of the most popular models of $1/f$ noise, including those based on a superposition of exponential relaxation processes and those based on power law renewal processes.

Dedicated to my father, Dr. Brian F. Davis

ACKNOWLEDGEMENTS

I would like to express the utmost gratitude to my advisor, Dr. Ralph V. Chamberlin, for his guidance through these years, for the things he has taught me, the freedom he granted me, his curiosity, his patience, and the many thoughtful discussions we shared.

For their guidance and patience, I would also like to thank my supervisory committee: Dr. Oliver Beckstein, Dr. Philip Mauskopf, and Dr. George Wolf.

For their friendship and enlightening conversations, I would like to thank Dr. Jack R. Staunton, Dr. Jeffrey M. Hyde, and Mr. Norman L. Bemelmans.

For her love and support, I would like to thank Ariel L. Molk.

Finally, most of all, I would like to thank my family: my parents, Brian and Cynthia, my sister Haley, and my brother Bret.

TABLE OF CONTENTS

CHAPTER Page

CHAPTER Page

LIST OF FIGURES

Figure Page

Chapter 1

BACKGROUND

1.1 $1/f$ Noise: Its Discovery and Prevalence

Some of the earliest investigations of the spectral distribution of noise power were carried out by J.B. Johnson on the voltage fluctuations of vacuum tube amplifiers and resistors. Johnson was able to measure three distinct categories of noise. First, he measured a noise with a spectrum independent of the frequency, originating from the thermal motion of electrons present in all conductors, now known as *Johnson-Nyquist noise* [57]. In an analogy to white light, having equal contributions to its intensity from every visible wavelength, noise that has a frequency-independent spectral density is known as *white noise*. Second, Johnson measured another white noise, but with its origins in the thermionic emission of single electrons from the surface of the cathode in the vacuum tube amplifier, now known as *shot noise*. The third, initially named *flicker noise*, now more commonly called *pink noise* and most often $1/f$ *noise*, with a spectral density that increased with decreasing frequency, was the most puzzling to Johnson [56].

This first type of noise, Johnson-Nyquist noise, was noted by Johnson to have two important characteristics: it was proportional to the resistance R and temperature T of the conductor under investigation. Otherwise, the composition, size, etc. of the conductor were immaterial. The only dependence upon the measurement apparatus was a linear dependence of the magnitude upon the bandwidth, indicating that the voltage fluctuations δV were distributed uniformly over all frequencies; that is, the power spectral density S_V was constant as a function of frequency f [57].

The same year, H. Nyquist (the second namesake of Johnson-Nyquist noise) provided a theoretical treatment of Johnson-Nyquist noise [95]. Nyquist considered two resistors connected in a circuit, in thermal equilibrium with one another. Recognizing that the power dissipated in a resistor from fluctuations in voltage of the other resistor must be the same for both resistors, he developed what is now called the Nyquist relation for the spectral density of voltage fluctuations:

$$S_V(f) = \frac{d}{df}\langle(\delta V)^2\rangle = 4k_B T R \tag{1.1}$$

where k_B is Boltzmann's constant. This expression is the first instance of a *fluctuation-dissipation relation*, relating dissipative processes (through R, the resistance) to equilibrium fluctuations (in voltage, δV).

The second type of noise, shot noise, also has a white noise spectrum. However, its origin is not the thermal fluctuations of electrons, but instead is due to the discrete nature of the electron. The spectrum was predicted in 1918 by W. Schottky, who modeled the current from the thermionic emission of electrons in a tube amplifier as a series of uncorrelated pulses, essentially a Poisson process. By calculating the autocorrelation function for a Poisson process and Fourier transforming, he arrived at the spectral density for shot noise in the current of a tube amplifier:

$$S_I(f) = 2e\langle I\rangle \tag{1.2}$$

where e is the electron charge and $\langle I\rangle$ is the mean current through the vacuum tube. This expression holds at frequencies below the inverse characteristic time of a pulse, which in this case is the emission of an electron [115].

The first successful measurement of the white noise spectrum of shot noise was performed by Johnson in 1925 [56]. However, while measurement of the shot noise may have been his primary purpose, perhaps more significant was Johnson's discovery

of the third type of noise, an excess noise in the low frequency end of the measured spectrum, which, because of its distinct dependence upon the *square* of the current, he surmised was a phenomenon separate from the shot noise. The power contained in the noise was seen to increase with decreasing frequency as a power law, $S(f) \sim 1/f$, down to the lowest frequency measured [56].

Since being first discovered by Johnson, $1/f$ noise has been measured in carbon resistors [10, 33], semiconductors [87, 41, 128, 79], metals [44, 42, 132, 136, 43], spin glasses [137, 2, 123, 18], metal-oxide-semiconductor field effect transistors [102], operational amplifiers [22], nanowires [8], nanoelectrodes [68], nanopores [122], graphene and other carbon allotropes [9, 113, 59], biomolecular systems [12, 141, 140, 75, 121], turbulence [120], quantum dots [112, 99], Josephson junctions [96, 142, 97, 58], long-term fluctuations in rainfall [83], and the fluctuations in pitch and volume of music and human speech [131]. Of the published literature on noise, more than a third of it is on $1/f$ noise [65].

Given the number and the variety of systems exhibiting $1/f$ noise listed above, it is of practical concern for many different fields. Its appearance in resistors [44, 42, 132, 136, 43], MOSFETs [102], and op-amps [22] limits the performance of traditional electronics devices. Furthermore, its presence in graphene [9, 113, 59], Josephson junctions [96, 142, 97, 58], nanoscale devices [8, 68, 122], etc., means it degrades the most sensitive and sophisticated of current and future devices, including graphene FETs [9], chemical and biological sensors [113], superconducting quantum interference devices (SQUIDs) [62, 4], qubits and quantum computers [97, 96, 35, 58], etc.. In these systems, $1/f$ noise is particularly problematic: because of its divergence at low frequencies, extending the measurement time of a variable exhibiting $1/f$ noise tends not to improve, and can often diminish, the accuracy of the measurement.

Although a nuisance in the systems listed above, $1/f$ noise is necessary to the

function of other systems. In general, slow, low-frequency fluctuations have been found to be crucial to the functionality of biomolecules [75, 17]. For example, the low frequency $1/f$ fluctuations in the residence time of water molecules on a lipid membrane have been found in molecular dynamics simulations to contribute to the stability of the membrane's hydration layer, which is necessary for its biological function [141]. Dynamic force spectroscopy experiments have shown a $1/f$ spectrum in the force associated with the exploration of a rugged free energy landscape in the process of biorecognition [12, 13]. $1/f$ noise is also present in the regulation of water transport through aquaporins [140], the spectrum of sequence in DNA [75], and fluctuations of ionic currents through membrane nanopores [121].

Irrespective of these practical implications, the ubiquity of $1/f$ noise has led many to speculate on its origin: whether there is a universal mechanism or, in the absence of such, what other features do systems exhibiting $1/f$ noise have in common? The connection of fluctuations to dissipation and relaxation through fluctuation-dissipation relations, an innovation that has developed alongside the growing literature on $1/f$ noise, continues to provide insights and open new questions. Its divergence at low frequencies, and therefore over long time scales, suggests that $1/f$ noise is fundamentally connected to deep statistical properties like ergodicity, stationarity, and the aging observed in glasses and other systems. The scale invariance of the spectrum and the associated self-similarity of a time-series possessing $1/f$ fluctuations has led many to speculate that this property is the cornerstone of a universal model.

The fundamental aspects of $1/f$ noise, its practical importance, and its seeming omnipresence mean that models for it run the gamut from universal to highly system-specific to models with no readily-apparent physical meaning. These include the superposition of exponential relaxation processes, power law distributed relaxation processes, time-correlated relaxation processes, sub-diffusion processes, multiplicative

as well as fractional stochastic differential equations, self-organized criticality, and more.

In this dissertation, I will offer a new account of the origin of $1/f$ noise. By relaxing the assumption used in standard statistical mechanics of ideal coupling to an infinite thermal reservoir, this explanation produces $1/f$ noise by linking the characteristic times of fluctuations to the multiplicity of the fluctutating variable. This interpretation will be tested using the results of numerical simulations of two models and comparison to experimental results in the literature. While perhaps not the sought-after universal account, this explanation will hopefully uncover some common ground among the many systems exhibiting $1/f$ noise and the models used to describe them.

Before discussing these multiplicity-dependent characteristic times from finite, local baths in § 2, and the models employed to study them in § 3 and 4, the mathematical background and literature relevant to $1/f$ noise will be discussed in this chapter. In § 1.2 the autocorrelation function and the power spectral density of fluctuations will be discussed, and their relationship through the Wiener-Khinchin theorem will be derived. In § 1.3, some properties of $1/f$ noise, including the form of its autocorrelation function and probability density function (§ 1.3.1), its Gaussianity and linearity (§ 1.3.2), and its stationarity and ergodicity (§ 1.3.3) will be discussed. Finally, in § 1.4, three of the most popular classes of models of $1/f$ noise will be presented: those based on a distribution of exponential relaxation processes (§ 1.4.1), power law renewal processes (§ 1.4.2), and self-organized criticality (§ 1.4.3).

1.2 The Autocorrelation Function and the Spectral Density of Fluctuations

Many processes in nature can be described as *stochastic* or *random*. A stochastic process is defined by its time series $x(t)$, a random function that gives the value of

some variable x as a function of time t. The time series $x(t)$ of a stochastic process can be characterized by a probability density function, $w(x,t)$, which is defined such that

$$P\{a \leq x \leq b, t\} = \int_a^b w(x,t)dx \tag{1.3}$$

where $P\{a \leq x \leq b, t\}$ is the probability that the value of $x(t)$ lies between $x = a$ and $x = b$ at time t. For a *stationary* process, the probability density function is independent of the time t, and we can drop the dependence on time from our notation. The mean value is then well-defined through the *expectation value* of the process $x(t)$:

$$\mathbf{E}[x] = \mathbf{E}[x(t)] = \int_{-\infty}^{\infty} x \cdot w(x)dx \tag{1.4}$$

This quantity is time-independent for a stationary process. Let $\delta x(t)$ denote the *fluctuation* of $x(t)$; that is, the deviation of $x(t)$ from its mean value: $\delta x(t) \equiv x(t) - \langle x \rangle$. The mean value of the fluctuation is by definition zero, so to characterize the degree to which $x(t)$ deviates from its mean value, we define the variance as the mean fluctuation squared:

$$\mathbf{E}[(\delta x)^2] = \mathbf{E}[\{\delta x(t)\}^2] = \mathbf{E}[\{x(t) - \mathbf{E}[x]\}^2] = \mathbf{E}[x^2] - \mathbf{E}[x]^2 \tag{1.5}$$

Like the mean value, this quantity is time-independent for a stationary process.

In a typical experiment, the mean value of the random quantity x is not determined using equation 1.4. To practically determine the mean value, one of two methods of averaging can be used. The random quantity $x(t)$ can be averaged over one realization of a time series of length t_m, to give a *time average*:

$$\overline{x} = \lim_{t_m \to \infty} \frac{1}{t_m} \int_{-t_m/2}^{t_m/2} x(t)dt \tag{1.6}$$

The random quantity $x(t)$ can also be averaged over an ensemble of N identically

prepared systems, to give an *ensemble average*:

$$\langle x \rangle = \lim_{N \to \infty} \frac{1}{N} \sum_{i=1}^{N} x_i(t) \tag{1.7}$$

Note that time averages and ensemble averages are distinguished by an overbar and angle brackets, respectively. Though, intuitively it might seem that these are equivalent in the limits of very large t_m and N, this is not always the case, and it is important to differentiate the two. If time averages and ensemble averages are both well-defined and converge to the same value in the limits of very large t_m and N, the system is said to be *ergodic* [66, 55]. This fundamental property, its meaning, and its relation to stationarity, will be discussed in § 1.3.3.

In addition to the mean value of a random quantity and the variance describing the magnitude of fluctuations about this mean, it would be useful to have a non-random function to describe the time-evolution of fluctuations about the mean. Using equation 1.4, the two-time autocorrelation function is defined

$$\begin{aligned} \xi_x(t_1, t_2) &= \mathbf{E}[\delta x(t_1) \delta x(t_2)] \\ &= \sum \delta x(t_1) \delta x(t_2) w(x_1, t_1; x_2, t_2) \end{aligned} \tag{1.8}$$

where $w(x_1, t_1; x_2, t_2)$ is the two-dimensional probability density function giving the probability that $x = x_1$ at time $t = t_1$ and $x = x_2$ at time $t = t_2$. Defining the joint conditional probability $P(x_2, t_2 | x_1, t_1)$ as the probability that $x = x_2$ at time $t = t_2$ given the condition that $x = x_1$ at time $t = t_1$, this can be written as

$$\xi_x(t_1, t_2) = \sum \delta x(t_1) \delta x(t_2) P(x_2, t_2 | x_1, t_1) w(x, t_1) \tag{1.9}$$

Using ensemble averaging, the autocorrelation function is:

$$\begin{aligned}\xi_x(t_1,t_2) &= \langle \delta x(t_1)\delta x(t_2)\rangle \\ &= \langle x(t_1)x(t_2)\rangle - \langle x(t_1)\rangle\langle x(t_2)\rangle \\ &= \lim_{N\to\infty}\frac{1}{N}\sum_{i=1}^{N}\delta x_i(t_1)\delta x_i(t_2)\end{aligned} \tag{1.10}$$

Or, equivalently for an ergodic system, using time averaging:

$$\begin{aligned}\xi_x(t_1,t_2) &= \overline{\delta x(t_1)\delta x(t_2)} \\ &= \lim_{t_m\to\infty}\frac{1}{t_m}\int_{-t_m/2}^{t_m/2}\delta x(t_1+t)\delta x(t_2+t)dt\end{aligned} \tag{1.11}$$

As with the mean and variance, the autocorrelation function is time-independent for a stationary process. However, it does depend upon the difference $t_1 - t_2$, permitting it to be written as a function of a single variable $\xi_x(t_1,t_2) = \xi_x(t_1 - t_2)$. As can be seen from equation 1.9, the autocorrelation function at $t_1 = t_2$ is equal to the variance, equation 1.5: $\xi_x(0) = \langle(\delta x)^2\rangle$. For a stochastic process, the autocorrelation function is typically a monotonically decreasing function of $|t_1 - t_2|$.

With a view toward expressing the autocorrelation function in spectral terms, the Fourier transform of a fluctuation is defined

$$\widetilde{\delta x}(\omega) = \int_{-\infty}^{\infty}\delta x(t)e^{i\omega t}dt \tag{1.12}$$

or equivalently, through the inverse Fourier transform,

$$\delta x(t) = \int_{-\infty}^{\infty}\widetilde{\delta x}(\omega)e^{-i\omega t}\frac{d\omega}{2\pi} \tag{1.13}$$

Assuming ergodicity, equation 1.13 can be substituted into equation 1.10 for the ensemble-averaged autocorrelation function

$$\begin{aligned}\xi_x(t_1,t_2) &= \langle \delta x(t_1)\delta x(t_2)\rangle \\ &= \int_{-\infty}^{\infty}\int_{-\infty}^{\infty}\langle\widetilde{\delta x}(\omega)\widetilde{\delta x}(\omega')\rangle e^{-i(\omega t_1+\omega' t_2)}\frac{d\omega}{2\pi}\frac{d\omega'}{2\pi}\end{aligned} \tag{1.14}$$

Looking at the argument of the exponential, it is clear that for the autocorrelation function to be a function of $t_1 - t_2$ alone, the integrand, specifically $\langle\widetilde{\delta x}(\omega)\widetilde{\delta x}(\omega')\rangle$, can only be nonzero for $\omega = -\omega'$. That is, it must contain a delta function: $\langle\widetilde{\delta x}(\omega)\widetilde{\delta x}(\omega')\rangle = A(\omega) \times \delta(\omega + \omega')$. Making this substitution in equation 1.14 and performing the integral over ω'

$$\xi_x(t_1 - t_2) = \int_{-\infty}^{\infty} A(\omega) e^{-i\omega(t_1 - t_2)} \frac{d\omega}{(2\pi)^2} \tag{1.15}$$

Comparing equation 1.15 to equation 1.13, it is clear that the coefficient of the delta function is $A(\omega) = 2\pi\widetilde{\xi_x}(\omega)$, where $\widetilde{\xi_x}(\omega)$ is the Fourier transform of the autocorrelation function $\xi_x(t_1 - t_2)$:

$$\langle\widetilde{\delta x}(\omega)\widetilde{\delta x}(\omega')\rangle = 2\pi\widetilde{\xi_x}(\omega)\delta(\omega + \omega') \tag{1.16}$$

As noted above, the autocorrelation function at $t_1 - t_2 = 0$ is equal to the variance:

$$\begin{aligned} \langle(\delta x)^2\rangle &= \xi_x(0) \\ &= \int_{-\infty}^{\infty} \widetilde{\xi_x}(\omega)\frac{d\omega}{2\pi} \\ &= \int_{0}^{\infty} 2\widetilde{\xi_x}(\omega)\frac{d\omega}{2\pi} \end{aligned} \tag{1.17}$$

Where the fact that $\widetilde{\xi_x}(-\omega) = \widetilde{\xi_x^*}(\omega)$ (the * indicating complex conjugation), since $\xi_x(t_1 - t_2)$ is real-valued, has been used to express the integral over positive frequencies only. The form of equation 1.17 suggests that the integrand in the final integral is a kind of density. Specifically, it is the mean fluctuation squared in an infinitesimal frequency band centered around f, known as the *power spectral density*:

$$S_x(f) \equiv 2\widetilde{\xi_x}(\omega) = 2\int_{-\infty}^{\infty} \xi_x(t_1 - t_2) e^{i\omega(t_1 - t_2)} d(t_1 - t_2) \tag{1.18}$$

The above relationship is known as the Wiener-Khinchin theorem. The power spectral density does not necessarily correspond to a physical power. Instead, in this context

it refers to the square of any signal that is fluctuating about its mean, known as *noise power* [66].

In order to practically determine the power spectral density from an experiment or simulation, it is more useful to express it in terms of the time series of fluctuations. In fact, the power spectral density can be expressed simply as $S_x(f) = 2\widetilde{\delta x}(\omega)\widetilde{\delta x^*}(\omega)$. To show this, the time-averaged definition for the autocorrelation function in equation 1.11 is substituted into the Wiener-Khinchin theorem, equation 1.18:

$$\begin{aligned} S_x(f) &= 2\int_{-\infty}^{\infty} \xi_x(t_1 - t_2) e^{i\omega(t_1 - t_2)} d(t_1 - t_2) \\ &= 2\int_{-\infty}^{\infty} \left\{ \int_{-\infty}^{\infty} \delta x(t_1 + t)\delta x(t_2 + t) dt \right\} e^{i\omega(t_1 - t_2)} d(t_1 - t_2) \\ &= 2\int_{-\infty}^{\infty} \left\{ \int_{-\infty}^{\infty} \delta x(t)\delta x(t + t_1 - t_2) dt \right\} e^{i\omega(t_1 - t_2)} d(t_1 - t_2) \\ &= 2\int_{-\infty}^{\infty} \left\{ \int_{-\infty}^{\infty} \delta x(t + t_1 - t_2) e^{i\omega(t_1 - t_2)} d(t_1 - t_2) \right\} \delta x(t) dt \end{aligned} \tag{1.19}$$

A change of variables $t' \equiv t + t_1 - t_2$ in the bracketed integral allows the integrals to be separated. Recognizing that $\delta x(t)$ is, of course, real-valued, the desired result manifests

$$\begin{aligned} S_x(f) &= 2\int_{-\infty}^{\infty} \left\{ \int_{-\infty}^{\infty} \delta x(t') e^{i\omega t'} e^{-i\omega t} d(t' - t) \right\} \delta x(t) dt \\ &= 2\int_{-\infty}^{\infty} \delta x(t') e^{i\omega t'} dt' \int_{-\infty}^{\infty} \delta x(t) e^{-i\omega t} dt \\ &= 2\left| \int_{-\infty}^{\infty} \delta x(t) e^{i\omega t} dt \right|^2 \\ &= 2\widetilde{\delta x}(\omega)\widetilde{\delta x^*}(\omega) \end{aligned} \tag{1.20}$$

This quantity is known as the *periodogram*. Of course, for a real experiment or simulation, the time series can only be collected over a finite interval of time, $-t_m <$

$t < t_m$. So, the truncated Fourier expansion has to be used:

$$S_x(f) = \frac{1}{t_m}\left| \int_{-t_m}^{t_m} \delta x(t) e^{i\omega t} dt \right|^2 \tag{1.21}$$

Finally, in actuality, any time series obtained will not be continuous, but a discrete set of N points collected over the time t_m:

$$S_x(f) = \frac{1}{N}\left| \sum_{n=0}^{N-1} \delta x_n e^{i\omega n/N} \right|^2 \tag{1.22}$$

This estimation of the power spectral density will be used throughout this dissertation.

1.3 Properties of $1/f$ Noise

$1/f$ noise, or perhaps more appropriately noise of $1/f$-type, can be defined as any fluctuation of a physical quantity that exhibits a power spectral density $S(f) \propto 1/f^{\alpha}$, where the spectral exponent $0 < \alpha < 2$, over some range of frequencies f. In this sense, it describes all fluctuations with a power spectral density that obeys a power law with a spectral exponent between that of white noise, where $\alpha = 0$ and all frequencies contribute equally to the noise, and what is known as red or brown noise, where $\alpha = 2$ and all cycle-times contribute equally, which describes the power spectral density of velocity fluctuations of a Brownian particle [66].

In this section, a number of notable properties of $1/f$ noise will be discussed. In § 1.3.1, the autocorrelation function, intimately related to the power spectral density through the Wiener-Khinchin theorem, will be discussed. In addition, the probability density function of $1/f$ processes will be described. In § 1.3.2, the Gaussianity and linearity of $1/f$ noise, and the processes which underlie it, will be discussed. Finally, in § 1.3.3, the divergence of $1/f$ noise at zero frequency, the so-called *paradox of infinite fluctuations* will be discussed. This long standing problem has attracted a large amount of attention, and is a consequence of the fractal nature of $1/f$ noise.

The stationarity and ergodicity of $1/f$ noise will also be discussed in general. All of these properties will be used to distinguish the models discussed in § 1.4 as well as the original models and results in § 3 and 4.

1.3.1 Heavy-Tailed Autocorrelation Functions and Probability Density Functions

The form of the spectral density of a process determines the form of its autocorrelation function by way of the Wiener-Khinchin theorem, equation 1.18:

$$S_x(f) = 2\int_{-\infty}^{\infty} \xi_x(t) e^{i\omega t} dt \tag{1.23}$$

In equation 1.23 and from this point on, the autocorrelation function will be denoted for convenience as $\xi_x(t)$ instead of $\xi_x(t_1 - t_2)$. Noting that $\lim_{f\to 0} S_x(f) = \infty$, it can be seen from equation 1.23 that the integral over time of the autocorrelation function for a $1/f$-type process is divergent:

$$S_x(0) = 2\int_{-\infty}^{\infty} \xi_x(t) dt = \infty \tag{1.24}$$

From this it can be concluded that the autocorrelation function of a $1/f$-type process is *heavy-tailed*, meaning that it decays more slowly than functions of exponential form and may in fact be dependent upon its initial state for all time. Qualitatively, this implies that $1/f$-type processes have long-range correlation over time. Indeed, the defining characteristic of many processes exhibiting $1/f$ noise is diverging characteristic times, decaying according to, e.g., a power law, $\xi_x(t) \propto t^{-\beta}$, or a stretched exponential, $\xi_x(t) \propto e^{-t^\beta}$ [74].

More precisely, for an exact $1/f$ spectrum, $S(f) \propto 1/f$, over the range $f_1 < f < f_2$, the autocorrelation function can be calculated using the inverse of the Wiener-Khinchin theorem, equation 1.18, over the range $(2\pi f_2)^{-1} < t < (2\pi f_1)^{-1}$. Assuming

that $f_2 \gg f_1$ and retaining the leading terms

$$\begin{aligned} \frac{\xi_x(t)}{\langle(\delta x)^2\rangle} &= \int_{f_1}^{f_2} \frac{\cos(2\pi f t)}{f} df \\ &\approx 1 - \frac{1}{\ln(f_2/f_1)}[\gamma + \ln(2\pi f_2 t)] \end{aligned} \tag{1.25}$$

where $\gamma = 0.577...$ is the Euler-Mascheroni constant. Again, it is found that the autocorrelation function decays non-exponentially. Specifically, for an exact $1/f$ spectrum over the range $f_1 < f < f_2$, the autocorrelation function decays logarithmically in the range $(2\pi f_2)^{-1} < t < (2\pi f_1)^{-1}$.

The non-exponential decay of the autocorrelation function suggests that the probability density functions of $1/f$ processes are also heavy-tailed, through equation 1.8. It is known that heavy-tailed probability distributions (e.g. the Pareto distribution, Lévy distribution, Cauchy distribution, etc..) will result in autocorrelation functions that decay non-exponentially. Physically, the heavy tails of a probability distribution mean an enhanced probability of rare processes. A well-known property of heavy-tailed probability density functions is that they often do not have a well-defined mean and/or variance, implying processes that are divergent or unbounded [74]. Processes with infinite mean and variance, their meaning, and their relevance to $1/f$ noise will be further discussed in § 1.3.3 and 1.4.2.

1.3.2 Gaussianity and Linearity

Though the discussion of heavy-tailed probability density functions in § 1.3.1 is suggestive, it is possible to have a non-exponential autocorrelation function from a *Gaussian process*. A *Gaussian distribution* is characterized completely by its mean value and variance and has the single-time probability density function:

$$w(x,t) = \frac{1}{\sqrt{2\pi\langle(\delta x)^2\rangle}} \exp\left(-\frac{(x-\langle x\rangle)^2}{2\langle(\delta x)^2\rangle}\right) \tag{1.26}$$

A process is Gaussian if all its higher order probability density functions (that is, $w(x_1, t_1; x_2, t_2; ...; x_n, t_n)$, for all n) are also distributed as such. Consequently, all higher-order moments of a process can be expressed as a function of the second-order moment, the variance [66].

According to a result known as the *central-limit theorem*, the probability density function of a random variable that is the sum of N uncorrelated and identically distributed random variables, whether they are distributed according to a Gaussian or not, will approach a Gaussian distribution in the limit of a very large number $N \to \infty$ of random variables being summed [106]. The central-limit theorem therefore limits what a macroscopic measurement can reveal about the underlying processes producing $1/f$ noise. If the microscopic kinetics are Gaussian, then a measurement will result in Gaussian fluctuations, regardless of the system size. If, on the other hand, the microscopic kinetics are non-Gaussian or nonlinear, a measurement will result in Gaussian fluctuations *only if* the system is sufficiently large and the fluctuations will not retain their Gaussian character as system size is reduced.

Therefore, if $1/f$ fluctuations are necessarily the result of a superposition of a great number of degrees of freedom (as *e.g.* the models discussed in § 1.4.1), then $1/f$ fluctuations will always be closely Gaussian regardless of the underlying processes. If the underlying processes are not Gaussian, then the Gaussian character *and* the $1/f$ character of the fluctuations will break down as system size is reduced. On the other hand, if $1/f$ fluctuations are *not* necessarily the result of a large number of degrees of freedom, they will be seen to persist at small system sizes even if their Gaussian character breaks down. The Gaussianity of $1/f$ fluctuations at smaller system sizes is therefore an important indicator of their origin [65].

Naturally, the first test of Gaussianity is to measure the single-time probability density function to verify if it matches equation 1.26. Failure of this test would mean

the process is certainly not Gaussian, though success does not necessarily verify that it is. As mentioned, to absolutely confirm that a process is Gaussian, the probability density functions of all orders have to be tested. Measurements of the single-time probability density function of $1/f$ processes have been performed numerous times [101, 91, 21, 130].

A notable example is a series of measurements reported by R.F. Voss in 1978 on five different sources of $1/f$ noise: the voltage across a carbon resistor, the collector-base current and the emitter voltage of a reverse-biased n-p-n bipolar transistor, the current in a MOSFET, and the current through a reverse-biased p-n diode. What he found was that the single-time probability density functions in the carbon resistor and the MOSFET were almost exactly Gaussian, that the collector-base current and emitter voltage of the n-p-n transistor deviated from Gaussianity at the tails, and that the p-n junction current was strongly non-Gaussian [130]. Other measurements have been carried out that test the higher-order moments for Gaussianity [124, 93]. However, it suffices to say that $1/f$ fluctuations are not always Gaussian, therefore the underlying mechanisms are not always Gaussian.

In the course of testing the Gaussianity of these systems, Voss also tested their *linearity*. Fluctuations of a quantity are linear if the value of the variance and higher moments of the quantity do not depend upon the value of the quantity. Voss tested this by measuring the correlation function for realizations of the experiment with a specific initial value δx_0 of the fluctuation and reducing it by δx_0:

$$\phi(t|\delta x_0) = \frac{\langle \delta x(t)|\delta x_0\rangle}{\delta x_0} \tag{1.27}$$

If fluctuations of x are linear, this function of time will be independent of the value of δx_0. Voss found the deviation from linearity in these systems to follow that of the Gaussianity. That is the more non-Gaussian a system's fluctuations, the more

non-linear the fluctuations. Of course, much like the Gaussianity, this says nothing regarding the kinetics of the underlying processes producing the noise in these systems, but only of the observed phenomenology.

These considerations and tests of the Gaussianity and linearity, particularly for systems of varying size, are important in restraining models of $1/f$ noise. For example, the $1/f$ noise measured in the flux of SQUIDs is known to be non-linear. Since the spectral density of fluctuations of the flux are related to the SQUID inductance through the fluctuation-dissipation relation, this has important ramifications on the operation of SQUIDs [119, 4].

1.3.3 The Paradox of Infinite Fluctuations, Ergodicity, and the Stationarity of $1/f$ Noise

Regardless of where the spectral exponent falls in the range $0 < \alpha < 2$, a question of immediate importance presents itself: *over what range of frequencies is the noise of $1/f$-type present?* The potential problem is apparent upon integrating a power spectral density of $1/f$-type over the range $f_1 < f < f_2$ to find the total power of fluctuations in that range:

$$\int_{f_1}^{f_2} S_x(f)df \propto \int_{f_1}^{f_2} \frac{1}{f^\alpha}df \propto \begin{cases} \ln\left(\frac{f_2}{f_1}\right) & \alpha = 1 \\ \frac{1}{1-\alpha}\left[\frac{1}{f_2^{\alpha-1}} - \frac{1}{f_1^{\alpha-1}}\right] & \alpha \neq 1 \end{cases} \tag{1.28}$$

Apparently, if fluctuations of $1/f$-type persist over all frequencies, the variance of the quantity is infinite. For $0 < \alpha < 1$, the above integral diverges in the high frequency limit; for $1 < \alpha < 2$, it diverges in the low frequency limit; and for an exact $1/f$ spectrum ($\alpha = 1$), it diverges in both limits, albeit logarithmically. Experimental considerations usually remove any concerns about this divergence. In the high frequency limit, $1/f$ noise is always subsumed by some other source of noise, and in

both the low and high frequency limits, the noise is limited either by filters in the experimental apparatus or simply by the time of measurement. However, this does not resolve the fundamental paradox of infinite fluctuations.

Typically, the assumption is that there is a low frequency cutoff of $1/f$ noise and in fact, a low-frequency cutoff is a natural feature of many of the most popular models for $1/f$ noise, particularly those discussed in § 1.4.1 [10, 87, 42]. However, for most systems, no such cutoff has been observed experimentally. The lowest frequency measurement of the a $1/f$-type spectrum was reported by M.A. Caloyannides in 1974, down to a frequency of $10^{-6.3}Hz$ in a measurement of current noise through operational amplifiers that lasted approximately three weeks [22]. A similarly lengthy measurement was performed on thick-film resistors by B. Pellegrini, R. Saletti, P. Terreni, and M. Prudenziati and showed the same result: a $1/f$-type spectrum over six decades of frequency with no sign of flattening at the lowest frequencies [98]. In a more exotic example, using 300 years worth of weather data, B.B. Mandelbrot and J.R. Wallis reported in 1968 no low-frequency cutoff in the $1/f$ behavior of fluctuations in rainfall [83]. Of course, all of these quantities being bounded, the idea of an infinite variance is non-sensical.

Aside from a low-frequency cutoff, a possible resolution to the paradox of infinite fluctuations is in the answer to another question that has long been a point of contention in the field of $1/f$ noise: whether or not the processes that produce $1/f$ noise are *stationary*. A stationary process is a stochastic process in which the probability density function is invariant under a shift in time [65]. As a result, properties like the mean and variance, if otherwise well-defined, are independent of time. Autocorrelation functions, as well, are time-independent for stationary processes and consequently, so are power spectral densities. A *non-stationary* process, on the other hand, could have a spectral density that is generally $1/f$, but can wander over time in

shape and amplitude [127] or scale in amplitude with the time over which the process is observed [127, 107, 94, 112].

With the appropriate time-dependence of the spectral density, the integral in equation 1.28 could remain finite even for a spectral density having a $1/f$ dependence with no low-frequency cutoff, thus resolving the paradox of infinite fluctuations. To wit, if equation 1.28 is evaluated over the interval $1/t_m < f < \infty$ for a spectral density with $1 < \alpha < 2$, where the time of measurement t_m restricts the lowest measurable frequency, the total noise power depends upon measurement time as $\propto {t_m}^{\alpha-1}$. Therefore, a spectral density with the form

$$S(f) \propto {t_m}^{1-\alpha}/f^{\alpha} \tag{1.29}$$

will see its amplitude decrease with measurement time in such a way that the variance $\int_0^\infty S(f)df$ remains bounded. Models that possess this property and physical systems that has been observed to possess it, will be discussed in SEC 1.4.2.

The suggestion that non-stationary processes are necessary for a $1/f$-type spectrum was first made by Mandelbrot in 1967 [80] and, as a possible resolution to the paradox of infinite fluctuations, it was an attractive proposition. A number of experiments into the current noise spectra of carbon resistors and semiconductor diodes following Mandelbrot's suggestion appeared to indicate that $1/f$ noise is in fact non-stationary [101, 91, 21]. The indicator of non-stationarity was a measured variance of the variance; that is, the noise spectrum itself seemed to fluctuate and exhibit noise, what J.J. Brophy termed *noisy noise* [21]. This noisy noise is often assessed using the *second spectrum*, $S^{(2)}(f_1, f_2)$, which is the spectrum of fluctuations as a function of frequency f_1 in the octave sums of the first power spectral density $S(f)$ about frequencies f_2 [65].

In 1976, when the suspicion that $1/f$ noise was a non-stationary process was

at its peak, J.L. Tandon and H.R. Bilger showed that a stable $1/f$ mean spectral density could be obtained from a time-dependent autocorrelation function [127]. The peculiar form of the autocorrelation function, however, did not and does not appear to correspond to any known physical system [43]. The same year, measurements by M. Stoisiek and D. Wolf [124] of the systems that originally appeared to exhibit non-stationarity, failed to reproduce the original results. Subsequent experiments have also indicated that $1/f$ noise is a stationary process in metals, carbon resistors, and semiconductors and that has become the operating assumption of most, but not all, investigations [43]. Recently, however, with the advent of more sophisticated measurement techniques that allow the observation of intrinsically non-stationary $1/f$ noise in nano-sized systems, these ideas of Mandelbrot's have regained currency. The physical systems exhibiting non-stationarity, and the theoretical models used to describe them, will be discussed in § 1.4.2.

Stationarity is closely connected to another fundamental statistical property: ergodicity. As mentioned above, a system is ergodic when ensemble averages $\langle x \rangle$ (equation 1.7) and time averages $\overline{x}$ (equation 1.6) are well-defined and equivalent in the limit of a large number of ensembles N and long times of measurement t_m, $\langle x \rangle = \overline{x}$. Aside from equivalence of the moments, mean and variance, this also includes correlation functions and spectral densities. To understand how ergodicity is broken and what it means for the fluctuations of a system, fluctuations have to be understood in the context of statistical mechanics.

A system is considered macroscopic when it is composed of a very large number of degrees of freedom. A complete specification of all the degrees of freedom is called a *microstate* and the number of microstates that a system can find itself in is typically very large. The state of the system can also be specified using a much coarser measure by considering the value of a measurable, macroscopic variable, e.g. temperature,

potential difference, net magnetization, etc.. The set of microstates that correspond to a single value of a macroscopic variable is called a *macrostate*. In these terms, fluctuations of a variable correspond to transitions between various macrostates of the system.

For a system that is in ideal thermal contact with an effectively infinite thermal reservoir at temperature T, the probability that the system is in a specific microstate, denoted by j, depends upon the energy E_j of the microstate through the Gibbs distribution:

$$w_j = \frac{e^{-E_j/k_BT}}{\sum_j e^{-E_j/k_BT}} \tag{1.30}$$

where the sum in the denominator is over all microstates and k_B is Boltzmann's constant. The mean value of a macroscopic variable x is found from the probability distribution using equation 1.4 in discrete form:

$$\mathbf{E}[x] = \sum_j x_j w_j = \frac{\sum_j x_j e^{-E_j/k_BT}}{\sum_j e^{-E_j/k_BT}} \tag{1.31}$$

where x_j is the value of the variable x when the system is in the j^{th} microstate. Since an ensemble of identically prepared systems will be distributed according to equation 1.30, equation 1.31 is equivalent to the ensemble average, equation 1.7: $\mathbf{E}[x] = \langle x \rangle$. For very large systems, the probability that the system will be found in states with energies significantly different from the mean energy $\langle E \rangle$ becomes vanishingly small. In this case, $w_j \to 1/\Omega$, where Ω is the number of states with energy $E_j = \langle E \rangle$, called the *multiplicity*. Therefore, in the space of possible configurations, known as *phase space*, the system is confined to a surface of definite energy. The mean value of x in equation 1.31 becomes:

$$\langle x \rangle = \frac{1}{\Omega} \sum_{E_j = \langle E \rangle} x_j \tag{1.32}$$

where the sum is performed over microstates j with $E_j = \langle E \rangle$; that is, over the microstates of a single macrostate.

By definition, a system is ergodic when ensemble averages are equivalent to time averages, $\langle x \rangle = \overline{x}$. For this to be the case, the system must have occupied, in the time of measurement t_m, all of phase space, or at least a portion of phase space significant enough that the condition $\langle x \rangle = \overline{x}$ is satisfied. If this condition is satisfied, it is clear that for even longer times of measurement, the time average is the same, so that stationarity is satisfied as well. The condition for ergodicity can then be stated:

$$t_m > t_\phi \tag{1.33}$$

where t_ϕ is the time it takes for a system to explore enough of phase space to satisfy $\langle x \rangle = \overline{x}$. This can be stated another way: after a sufficiently long period of time, an ergodic system spends an equal amount of time in each microstate. This postulate, known as the *ergodic hypothesis*, is central to the standard derivation of the second law of thermodynamics [55].

Ergodicity is broken in systems in which t_ϕ diverges and equation 1.33 cannot be realistically satisfied. This occurs when the phase space is divided into regions which are not connected to one another by a dynamic pathway. In other words, valleys of phase space are separated by barriers which are not crossable in a realistic period of time. A distribution of barrier heights can mean the system will wander different regions of phase space on arbitrarily long time scales, meaning diverging characteristic rates, which were pointed out above to be associated with $1/f$ noise [74]. This picture is often associated with glasses. Indeed, $1/f$ noise in glasses, particularly spin glasses, has been extensively reported upon [137, 2, 123, 18]. The spectral wandering of $1/f$ noise, associated with the system making rare transitions to different regions of phase space, has been directly observed through the second spectrum and used to distinguish between the two most popular models for spin glass dynamics: the droplet model and the hierarchical kinetics model [137]. This same observation has also been used to

justify the model for $1/f$ noise based on the superposition of exponential relaxation processes, described is § 1.4.1.

1.4 Models of $1/f$ Noise

Having reviewed the properties of $1/f$ noise, three of the most popular models, or classes of models, of $1/f$ noise will be discussed. The first of these, § 1.4.1, is based on a distribution of exponential, or Poissonian, relaxation processes. It is the most widely employed class of models of $1/f$ noise, as well as the earliest. It relies upon the superposition of processes with a certain distribution of characteristic times. The distribution, though specific, has been shown to be a natural feature of many physical systems. The next class of models, § 1.4.2, is based upon renewal processes, in which transition times of a single process have a power law probability distribution function. Models based on power law renewal processes were first proposed by Mandelbrot in the early 1960s. Though they did not gain much traction aside from some initial interest, they have recently regained relevance as models of $1/f$ noise in nanoscopic systems, such as stimulated quantum dots. These models are intrinsically non-stationary, exhibiting aging like that described in § 1.3.3. The last model, § 1.4.3, discussed only briefly here, is the subject of the most cited paper in the $1/f$ noise literature. It is based on, and is the first paper describing, self-organized criticality. All of these models will be compared to the original models and results presented in § 3 and 4.

1.4.1 $1/f$ Noise From a Distribution of Exponential Relaxation Processes

The earliest model for $1/f$ noise remains today the most popular. The essential idea is that by superposing exponential relaxation processes with the correct distribution of characteristic frequencies a $1/f$ spectrum over an appropriately broad range of frequencies can develop. Such conditions are often found in heterogeneous systems.

Models of this basic type have been used to explain $1/f$ in many systems and to review them, it is best to follow their development since the very discovery of $1/f$ noise.

In the same year that Johnson reported his measurement of excess noise in the low frequency end of the shot noise spectrum, Schottky provided a mathematical treatment of what he deemed *the flicker effect*. Following suggestions from Johnson, Schottky's proposition was that impurities on the surface of the cathode created sites where electrons were being trapped and undergoing emission at a rate given by an exponential with a single characteristic time [116]. For a system variable x (in Schottky's case, the current due to capture and emission of trapped electrons) undergoing fluctuations that decay with a single characteristic time, τ_c, the autocorrelation of a fluctuating quantity is exponential

$$\xi_x(t) = \langle (\delta x)^2 \rangle e^{-|t|/\tau_c} \tag{1.34}$$

where $(\delta x)^2$ is the variance of the variable x. By way of the Wiener-Khinchin theorem, EQ 1.18, the spectral density is proportional to the Fourier transform of the autocorrelation:

$$\begin{aligned} S_x(f) &= \int_{-\infty}^{\infty} \xi_x(t) e^{-i\omega t} dt \\ &= 4 \int_0^{\infty} \xi_x(t) \cos(\omega t) dt \\ &= \langle (\delta x)^2 \rangle \frac{4\tau_c}{1 + \omega^2 \tau_c^2} \end{aligned} \tag{1.35}$$

This function is known as a *Lorentzian*. Qualitatively, this spectrum would be constant (white) at low frequencies and roll over to noise with a $1/f^2$ dependence at the characteristic frequency $f_c \approx 1/\tau_c$. Admitting the Lorentzian to be a rather rough fit to Johnson's data, Schottky pointed out a $1/f^2$ dependence in the high end of

Johnson's measurements to comport with his theory, but noted that the bend at low frequencies in the data did not quite flatten out to constant, as does a Lorentzian [116].

Further measurements on the same and different materials showed a $1/f$ dependence over a broad range of frequencies and no flattening at low frequencies, and it became clear that Schottky's explanation was not sufficient. In an attempt to explain measurements of $1/f$ noise in the current of carbon microphones made by C.J. Christensen and G.L. Pearson at Bell Labs [33], J. Bernamont pointed out that, instead of a single Lorentzian, the correct distribution of Lorentzians having different characteristic times has the properties necessary to reproduce the observed spectra: a $1/f$ dependence at low frequencies transitioning to $1/f^2$ at higher frequencies [10]. Specifically, the power spectral density is integrated over the characteristic time, τ_c, weighted by a distribution, $p(\tau_c)$:

$$S_x(f) = \int_0^\infty p(\tau_c) \frac{4\tau_c}{1+\omega^2\tau_c^2} d\tau_c \tag{1.36}$$

The quantity $p(\tau_c)d\tau_c$ includes in it both the abundance of fluctuators as well as the strength of the contribution from a single fluctuator with characteristic times between τ_c and $\tau_c + d\tau_c$. Therefore, the total variance is absorbed into the distribution $p(\tau_c)$, so that

$$\int_0^\infty p(\tau_c)d\tau_c = \int_0^\infty S_x(f)df = \langle(\delta x)^2\rangle \tag{1.37}$$

Bernamont showed that to yield a power spectral density with a $1/f$ region in the range $f_1 < f < f_2$, it must be that the distribution $p(\tau_c) \propto 1/\tau_c$ in the range $1/f_1 < \tau_c < 1/f_2$ [65]. That is, for exact $1/f$ noise, $p(\tau_c)$ is constant on a logarithmic scale. To yield $1/f$ noise, the problem then becomes to develop some physical justification of characteristic modes distributed as $\sim 1/\tau_c$ over the range $1/f_1 < \tau_c < 1/f_2$.

The first of such models to physically justify this distribution was developed in

1957 by A.L. McWhorter [87]. McWhorter was attempting to explain $1/f$ type noise in the current through semiconductor (germanium) filaments. His supposition was that these fluctuations are due to fluctuations of the charge carrier density at the germanium-oxide interface, which in turn are due to the occasional capture and release of electrons in sites within the oxide layer. If the process by which the electrons are captured and released is tunneling, the rate, or inverse characteristic time, of this process falls off exponentially with increasing distance x between the surface and the trap: $\tau_c^{-1} = \tau_0^{-1} \exp(-x/x_0)$, where the attempt frequency τ_0 depends upon x weakly enough to be ignored, and x_0 is a scattering length. To surmise the distribution, $p(x)$, of barrier widths, x, necessary to yield $p(\tau_c) \propto 1/\tau_c$, McWhorter observed:

$$\begin{aligned} p(\tau_c)d\tau_c &= p(x)dx \\ \rightarrow p(\tau_c) &= \frac{p(x)}{|d\tau_c/dx|} = p(x)\frac{x_0}{\tau_c} \end{aligned} \tag{1.38}$$

So, to yield a distribution of characteristic times $p(\tau_c) \propto 1/\tau_c$, it must be that $p(x)$ is constant over some range of barrier widths, x. Because of the exponential dependence of the characteristic time upon barrier width, the constant distribution of barrier widths can be relatively narrow and still yield a power law distribution of characteristic times over a wide range [65]. For example, values of $\tau_0 \approx 10^{-12}$ s and $x_0 \approx 1$ $\mathring{A}$, physically reasonable values, would require that the distribution of barrier widths be constant only in the range 0.1 $\mathring{A} < x < 0.4$ $\mathring{A}$ in order to yield $1/f$ noise over the observed range [136, 87].

McWhorter's model was the first of its kind to attempt to model a specific physical system exhibiting $1/f$ noise. However, it was not the first time that an exponential dependence of characteristic time on a barrier height with a constant distribution was postulated to derive the $1/\tau_c$ distribution of characteristic times needed for $1/f$ noise. Without mentioning a specific system, F.K. du Pre [41] and A. van der Ziel

[128] independently suggested that a collection of Arrhenius-type activation processes, $\tau_c = \tau_0 \exp(E/k_B T)$, with a uniform distribution of activation energies, E, could produce $1/f$ noise. This model gives a dependence upon temperature of the spectral density, observed in metals [136, 42], which is absent in McWhorter's model [87] and generally absent in the low frequency noise of semiconductors [136].

The first model to ascribe the temperature-dependent $1/f$ noise observed in metals (specifically, thin Ag films) to a distribution of Arrhenius-type activation processes is due to P. Dutta, P. Dimon, and P.M. Horn [42]. Along with the assumption of Arrhenius-type activation processes coupling linearly to the observable exhibiting $1/f$ noise, in this case, resistivity ρ, they assumed that the samples exhibiting $1/f$ noise were heterogeneous, having a distribution $p(E)$ of activation energies E. Under these assumptions, the spectral density of fluctuations in resistivity is

$$\begin{aligned} S_\rho(f,T) &= \int_0^\infty p(E) \frac{4\tau_0 e^{E/k_B T}}{1+\omega^2 \tau_0^2 e^{2E/k_B T}} dE \\ &= \frac{2}{\omega} \int_0^\infty p(E) \frac{1}{\cosh(E-E^*)/k_B T} dE \end{aligned} \tag{1.39}$$

Here, τ_0 is the inverse characteristic attempt frequency of the material, often the phonon frequency of that material [42]. Typically, for solids, $10^{-14}\ s < \tau_0 < 10^{-11}\ s$ [65]. Therefore, for the range of ω over which $1/f$ noise is typically observed, the energy

$$E^* \equiv -k_B T \ln(\omega \tau_0) \tag{1.40}$$

is of the order of typical activation energies $\approx 1\ eV$. Note that, because of the logarithmic dependence upon τ_0 of this energy, E^* is very insensitive to the value of τ_0 [42].

The factor $\cosh^{-1}[(E-E^*)/k_B T]$ appearing in the integrand of the spectral density is peaked about $E = E^*$ with a width $\approx k_B T$, exponentially suppressing energies with $|E - E^*| > k_B T$. Physically, this means that as temperature is increased, more

activation processes are thermally allowed, anticipating a dependence of the spectral density upon temperature. If it is the case that the distribution of activation energies $p(E)$ is approximately constant over this range, then it is a safe approximation to replace $p(E)$ with $p(E^*)$ and remove it from the integral. The integral can then be evaluated to give

$$S_\rho(f,T) \propto k_B T p(E^*) \frac{1}{f} \tag{1.41}$$

The spectral density has the desired $1/f$ dependence. It is also linearly dependent upon T, reflecting the fact that the power of the noise grows as the temperature is increased and more activation processes are thermally allowed.

However, as Dutta, Dimon, and Horn pointed out, J.W. Eberhard and P.M. Horn found that the spectral exponent α (in the relationship $S(f) \propto 1/f^\alpha$) of metals is temperature dependent with α decreasing in the range $0.8 \lessapprox \alpha \lessapprox 1.4$ with increasing temperature [44]. Dutta, Dimon, and Horn supposed that this meant a failure of the assumption that $p(E)$ is independent of temperature, altering the spectral density's exact $1/f$ dependence upon frequency as well as its linear dependence upon temperature. To characterize these deviations, they assumed that $p(E)$ depends only upon temperature implicitly through E^*. They then related the temperature and frequency dependences of the spectral density while simultaneously removing their dependence upon $p(E^*)$.

Taking the logarithm of equation 1.41 and taking the derivative of this expression with respect to $\ln(\omega)$ yields

$$\begin{aligned} \frac{\partial \ln(S_\rho(\omega,T))}{\partial \ln(\omega)} &= \frac{\partial \ln(p(E^*))}{\partial \ln(\omega)} - 1 \\ &= \frac{1}{p(E^*)} \frac{\partial p(E^*)}{\partial E^*} \frac{\partial E^*}{\partial \ln \omega} - 1 \\ &= -\frac{k_B T}{p(E^*)} \frac{\partial p(E^*)}{\partial E^*} - 1 \end{aligned} \tag{1.42}$$

Again, taking the logarithm of equation 1.41, but now taking the derivative with respect to $\ln(T)$ yields

$$\begin{aligned}\frac{\partial \ln(S_\rho(\omega,T))}{\partial \ln(T)} &= \frac{\partial \ln(p(E^*))}{\partial \ln(T)} + 1 \\ &= \frac{1}{p(E^*)}\frac{\partial p(E^*)}{\partial E^*}\frac{\partial E^*}{\partial \ln T} + 1 \\ &= -\ln(\omega\tau_0)\frac{k_B T}{p(E^*)}\frac{\partial p(E^*)}{\partial E^*} + 1\end{aligned} \tag{1.43}$$

Equations 1.42 and 1.43 are combined to eliminate the terms containing $p(E^*)$. Finally, solving for the spectral exponent $\alpha(f,T) = -\partial \ln\big(S_\rho(\omega,T)\big)/\partial \ln(\omega)$

$$\alpha(f,T) = 1 - \frac{1}{\ln(\omega\tau_0)}\left[\frac{\partial \ln(S_\rho(\omega,T))}{\partial \ln(T)} - 1\right] \tag{1.44}$$

As can be seen from equation 1.44, a linear relationship between the power spectral density and temperature will result in a pure $1/f$ spectrum. Dutta, Dimon, and Horn found agreement with this model for silver, gold, copper, and bismuth for temperatures up to $550K$ [42], verified by Eberhard and Horn for those metals as well as for nickel [44]. In all of these cases it was found that fits to data gave reasonable values for activation energies $E^* = -k_B T \ln(\omega\tau_0) \approx 1\ eV$ [43].

In the above, no mention was made of the nature of the heterogeneity that leads to the distribution of characteristic times aside from the fact that they obey an Arrhenius-like activation law and some further assumptions about the distribution of activation energies. However, $1/f$ noise was known to persist in metals below temperatures where *any* Arrhenius processes would be thermally active [43]. Fortunately, at the time that Dutta, Dimon, and Horn proposed their model for $1/f$ noise in metals, a class of excitations yielding the correct distribution of characteristic times had already been used to explain many material properties. In 1971, P.W. Anderson, B.I. Halperin, and C.M. Varma used a model based on two-level tunneling systems

(TLTS) to explain the anomalous linear dependence upon temperature of the low-temperature specific heat and thermal conductivity in disordered materials [3]. The crux of their model is the existence in disordered materials of atoms or collections of atoms that can occupy one of only two states and are able to tunnel between these states. These two-level tunneling systems can then be represented by a double-well potential and the probability of transitioning from one well to another is controlled by a tunneling parameter, which in turn is determined by the height of the barrier, the distance over which the atoms must tunnel, and the mass of the tunneling atoms. Finally, the transitions of these two-level tunneling systems are coupled to macroscopic quantities, such as resistivity or dielectric function, leading to observable fluctuations [67, 77].

The results of Dutta, Dimon, and Horn were quickly reformulated in terms of TLTS [67, 136, 16, 15, 77], so that $1/f$ behavior, due to classical Arrhenius activation processes at high temperatures, could be seen to continue at low temperatures, where tunneling dominates. The manner in which TLTS lead to $1/f$ noise is only qualitatively outlined here; very complete overviews can be found in reference [65, 14]. It was noted that as temperature is reduced, and most thermally activated transitions become inaccessible, the fluctuations are dominated instead by tunneling. In order to ascribe $1/f$ noise to the tunneling, the transition times must be distributed as $p(\tau_c) \propto 1/\tau_c$, and this usually comes about from the transition time τ_c depending upon the exponential of a quantity that is distributed uniformly over some range. In this case, the transition time is found through Fermi's golden rule of time-dependent perturbation theory to depend upon the tunneling parameter λ as $\tau_c \propto e^{2\lambda}$, where λ depends upon the barrier's height and width and the mass of the tunneling atoms. Physical arguments lead to the conclusion that this tunneling parameter λ is indeed uniformly distributed [67, 77, 14], and so the necessary ingredients for $1/f$ noise are

present. The model of two-level tunneling systems is today one of the more popular models for $1/f$ noise and has been applied to a number of systems and devices which typically operate at low temperatures, e.g. Josephson junctions [97, 143].

Regardless of the origins of the heterogeneity in these models, a natural test for any model of $1/f$ noise based on a broad distribution of characteristic times is to reduce the system size until few enough modes contribute to the noise spectrum that features in the spectrum corresponding to single Lorentzians can be distinguished. The first such test was reported in 1984 by K.S. Ralls et al. by observing changes in resistance of the inversion channels of MOSFETs of very small size, $\approx 1\ \mu m \times 0.1\ \mu m$. They observed time series of resistance that switched between two states with noise spectra that were Lorentzian and in one case were able to measure a time series with a spectrum that consisted of two Lorentzians superposed. A transistor with an inversion channel with larger dimensions $\approx 10\ \mu m \times 20\ \mu m$, manufactured simultaneously from the same wafer as the submicron transistors, showed no distinguishable two-state switching in the time series or features in the spectra, only the $1/f$ spectrum expected in macroscopic transistors. However, while they did observe the two-state switching that is expected to lead to $1/f$ noise, they did not have sufficient data to see the emergence of a $1/f$ spectrum from a few Lorentizan spectra [102]. In the same year, C.T. Rogers and R.A. Buhrman reported just such observations in the voltage fluctuations of a submicron metal-insulator-metal tunnel junction, resolving an approximate $1/f$ spectrum with features that were able to be fit to a superposition of just a few Lorentzian spectra [108].

E.V. Russell and N.E. Israeloff have also reported evidence for $1/f$ arising from heterogeneity in a structural glass. By biasing the probe of an atomic force microscope and a sample of the polar, glass-forming molecule polyvinylacetate they were able to measure fluctuations in the polarization of a volume of $\approx 2 \times 10^{-17}\ cm^3$ of the sample,

recording a time series over approximately a day. This volume probed is comparable to the size of cooperative clusters in polyvinylacetate found from nuclear magnetic resonance experiments, $\approx 2-4\ nm$, so that only a few clusters contributed to the fluctuations. From full, day-long time series, a $1/f$ type spectrum was observed. However, for time series on the order of an hour, the shape of the spectrum was found to wander, and at times spectral features identified as individual Lorentzians would grow and subsequently relax. These observations provide evidence not just of heterogeneity, but specifically of *dynamic* heterogeneity, with the strength and characteristic time of fluctuations changing with time as the probed volume moves slowly among configurations with different sets of characteristic times [110]. Similar observations of distinct spectral features have been made in mesoscale experiments in spin glasses [136] and semiconductor devices [92].

Some of the best evidence for these models is that heterogeneity and the resultant distribution of characteristic times is also the most popular explanation for a number of other properties of disordered systems. It was pointed out above that the two-level tunneling systems used by Anderson, Halperin, and Varma to explain some properties of disordered materials [3] have been extensively used in models of $1/f$ noise [67, 136, 15, 16, 77]. Another significant property of heterogeneity is the nonexponential characteristic of supercooled liquids and structural glasses [133, 19, 105, 26]. For systems such as these, the relaxation and autocorrelation functions $\xi(t)$ are not found in experiments to be exponential, but more often follow a stretched exponential form known as the Kohlrausch-Williams-Watt function:

$$\xi(t) \propto e^{-(t/\tau_c)^{\beta}} \tag{1.45}$$

where the parameter $\beta = 1$ at high (typically inaccessible in experiments) temperatures, meaning standard exponential characteristic, and decreases to some value

$\beta < 1$ near the glass transition temperature, yielding the much slower characteristic associated with glasses. While it remains a possibility that this stretching is a phenomenon intrinsic to individual molecules, allowing the liquid to relax homogeneously, the explanation supported by the experimental evidence is that molecular cooperativity near the glass transition results in the creation of clusters of molecules with their own relaxation rates. Like the power spectral density, this means that to find the relaxation function for the bulk sample, the exponential relaxation of an individual region needs to be integrated over its characteristic time, weighted by a distribution $p(\tau_c)$:

$$\xi(t) \propto \int_0^\infty p(\tau_c) e^{-t/\tau_c} d\tau_c \tag{1.46}$$

The heterogeneous explanation for the stretched form of relaxation and autocorrelation functions has been known for some time. However, in the past twenty years, with the advent of molecular dynamics simulations and experimental techniques such as reduced 4D nuclear magnetic resonance and non-resonant spectral hole burning that allow for the direct observation of characteristic of individual clusters of molecules, evidence has suggested more and more that heterogeneity is in fact the solution to this long-standing problem [133].

Similarly, experimental limitations for some time obfuscated the heterogeneous explanation of $1/f$ noise. While nonexponential relaxation may clearly be a property of supercooled liquids, most early observations of $1/f$ noise were made in metals, carbon resistors, etc., where those effects are not readily observable. Ironically, while it was the noise that prevented direct measurement of the susceptibility, it was through measurement of the noise that the susceptibility could be found indirectly, by way of the fluctuation-dissipation relation [65, 110].

As previously discussed, no low frequency cutoff of a continuous $1/f$ type spectrum has been observed. By definition, this means that ergodicity is broken in these

systems. Absent of a cutoff, the lowest frequency characteristic modes cannot have been observed to have made a transition, so that the system, in the time of observation, has not fully explored its phase space. These models, at their core, are based upon a constant distribution of barrier heights. However, because of the characteristic time's exponential dependence upon barrier height, this distribution can be relatively narrow and still yield a very broad distribution of characteristic times. It therefore comes as no surprise that the low frequency cutoff is inaccessible. It should also be pointed out that the underlying processes in these models are stationary, linear, and Gaussian. Instead, the power law nature of the $1/f$ noise in these models come from the distribution $p(\tau_c) \sim 1/\tau_c$. This is in contrast to the models in the next section, § 1.4.2, in which the underlying processes themselves are based on power laws and are therefore intrinsically non-stationary.

1.4.2 $1/f$ Noise From Power-Law Renewal Processes

For models based on the superposition of exponential relaxation processes with distributed characteristic times, the resolution to the paradox of infinite fluctuations is found in the assurance that there exists some low-frequency cutoff to the $1/f$ spectrum. The underlying processes of these models are stationary, and the power law nature of $1/f$ noise comes from a power law distribution of relaxation times. However, there also exist classes of models that resolve this paradox by considering non-stationary and/or non-ergodic processes which demonstrate aging like that described in § 1.3.3, specifically equation 1.29. One such class of models is based on *renewal processes* [50]. The use of renewal processes to generate $1/f$ type spectra that could avoid the paradox of infinite fluctuations was first suggested by B.B. Mandelbrot in the mid 1960s [82, 135]. The simplest of these are two-state random processes, in which a system switches between two discrete states, described by a random variable

I that assumes one of two values, say

$$I(t) = \pm I_0 \tag{1.47}$$

at times $t = t_1, ...t_n, ...$ In this case, not only is $I(t)$ a random variable, but so are the *sojourn times* $\tau_i = t_i - t_{i-1}$ that the system spends in each state [46]. An early investigation of two-state random noise was conducted by S.O. Rice in 1944 [104]. Rice considered a Poisson process, where the sojourn times τ_i are exponentially distributed with a single intensity μ. The probability density function from such a process is

$$\psi(\tau) = \mu e^{-\mu\tau} \tag{1.48}$$

and the number of switching events n occuring in time t follow a Poisson distribution: $P(n,t) = (\mu t)^n e^{-\mu t}/n!$. An example of a time series of such a process is shown in figure 1.1a. The mean sojourn time is well defined:

$$\overline{\tau} = \int_0^\infty \tau\psi(\tau)d\tau = \frac{1}{\mu} \tag{1.49}$$

The power spectral density is a Lorentzian, and as such Poisson processes are often the fluctuators appearing in the models of distributed characteristic times in § 1.4.1, where μ^{-1} is interpreted as the characteristic time τ_c. Indeed, McWhorter employed a Poisson process to describe the occupation of defects by electrons in his model of noise in semiconductors [87], described in § 1.4.1.

In addition to having a well-defined mean sojourn time, the correlation function of a Poisson process depends only upon the lag and not upon the measurement time t_m, converging to a delta function as $t_m \to \infty$ [46, 84]. The process is therefore ergodic and stationary. However, the sojourn times of a two-state process need not be exponentially distributed, and not all such processes are ergodic or stationary. One example comes from sojourn times following a Mittag-Leffler distribution, a survival

function interpolating between a power law distribution $\psi(\tau) \propto \tau^{-\beta}$ for $\tau \to \infty$ and a stretched exponential $\psi(\tau) \propto e^{-\tau^{\beta}}$ for $\tau \to 0$. Time series from models of this type are non-stationary and non-ergodic and fluctuate with a $1/f$ type spectrum that has been found to exhibit aging [94, 46]. Importantly, this aging preserves the shape of the spectrum as a function of frequency, yielding an α that is constant in time. Only the amplitude, separable as a time-dependent prefactor multiplying the frequency-dependent part of the spectrum, changes with time. The ensemble average of this prefactor has the proper time dependence, $\propto t^{1-\alpha}$, to avoid the paradox of infinite fluctuations [94].

Similarly, when sojourn times are distributed according to simply a power law, the resulting time series may not be ergodic and will fluctuate with a $1/f$ type spectrum [80, 84, 76]. For instance, a process obeying Lévy statistics, for which the sojourn times follow a probability distribution function

$$\psi(\tau) \sim \tau^{-1-\theta}, \qquad 0 < \theta \leq 2 \tag{1.50}$$

will fluctuate with a $1/f$ type spectrum and may be non-ergodic and non-stationary, depending on the value of θ. An example of such a time series, for $\theta = 0.5$ is shown in figure 1.1(b). The time-averaged mean and variance of τ are

$$\begin{aligned} \overline{\tau} &= \int_0^{\infty} \tau \psi(\tau) d\tau \propto \lim_{\tau \to \infty} \tau^{1-\theta} \\ \overline{\tau^2} &= \int_0^{\infty} \tau^2 \psi(\tau) d\tau \propto \lim_{\tau \to \infty} \tau^{2-\theta} \end{aligned} \tag{1.51}$$

For $\theta = 2$, both the mean and the variance are bounded and the process simply describes Brownian motion. In this extreme case, the mean sojourn time remains small, yielding a variance that is finite. It will therefore have a power spectral density that decays as $1/f^2$ and is stationary. For $1 < \theta < 2$, the tail of the distribution is heavy enough that longer sojourns are allowed. Time series of this type, of

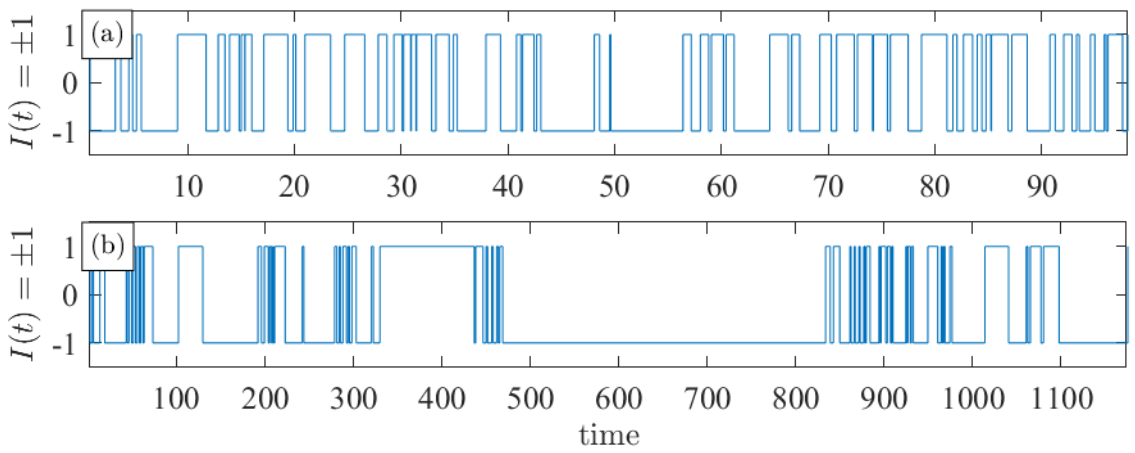

Figure 1.1: Illustration of ergodic (Poissonian) and non-ergodic (power law) time series. (a) Time series of a random variable $I(t) = \pm 1$ containing $N = 100$ transitions, where the sojourn time between two transitions $\tau_i = t_i - t_{i-1}$ is itself a random variable distributed according to equation 1.48 with $\mu = 1$. It is clear that τ has a finite time-average and that $\overline{I(t)} \to 0$. (b) Another time series of $I(t) = \pm 1$ containing $N = 100$ transitions, where τ_i is distributed according to equation 1.50 with $\theta = 0.5$. Since $0 < \theta < 1$, the time-averaged mean and variance of τ, equation 1.51, diverge. Therefore, $\overline{I(t)}$ does not converge, the process is non-stationary and non-ergodic, and the power spectral density will exhibit aging.

which Brownian motion is a special case, are known as Lévy flights, a term coined by Mandelbrot after Paul Lévy, a mathematician whose work anticipated much of Mandelbrot's [81]. The mean sojourn time remains bounded and consequently so does the time-averaged mean of $I(t) = \pm I_0$: $\overline{I(t)} = 0$. The variance, on the other hand, diverges and the power spectral density is non-stationary. For $0 < \theta \leq 1$, both the mean and the variance of τ diverge, and $\overline{I(t)}$ is a random variable for all measurement times [135, 80, 84]. This highly non-ergodic case has attracted the most attention in recent years [84, 94, 73].

From figure 1.1 it can be visualized how a time series with sojourn times distributed as in equation 1.50 can lead to the aging described by equation 1.29. In figure 1.1a is shown a time series with $N = 100$ transitions and sojourn times distributed exponentially, as in equation 1.48, with $\mu = 1$. It is clear from the time

series alone that the average sojourn time is finite and $\overline{I(t)} \to 0$. In figure 1.1b is shown a time series with the same number of transitions, $N = 100$, but sojourn times distributed according to equation 1.50, with $\theta = 0.5$. Because the distribution $\psi(\tau)$ is heavy tailed, unlike the exponentially distributed sojourn times seen in figure 1.1a, the mean sojourn time, equation 1.51, is infinite. This means that there is always finite probability of a sojourn time of *any* length occuring. This includes sojourn times greater than the length of the measurement itself, $\tau > t_m$. If such a sojourn time occurs during and beyond the end of a measurement, extending the length of the measurement only extends the time over which no fluctuations occur. Essentially, as time passes the cumulative probability of encountering a sojourn time $\tau \sim t_m$ increases. As a result, ensemble averages of power spectral densities calculated from successively longer measurements of the same time series will decay with time. Another consequence of non-stationarity that becomes clear from these considerations is that the time-averaged mean value of $I(t)$ is not well-defined. Encountering a sojourn time $\tau \sim t_m$ over which either $I(t) = +I_0$ or $-I_0$ will bias $\overline{I(t)}$ toward this value, so that $\overline{I(t)} \neq 0$ for any t_m. Of course, the ensemble-averaged mean value $\langle I \rangle = 0$, confirming that the process is nonergodic in addition to being non-stationary.

In figure 1.2, another property of time series of this type, and a property of $1/f$ noise in general, is illustrated: its *scale invariance*, or *self-similarity*. FIG 1.2 shows successively shorter portions of a single time series of a two-state random process with sojourn times taken from equation 1.50 with $\theta = 0.3$. The top figure, figure 1.2a, shows the full time series, containing $N = 10^5$ transitions over a unitless length of time $t_m \approx 10^7$. The red vertical lines in figure 1.2a indicate the range shown in (b), an order of magnitude smaller than that of (a), and so on for (c), (d), and (e). The visual similarity of these demonstrates that this process has no natural scale; it is scale invariant, or self-similar. Continually cutting out smaller portions

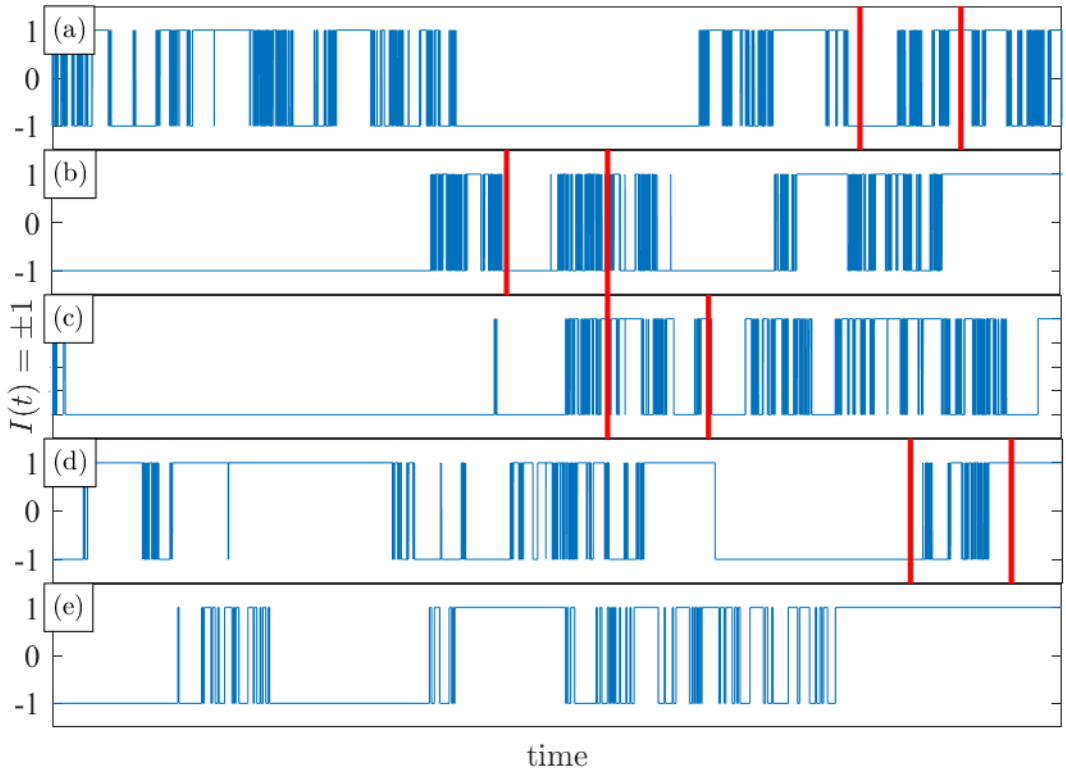

Figure 1.2: A demonstration of the fractal nature of the processes underlying $1/f$ noise, specifically their scale invariance, or self-similarity. (a) The full time series, containing $N = 100$ over a unitless length of time $t_m \approx 10^7$. The vertical red lines indicate the range shown in (b), an order of magnitude smaller than that of (a), and likewise for (c), (d), and (e). Shrinking or expanding the measurement time yields the same distribution of sojourn times. The mean sojourn time therefore diverges with measurement time. As a result, $\overline{I(t)}$ never converges and the process is non-stationary and, since $\langle I \rangle = 0$, non-ergodic. In (e) it becomes clear to the eye that the time series only contains a finite number of transitions, marking the end of the self-similarity.

of a time series of such a process produces the same distribution of sojourn times. Likewise, continually extending the time of measurement, the time series will have the same distribution of sojourn times. This means that the time-averaged sojourn time increases with measurement time, so that $\overline{I(t)}$ never converges for any length of time. The exception to this is perhaps figure 1.2(e), where the finite number of transitions becomes visible to the eye.

As discussed in § 1.3.3, such non-stationary models, though generating excitement, failed to gain currency in the years immediately after their conception, since most

experiments concluded that the processes underlying $1/f$ noise are stationary [124, 43]. Only until recently have experiments begun to show conclusive evidence of non-stationarity in systems exhibiting $1/f$ noise through the mechanisms described in this section (often called *power law intermittency* in the experimental literature). Like $1/f$ noise in general, the systems showing power law intermittency are diverse, including: the current-voltage characteristic of nanoscale electrodes [68]; turbulence in weakly driven liquid crystals [120] and the magnetic field generated by the flow of liquid metals [54]; the relaxation of a number of glasses [2]; in experiments and simulations of the interface fluctuations of the (1+1)-dimensional Kardar-Parisi-Zhang (KPZ) universality class [126]; biorecognition observed through dynamic force spectroscopy [12]; and, most exhaustively, in the fluorescense spectra of laser-driven quantum dots [99, 34, 48, 112].

Non-stationarity and spectral aging are experimentally observed only in a relatively small fraction of the many systems exhibiting $1/f$ noise. However, it may be possible that non-stationarity and its resolution of the paradox of infinite fluctuations might be salvageable and reconcilable with stationary models of $1/f$ noise. This is accomplished through the concepts of *conditional measurements* and a *conditional spectra*. Once again, this idea was originally conceieved by Mandelbrot [80], though it is only recently gaining popularity in relation to the physics of $1/f$ noise [135, 73]. The power spectral densities of the processes described in this section are non-stationary because of the finite probability of a sojourn time occuring during the measurement that is on the order of the measurement time, $\tau \sim t_m$. However, the ensemble average of power spectral densities might be made stationary by considering only the subset of measurements from "active" processes, for which there are no such sojourn times, $\tau < t_m$. Expanding on this idea, Mandelbrot was able to show that the complete, ensemble-averaged power spectral density for the processes described

by equation 1.50 could be decomposed into a function of frequency and the parameter θ, and a function of the measurement time and θ [80, 135]:

$$\langle S_{t_m}(f)\rangle \propto \frac{t_m^{\theta-1}}{f^{2-\theta}} \tag{1.52}$$

Such a spectrum will age as required to avoid the paradox of infinite fluctuations, equation 1.29. Nearly 50 years after first being expressed by Mandelbrot [80], this idea has been revisited and analyzed precisely, both analytically and numerically [94].

equation 1.52 comes from considering a process that is intrinsically non-stationary. However, it has been shown recently by N. Leibovich and E. Barkai that the concepts of conditional measurements and conditional spectra can reconcile stationary and non-stationary models of $1/f$ noise [73]. The most popular model of $1/f$ noise, that based on the superposition of exponential relaxation processes with a distribution of characteristic times, § 1.4.1, was among those considered. How a non-stationary conditional spectrum can be recovered from this intrinsically stationary model, and how it might manifest in experiments, will be outlined here.

The process is composed of N underlying processes. These are two-state Poisson processes, equation 1.47, where sojourn times between switching events are distributed as in equation 1.48. The spectrum of a single underlying process is a Lorentzian

$$S_j(f) = I_0^2 \frac{4\overline{\tau_j}}{1+\overline{\tau_j}^2\omega^2} \tag{1.53}$$

where its characteristic time is the mean sojourn time $\tau_c = \overline{\tau}$, equation 1.49, and the magnitude of fluctuations I_0^2 is the same for all processes. If the characteristic times $\overline{\tau_j}$ of the underlying processes are distributed as $p(\overline{\tau}) = 1/\overline{\tau}^\beta$ in the interval $\tau_{min} < \overline{\tau_j} < \tau_{max}$, the total spectrum, equation 1.36, will be $S(f) \propto 1/f^{2-\beta}$ in the interval $1/\tau_{max} < f < 1/\tau_{min}$. Note that the magnitude of fluctuations I_0^2, being the same for all processes, is retained in the single-process spectra, equation 1.53.

Therefore, the distribution $p(\overline{\tau})$ is normalized to 1 as opposed to the total variance, as was the case in equation 1.37. The normalization constant is

$$\nu = \left[\int_{\tau_{min}}^{\tau_{max}} \overline{\tau}^{-\beta} d\overline{\tau} \right]^{-1} = (1-\beta)/[(\tau_{max})^{1-\beta} - (\tau_{min})^{1-\beta}] \tag{1.54}$$

Now, if the measurement time is shorter than at least the longest characteristic time, $t_m < \tau_{max}$, not all underlying processes will undergo transitions. Specifically, those with $\overline{\tau_j} \gg t_m$ are not active and do not contribute to the total, observed spectrum. The probability that a process with characteristic time $\overline{\tau_j}$ will undergo a transition in measurement time t_m is

$$P_{act}(t_m|\overline{\tau_j}) = 1 - e^{-t_m/\overline{\tau_j}} \tag{1.55}$$

To construct the conditional spectrum, the underlying processes are considered individually and measurements are subject to the condition that only active processes are considered, which is precisely the condition used in experiments of single fluctuators. The conditional spectrum is found from integrating the active processes weighted by the new distribution

$$p_{act}(\overline{\tau_j}) = \nu_{act} \times p(\overline{\tau_j}) P_{act}(t_m|\overline{\tau_j}) \tag{1.56}$$

where the new normalization constant ν_{act} is

$$\nu_{act}^{-1} = \int_{\tau_{min}}^{\tau_{max}} P_{act}(t_m|\overline{\tau_j}) p(\overline{\tau_j}) d\overline{\tau_j} \approx \Gamma(\beta) \left(\frac{t_m}{\tau_{max}} \right)^{1-\beta} \tag{1.57}$$

where $\Gamma(\beta) \equiv \int_0^\infty x^{\beta-1} e^{-x} dx$ is the gamma function. Since the conditional spectrum is found by integrating the spectra of active processes weighted by $p_{act}(\overline{\tau_j})$, it is also normalized by ν_{act}. Therefore, the conditional spectrum of active processes is non-stationary, decaying with measurement time as $\propto t_m^{\beta-1}$ for $0 < \beta < 1$, which yields an ensemble averaged conditional spectrum

$$\langle S_{act}(f, t_m) \rangle \propto I_0^2 \frac{t_m^{\beta-1}}{f^{2-\beta}} \tag{1.58}$$

With $\alpha = 2 - \beta$, so that $1 < \alpha < 2$, this conditional spectrum has the same form as that expressed in equation 1.29, thus avoiding the paradox of infinite fluctuations.

The conditional spectrum of equation 1.58 may correspond to actual measurements if an experiment were to observe individual processes, as is the case in studies of individual quantum dots or nanocrystals [99, 34, 48, 112]. On the other hand, in many experiments, the underlying processes cannot be resolved individually. That is to say, a macroscopic measurement is being made. In this case, the spectrum will grow with time as more processes become active and contribute to the observed spectrum. The number of active processes is

$$\begin{aligned} N_{act} &= N \int_{\tau_{min}}^{\tau_{max}} P_{act}(t_m|\overline{\tau_j}) p(\overline{\tau_j}) d\overline{\tau_j} \\ &\approx N \times \Gamma(\beta) \left(\frac{t_m}{\tau_{max}} \right)^{1-\beta} \end{aligned} \tag{1.59}$$

Interpreting the conditional spectrum, equation 1.58, as the average spectrum of single active processes, the observed macroscopic spectrum is

$$\begin{aligned} S_{obs}(f) &= N_{act} \times \langle S_{act}(f, t_m) \rangle \\ &\propto N I_0^2 \tau_{max}^{\beta-1} \frac{1}{f^{2-\beta}} \end{aligned} \tag{1.60}$$

So, while the average spectrum of active processes decays as $t_m^{\beta-1}$, the number of processes contributing to $S_{obs}(f)$ grows as $t_m^{1-\beta}$. The observed spectrum is therefore independent of t_m and is stationary. However, the process remains non-ergodic on these time scales, as $t_m < \tau_{max}$ and the system has not explored all possible states.

Similarly, it has been shown that a macroscopic measurement of an intrinsically *non-stationary* process will yield a stationary spectrum [73]. In the case of blinking quantum dots, this explains why past measurements, which were not performed on individual quantum dots, hid the intrinsic non-stationarity of the underlying processes [112]. This opens up the possibility that more systems exhibiting $1/f$ noise are

composed of intrinsically non-stationary processes. In this case, no natural cutoff frequency would be necessary to avoid the paradox of infinite fluctuations.

1.4.3 $1/f$ Noise From Self-Organized Criticality

The final model considered here is the subject of the most highly-cited paper in the $1/f$ literature, with over 4,000 citations. The paper, published in 1987 by Per Bak, Chao Tang, and Kurt Wiesenfeld, has garnered so much attention not for its utility as a general model of $1/f$ noise, but for introducing the concept of *self-organized criticality* [7]. This paper will be briefly described here.

Self-organized criticality is an attempt to explain the self-similarity and power law distributed length and time-scales observed in nature, *e.g.* the shape of coast lines, correlations in turbulence, etc.. As discussed in the previous section, these phenomena are strongly linked to $1/f$ noise. Bak, Tang, and Wiesenfeld argued that these structures arise naturally in systems with extended degrees of freedom and represent an evolution of the system under weak perturbation to a state of minimal stability with a wide distribution of length scales. Because the system is in a state of minimal stability and length scales are widely distributed, small perturbations lead to cascades of larger perturbations on a wide distribution of length and time scales, generating $1/f$ noise. Because the system naturally evolves toward this critical state, it is distinct from the criticality observed at the critical point of a phase transition familiar from equilibrium statistical mechanics, which requires the tuning of external parameters, *e.g.* temperature, pressure, etc..

As an example of such a system, Bak, Tang, and Wiesenfeld considered sandpiles starting from an unstable configuration. If the slope of a sandpile exceeds a certain value K, the sand pile collapses until the slope equals K. This is the minimally stable position and a small perturbation, in the form of adding a little sand to the

top of the pile, will once again cause a collapse. The size and duration of this collapse will depend upon the size of the sandpile. Furthermore, the collapse will perturb neighboring sandpiles, causing them to collapse and perturb their neighbors, and a chain reaction ensues.

Bak, Tang, and Wiesenfeld simulated this system using cellular automata in one, two, and three dimensions. In two dimensions, each point is assigned a height of sand $z(x, y)$. If $z(x, y) > K$, the sandpile collapses, its height decreases and the sand moves to its neighbors, raising their height:

$$\begin{aligned} z(x, y) &\to z(x, y) - 4 \\ z(x \pm 1, y) &\to z(x \pm 1, y) + 1 \\ z(x, y \pm 1) &\to z(x, y \pm 1) + 1 \end{aligned} \tag{1.61}$$

Note that fluctuations in this sandpile model are independent of K. The boundary conditions are that $z = 0$ on the edges (imagine a table covered in sand). Initializing the system randomly under the condition that the system is far from equilibrium with all $z \gg K$, it will evolve into a state of minimal stability with all $z \leq K$. The system is perturbed by adding bits of sand to one z at a time and observing its evolution.

As predicted, Bak, Tang, and Wiesenfeld found that this system, under perturbation of a single site, exhibited collapses of sandpiles of all sizes s, where s is the extent of the sandpile's collapse in x and y. They found the size of sandpile collapses are distributed according to a power law $p(s) \sim s^{-\beta}$, with $\beta \approx 0.98$ and ≈ 1.35 in two and three dimensions, respectively.

Because the updating rule equation 1.61 is limited to nearest-neighbors, collapses propagate at a finite and constant speed. This is a crucial ingredient, as it means that, since collapse size is distributed according to a power law, so too is the duration

t_c of collapses. Say the collapse spreads over a duration t_c according to its size s as

$$t_c^{1+\gamma} \sim s \tag{1.62}$$

The distribution of collapse durations can be found from the distribution of collapse sizes:

$$p(t_c) = \frac{s}{t_c} p(s(t_c)) \frac{ds}{dt_c} \approx t_c^{-\beta(\gamma+1)+2\gamma} = t_c^{-\theta} \tag{1.63}$$

where $\theta \equiv \beta(\gamma + 1) - 2\gamma$ and $p(t_c)$ is weighted according to the average response of collapses s/t_c. Indeed, Bak, Tang, and Wiesenfeld found simulations produced power law distributions of t_c with $\theta \approx 0.42$ and ≈ 0.90 in two and three dimensions, respectively. As a result, the spectra of fluctuations are of the form $S(f) \approx 1/f^{\alpha}$ with $\alpha \equiv 2 - \theta \approx 1.58$ and ≈ 1.1 in two and three dimensions, respectively.

Though other models, including those discussed in § 1.4.1 and 1.4.2, are more popular as explanations of $1/f$ noise, this model has generated a vast literature surrounding self-organized criticality and its relevance to the self-similarity seen in nature. This model will also be relevant to the original models and results presented below in § 3 and 4. The similarity is somewhat tangential, as the models of § 3 and 4 do not exhibit self-organized criticality. They do, however, share the property that the time-scale of fluctuations of a quantity is related to the value of that fluctuating quantity. In the model of Bak, Tang, and Wiesenfeld, this property is encapsulated in the power law relation equation 1.62, and is crucial to the presence of $1/f$ noise [7].

Chapter 2

MULTIPLICITY-DEPENDENT CHARACTERISTIC TIMES

Before discussing the original models and work presented in § 3 and 4, their foundation is introduced: the concept of *multiplicity-dependent characteristic times*. That is to say, a stochastic variable M fluctuates with a characteristic time τ_c that depends upon M through its multiplicity $\Omega(M)$ as

$$\tau_c(M) \sim \frac{1}{\Omega(M)} \tag{2.1}$$

When this condition is satisfied, a system will exhibit fluctuations with a $1/f$ spectrum. This will be shown mathematically in § 2.1, for models based on a distribution of exponential relaxation processes and models based on power law renewal processes. In § 2.2, a physical interpretation of this condition will be offered: that equation 2.1 applies when the system is coupled to a finite, non-equilibrium bath, with which it shares a constant, maximized amount of entropy. This system + bath may then be coupled to an effectively infinite thermal reservoir, in the case that a system is only weakly coupled to the larger thermal environment and contact is mediated through the system's local environment.

2.1 Mathematical Motivation

In this section, equation 2.1 will be mathematically motivated. In § 2.1.1, it will be shown to result in $1/f$ fluctuations for a superposition of fluctuators in the manner of models discussed in § 1.4.1. In § 2.1.2, it will be shown to result in $1/f$ fluctuations for a single fluctuator, in the manner of the power law renewal processes discussed in § 1.4.2. Finally, in § 2.1.3 it will be compared to models based on self-organized

criticality, discussed in § 1.4.3. This mathematical motivation will also serve to clarify its physical interpretation in 2.1.3.

2.1.1 As a Distribution of Exponential Relaxation Processes

As discussed in § 1.4.1, a stochastic variable M (consider M stationary and $\langle M \rangle = 0$) will fluctuate with a $1/f$ spectrum if it is composed of fluctuators with Lorentzian spectra with time constants distributed as $p(\tau_c) \sim 1/\tau_c$. Given equation 1.37, the distribution $p(\tau_c)$ is interpreted as being the variance due to fluctuators with characteristic times between τ_c and $\tau_c + d\tau_c$ [65]. From this, $p(\tau_c)$ can be further interpreted as containing the density $\Omega(\tau_c)$ of fluctuators as well as the average amplitude squared $A^2(\tau_c)$ of a single fluctuation with characteristic time τ_c. It can be expressed as [51]

$$p(\tau_c) = A^2(\tau_c) \times \Omega(\tau_c) \tag{2.2}$$

So, with the proper relationship $A^2(\tau_c) \times \Omega(\tau_c) \sim 1/\tau_c$ between the density and the strength of fluctuations in the interval $\tau_1 < \tau_c < \tau_2$, fluctuations will have a $1/f$ spectrum in the frequency interval $1/\tau_2 < f < 1/\tau_1$. This is illustrated in figure 2.1, where 50 Lorentzian spectra are plotted along with their sum $S(f)$ for three different sets of $\Omega(\tau_c)$ and $A^2(\tau_c)$, each having the property $A^2(\tau_c) \times \Omega(\tau_c) \propto 1/\tau_c$.

Suppose that this stochastic variable M fluctuates with a characteristic time τ_c that depends upon M according to the condition of equation 2.1. This can be used to find the $\Omega(\tau_c)$ appearing in $p(\tau_c)$ in terms of $\Omega(M)$

$$\begin{aligned} &\Omega(\tau_c) d\tau_c = \Omega(M) dM \\ &\qquad \rightarrow \Omega(\tau_c) = \Omega(M) \left| \frac{d\tau_c}{dM} \right|^{-1} = \Omega^3(M) \left| \frac{d\Omega(M)}{dM} \right|^{-1} \end{aligned} \tag{2.3}$$

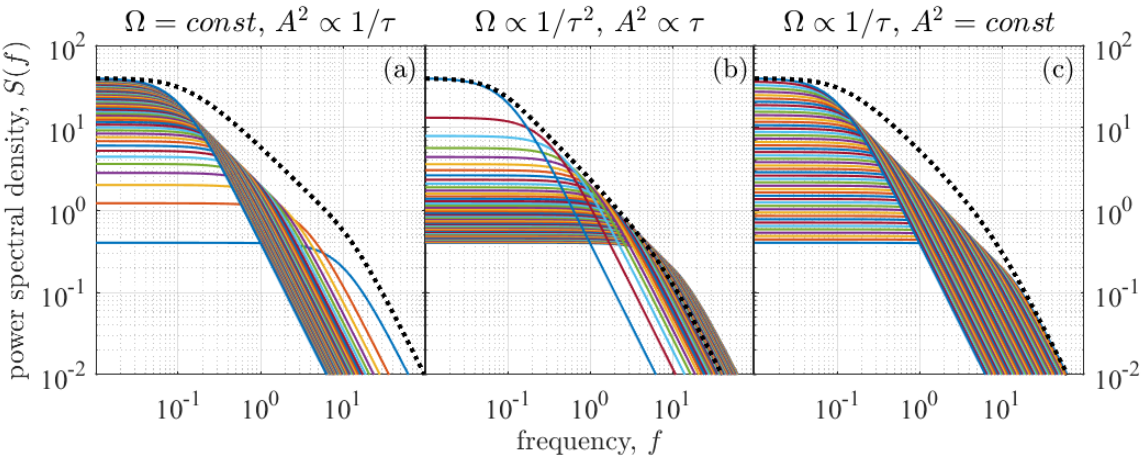

Figure 2.1: Log-log plot of 50 Lorentzian spectra (colored curves) and their sum (black dotted curve) corresponding to the total power spectral density as a function of frequency. Values of τ_c, in the interval $10^{-1} < \tau_c < 10^{1}$ from each set, were chosen according to the specified density $\Omega(\tau_c)$ of fluctuators and spectra are weighted by their corresponding amplitude $A^2(\tau_c)$. Each set has the property $p(\tau_c) = A^2(\tau_c) \times \Omega(\tau_c) \propto 1/\tau_c$ necessary to produce $1/f$ noise. For clarity of presentation, individual spectra are reduced by their amplitude and their sum is reduced in amplitude to match the low-frequency white noise level of the Lorentzian with the largest τ_c (lowest frequency mode). (a) $\Omega = const$, $A^2 \propto 1/\tau_c$. For a system consisting of linearly spaced characteristic times τ_c, the amplitude must be $\propto 1/\tau_c$. (b) $\Omega \propto 1/\tau_c^2$, $A^2 \propto \tau_c$. For a system consisting of characteristic times spaced as $1/\tau_c$, the amplitude must be $\propto \tau_c$. (c) $\Omega \propto 1/\tau_c$, $A^2 = const$. For a system consisting of logarithmically spaced characteristic times (linearly spaced on the log-log plot), the amplitude must be constant.

or in terms of τ_c as

$$\begin{aligned} \Omega(\tau_c)d\tau_c &= \Omega(M)dM \\ \rightarrow \Omega(\tau_c) &= \frac{1}{\tau_c}\left|\frac{dM}{d\tau_c}\right| \end{aligned} \tag{2.4}$$

Now consider the average amplitude $A^2(\tau_c)$ of a single fluctuation. The contribution to the total variance $\langle(\delta M)^2\rangle$ from a fluctuation of average size $|M|$ and duration τ_c, while dependent upon the shape of the fluctuation, is approximately

$$A^2 \sim M^2 \times \tau_c/t_m \tag{2.5}$$

where t_m is the total measurement time. Substituting equation 2.4 and 2.5 into

equation 2.2, the distribution of such multiplicity-dependent characteristic times τ_c is

$$p(\tau_c) = A^2(\tau_c) \times \Omega(\tau_c) \propto M^2(\tau_c)\left|\frac{dM}{d\tau_c}\right| \tag{2.6}$$

or, substituting equation 2.3 and 2.5 into equation 2.2, in terms of $\Omega(M)$,

$$p(\tau_c) \propto M^2\Omega^2(M)\left|\frac{d\Omega(M)}{dM}\right|^{-1} \tag{2.7}$$

In this case, of course, whether or not $p(\tau_c) \sim 1/\tau_c$ is satisfied and M exhibits fluctuations with a $1/f$ type spectrum will depend upon the form of $\Omega(M)$. A common situation, and one that will be relevant in the following, is that $\Omega(M)$ is Gaussian. If it isn't explicitly so, it can be approximated as such if a system undergoes small fluctuations about a state of maximum entropy. Here, Boltzmann's expression for the statistical entropy is used:

$$\mathcal{S} = k_B \ln \Omega \tag{2.8}$$

where Ω is the multiplicity of microstates corresponding to the macrostate of the system. In general, this multiplicity and the entropy of the system will depend upon the energy as well as any other parameters, including the variable M, which determine the macrostate of the system. For now, any dependency of M and $\mathcal{S}$ upon the energy E is ignored. The entropy considered is purely configurational so that equation 2.8 can be written $\mathcal{S}(M) = k_B \ln[\Omega(M)]$. This configurational entropy can be expanded as a function of M about its maximum $\mathcal{S}^{max}$

$$\mathcal{S}(M) = \mathcal{S}^{max} - \frac{1}{2}\frac{\partial^2 \mathcal{S}}{\partial M^2}M^2 + \mathcal{O}(M^4) \tag{2.9}$$

Retaining only the leading terms, the entropy is approximated as being quadratic in M so that the multiplicity is Gaussian, $\Omega(M) \propto e^{-const.\times M^2}$, and from equation 2.1, $\tau_c(M) \propto e^{const.\times M^2} \rightarrow M \propto \sqrt{\ln(\tau_c)}$. Either of these can be substituted into equation 2.6 or 2.7 to yield

$$p(\tau_c) \propto \frac{\sqrt{\ln(\tau_c)}}{\tau_c} \tag{2.10}$$

If the range of τ_c is sufficiently broad, $\sqrt{\ln(\tau_c)}$ being slow-growing, then this distribution is very nearly $\sim 1/\tau_c$. More precisely, for a distribution $p(\tau_c) \propto 1/\tau^\beta$, it is known that $S(f) \propto 1/f^{2-\beta}$ [73]. Therefore, taking $p(\tau_c) \sim \sqrt{\ln(\tau_c)}/\tau_c \sim 1/\tau_c^\beta$ locally in some range of τ_c, then $\beta < 1$, so that $\lim_{\tau\to\infty} \beta = 1^-$. So, the spectral exponent is $\alpha \sim 2 - \beta > 1$, so that $\lim_{\tau\to\infty} \alpha = 1^+$.

So, a variable M, fluctuating with a characteristic time τ_c depending upon M as in equation 2.1, will exhibit fluctuations with a $1/f$ spectrum if the multiplicity of states with M is Gaussian in M or as long as fluctuations in M are small enough that they may be approximated as such. Finally, if the value of M is bounded, so too is the value of τ_c. This defines the maximum characteristic time τ_{max}. For measurement times $t_m > \tau_{max}$, the system is ergodic. At frequencies $f < \tau_{max}^{-1}$ fluctuations are white and the power spectral density is flat.

2.1.2 As a Renewal Process

Equation 2.1 may also yield $1/f$ fluctuations in the fashion of a renewal process, as discussed in § 1.4.2. Consider a system which, unlike the two-state examples in § 1.4.2, has multiple states, corresponding to different values of the variable M, which may even be continuous. Further suppose that M is limited in how quickly it can change its value, if at all:

$$M(t+dt) = \begin{cases} M(t) \pm \delta M \\ \\ M(t) \end{cases} \tag{2.11}$$

If states are separated by a constant value $\delta M \sim const$, then each fluctuation can be considered as being between two states, and having a constant magnitude squared, $(\delta M)^2$. Therefore, though this process has multiple states, it is approximately reducable to the two-state systems discussed in § 1.4.2. Particularly, if the process is non-stationary and has no well-defined mean value, then the only meaningful measure

of the magnitude of each fluctuation is the separation δM between states adjacent in time. This also allows the characteristic time τ_c in § 2.1.1 to be considered equivalent to sojourn times τ in the analysis here.

If this single fluctuator obeys equation 2.1, then equation 2.4 holds and $\Omega(\tau) = \tau^{-1}|dM/d\tau|$. Once again, consider a system with a Gaussian multiplicity in M, $\tau \propto e^{const.\times M^2} \rightarrow M \propto \sqrt{\ln(\tau)}$ so that

$$\psi(\tau) \propto \Omega(\tau) \propto \frac{1}{\tau^2\sqrt{\ln(\tau)}} \tag{2.12}$$

where it was recognized that the probability density function of sojourn times $\psi(\tau)$ is the normalized multiplicity. Locally about some τ, this corresponds to equation 1.50, $\psi(\tau) \sim \tau^{-1-\theta}$, with $\theta > 1$ so that $\lim_{\tau\rightarrow\infty}\theta = 1^+$; therefore, $\alpha = 2 - \theta < 1$, so that $\lim_{\tau\rightarrow\infty}\alpha = 1^-$. So, this system will exhibit $1/f$ fluctuations. Furthermore, since $\theta > 1$, according to equation 1.51, M will have a well-defined, though slowly converging, mean, an infinite variance and a non-stationary power spectral density. However, if the value of M is bounded, so is the value of τ. The power law behavior of ψ will then be truncated at the maximum value of τ:

$$\psi(\tau) \sim \tau^{-1-\theta}e^{-\tau/\tau_{max}} \tag{2.13}$$

So, while the power spectral density may undergo large fluctuations for measurement times $t_m < \tau_{max}$, it will converge for $t_m > \tau_{max}$ and become stationary. In addition, fluctuations with $\tau > \tau_{max}$ will be white and the spectral density will be flat for $f < 1/\tau_{max}$.

2.1.3 Relationship to Self-Organized Criticality

Finally, systems obeying equation 2.1 bear some resemblance to models based on self-organized criticality, since in both cases the size of a fluctuation is related to its

duration. For the sandpile model of Bak, Tang, and Wiesenfeld, this is through the power law relation $t_c^{1+\gamma} \sim s$, equation 1.62 [7]. For the models based on multiplicity-dependent characteristic times presented here, this is through the relationship between the variable M, its multiplicity $\Omega(M)$, and the characteristic time, equation 2.1. While these relationships are crucial to $1/f$ fluctuations in both types of models, it is not clear that this similarity is anything more than cosmetic. Additionally, these are not the only two models of $1/f$ noise that depend upon a relationship between fluctuation size and duration. For instance, the droplet model of a spin glass, in which the magnetization fluctuates as $1/f$, has such a relationship, the size and duration of a fluctuation both being related the size of a cluster or droplet of spins [137]. However, there is another important property that originates from the relationship between fluctuation size and duration, shared by the multiplicity-dependent and self-organized criticality models: both models do not require the imposition of a specific distribution of sojourn times or characteristic times. Instead, $1/f$ noise arises naturally in both models without the tuning of a specific parameter.

2.2 Physical Interpretation

Having motivated equation 2.1 mathematically, and before moving on to its physical interpretation, the effects of this condition should be considered in general. Qualitatively, the condition equation 2.1 generates $1/f$ noise in a system by causing lower entropy states to live longer, causing the characteristic time of the system to evolve as the system moves among states of differing entropy. The system, then, is explicitly non-ergodic: different amounts of time are spent in different microstates. In fact, the probability of finding the system in a macrostate with M is

$$P(M) \propto \tau(M) \times \Omega(M) = constant \tag{2.14}$$

Apparently, imposing the condition equation 2.1 renders all macrostates and values of M equally likely in time. However, if the systems of an ensemble are prepared in such a way that ignores τ, so that their likelihood of being chosen is proportional to the multiplicity, then $P(M) \propto \Omega(M)$. Therefore, ensemble-averaged and time-averaged quantities will in general be different if equation 2.1 is satisfied, and the system is non-ergodic. Once again, however, if M is bounded, so too is the value of $\tau < \tau_{max}$. For measurement times $t_m > \tau_{max}$ time-averaged quantities become well-defined and the system is stationary for these times. However, these time averages may still differ from ensemble averages, so the system remains non-ergodic.

Another important consequence of equation 2.1 is that, since the fluctuations in M are directly related to M, models of this type are by definition non-linear (see § 1.3.2). This bodes well for models of this type for *e.g.* the flux noise in SQUIDs, which is known to be non-linear [119, 4]. The model presented in § 4 will be compared to SQUID flux noise, where its non-linearity allows it to reproduce the phenomenology of SQUID flux noise. On the other hand, linearity of the microscopic fluctuations of a system can serve as an experimental way to eliminate models of this type.

Below, the physical interpretation of what physical systems might obey the condition equation 2.1, and why, is explored. The interpretation used throughout this dissertation is that the system is in contact with a finite bath that can be pushed out of equilibrium according to the state of the system.

2.2.1 From a Finite, Non-Equilibrium Bath

Having outlined how the relationship expressed in equation 2.1 yields fluctuations with a $1/f$ type spectrum, it is left to describe the physical situation in which equation 2.1 might hold. The interpretation offered here is that equation 2.1 applies for a mesoscopic system in contact with a finite, local bath. The system + local bath may in

turn be considered to be coupled to an effectively infinite thermal reservoir, in the case that the system is not completely isolated, but also not ideally coupled to the thermal reservoir. On the other hand, ideal coupling to an infinite reservoir is assumed in the canonical ensemble, and is central to standard formulation of equilibrium statistical mechanics. Foundational to this formulation is the Boltzmann weight, which gives the probability of observing a system coupled to a thermal reservoir at temperature T to be in a state of energy E relative to the probability of observing a state with $E = 0$:

$$p \propto e^{-E/k_B T} \tag{2.15}$$

The sum over all Boltzmann weights of a system is known as the canonical partition function:

$$Z \equiv \sum_j e^{-E_j/k_B T} \tag{2.16}$$

The partition function, while doing much more, normalizes the Gibbs distribution to give definite values for the probabilities of states with energy E_j:

$$w_j = \frac{e^{-E_j/k_B T}}{Z} \tag{2.17}$$

Finally, the relative probability of two states having energies E_1 and E_2 separated by $\Delta E = E_1 - E_2$ is:

$$\frac{w_1}{w_2} = \frac{e^{-E_1/k_B T}}{e^{-E_2/k_B T}} = e^{-\Delta E/k_B T} \tag{2.18}$$

This is known as *Boltzmann's factor*. If the condition of detailed balance is satisfied, Boltzmann's factor also determines the probability of a transition between states of energy E_1 and E_2. In this role, Boltzmann's factor is the foundation of Markov chain Monte Carlo, most notably the heavily employed Metropolis-Hastings algorithm [89, 53].

Boltzmann's factor, equation 2.18, can be derived in a number of ways, *e.g.* using Lagrange's method of undetermined multipliers [55]. Here, to facilitate comparison

with the conditions necessary for equation 2.1, a derivation considering the linear change in the thermal reservoir's entropy due to the change ΔE in the internal energy of the system is employed [6]. Considering the system and the reservoir together, the probability of a fluctuation will be determined by the total change in entropy of the system and reservoir, $\Delta\mathcal{S}_{tot} = \Delta\mathcal{S}_S + \Delta\mathcal{S}_R$, where the subscripts R and S will denote reservoir and system quantities, respectively. Since the state of the system is known before and after the fluctuation, its entropy remains constant, $\Delta\mathcal{S}_S = 0$, so that $\Delta\mathcal{S}_{tot} = \Delta\mathcal{S}_R$. Now, the probability of the fluctuation is found by considering the relative probabilities of states to be proportional to their multiplicities, and inverting the Boltzmann entropy, equation 2.8:

$$p = e^{\Delta\mathcal{S}_R/k_B} \tag{2.19}$$

Expanding $\Delta\mathcal{S}_R$ as a function of the change in the reservoir's energy, ΔE_R, produces the fundamental equation of thermodynamics:

$$\Delta\mathcal{S}_R = \frac{\partial\mathcal{S}_R}{\partial E_R}\Delta E_R + \mathcal{O}((\Delta E_R)^2) \approx \frac{\Delta E_R}{T} \tag{2.20}$$

Where $T \equiv (\partial\mathcal{S}_R/\partial E_R)^{-1}$ defines the reservoir temperature. Higher order terms $\mathcal{O}((\Delta E_R)^2)$ are neglected under the assumption that the thermal reservoir is infinite. Further assuming that the only change in the energy of the reservoir comes from changes in the internal energy of the system, conservation of energy requires that $\Delta E_R = -\Delta E_S$. Substituting this and equation 2.20 into equation 2.19 gives Boltzmann's factor, equation 2.18. This derivation makes clear that the preference for the system to reduce its internal energy expressed in Boltzmann's factor fundamentally comes from a preference for raising the entropy of the thermal reservoir.

A number of assumptions go into deriving Boltzmann's factor. Two of these are (1) that the thermal reservoir to which the system is coupled is effectively infinite

and (2) that the coupling to this thermal reservoir is immediate. The sum of these considerations is that the thermal reservoir is not altered by changes in the state of the system and is therefore independent of the state of the system. However, when the system under consideration is small enough, the time scale of events short enough, or the system is not coupled ideally to the thermal reservoir, as may be the case at low temperatures, these assumptions might not hold. Instead, the local environment of the system, referred to here as the system's *local bath*, mediates contact and exchange of energy with the reservoir. Evidence for such imperfect coupling is found in the dynamical independence of nanometer size regions observed in many materials, as discussed is § 1.4.1 [133, 19, 105, 26]. Since the local bath is finite and of a size comparable to the system itself, changes in the system drive the local bath out of equilibrium, changing the thermal environment seen by the system. This violates the assumptions stated above which are necessary in deriving Boltzmann's factor to justify dropping the higher order terms $\mathcal{O}((\Delta E_R)^2)$ from the expansion in equation 2.20 and assuming that changes in the energy of the reservoir are accounted for entirely by the changes in the internal energy of the system.

To model this imperfect coupling, it is assumed that on the time scale of microscopic events, a maximized and constant amount of entropy is shared between the system and its local bath. Here, this constant amount of entropy is taken to be the maximum entropy of the system $\mathcal{S}^{max}_{system}$. The system + local bath are then coupled as a unit to the effectively infinite thermal reservoir. To maintain this situation, if the entropy of the system decreases, the entropy of its local bath must increase by a corresponding amount. As a result, if the system fluctuates into a state of low entropy, changes in its state are suppressed while the local bath, with its entropy now increased, explores newly available states and exchanges energy with the thermal reservoir. Specifically, changes are suppressed by a factor proportional to the fraction

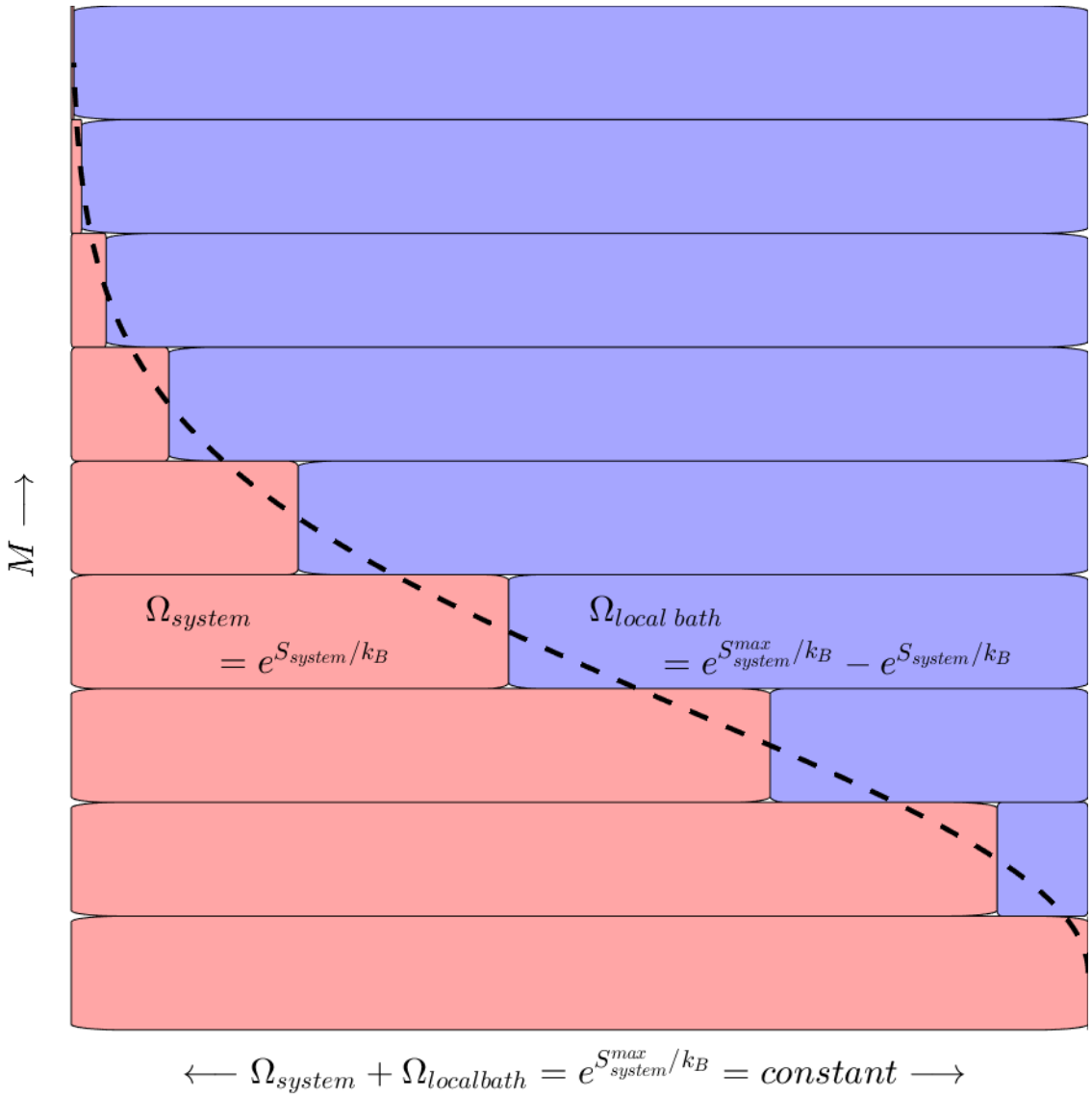

Figure 2.2: Schematic representation of a system (red) and its local bath (blue) sharing a constant amount of phase space. Depending on its entropy, transitions in the system are suppressed by a factor proportional to its relative share of the constant phase space: $\Omega_{system}/(\Omega_{system} + \Omega_{local\ bath}) = e^{\mathcal{S}_{system} - \mathcal{S}^{max}_{system}}$. This leads to the dependency of characteristic time upon multiplicity expressed in equation 2.1. The black dashed line depicts the smooth Gaussian dependence of the multiplicity upon M: $\Omega_{system} \equiv \Omega(M) \propto e^{-const. \times M^2}$.

of the total phase space $\Omega_{system} + \Omega_{local\ bath} = e^{S^{max}_{system}}$ that the system occupies:

$$\frac{\Omega_{system}}{\Omega_{system} + \Omega_{local\ bath}} = e^{\mathcal{S}_{system} - \mathcal{S}^{max}_{system}} \tag{2.21}$$

Suppressing the probability of transitions by a factor $\propto \Omega_{system}$ extends the lifetime of states with M by a factor of Ω^{-1}_{system}. This leads to the relationship between the characteristic time τ and the multiplicity $\Omega(M) \equiv \Omega_{system}$ expressed in equation 2.1. figure 2.2 illustrates this situation, depicting a constant amount of phase space being shared between the system and its local bath. Interpreting equation 2.1 as originating from the system's deviation from its state of maximum entropy suggests expressing it in another way:

$$\tau(M) \sim e^{\mathcal{S}^{max}_{system} - \mathcal{S}_{system}} \tag{2.22}$$

Under this interpretation, low entropy states of the system are preserved longer because the entropy of the local bath has been raised. Therefore, equation 2.22 (equivalent to 2.1) comes from a preference to keep the entropy of the local bath high, similar to Boltzmann's factor. However, equation 2.18 is different from Boltzmann's factor in that the local bath is pushed out of equilibrium by transitions in the system, whereas when the thermal reservoir is assumed infinite, its thermal equilibrium is unaltered by transitions in the system. One way that this difference manifests itself is that, while a *change* in entropy appears in equation 2.18, the *offset* from the maximum entropy appears in equation 2.22. This is because it is the offset from maximum entropy of the system that determines the state of the local bath, whose own offset from maximum entropy is determined by that of the system. If the total offset is considered to be the sum of changes in entropy from individual transitions, the local bath can be said to have a memory.

Another difference between the forms of equation 2.18 and 2.22 is that, while Boltzmann's factor comes solely from changes in the internal energy of the system,

equation 2.22 depends upon the configurational entropy as a function of M. However, fluctuations in configurational entropy may be accompanied by transfers of heat, independent of the interactions responsible for the internal energy of the system. A well-known example of work with an entirely entropic origin is the elasticity of a freely-jointed chain [47]. A well-studied practical realization of this is the cooling caused by the adiabatic demagnetization of non-interacting spins [70, 63]. If the transfers of entropy between the system and its local bath are indeed accompanied by transfers of heat, this allows the constraint to be viewed in another way: when the system fluctuates into a low entropy state, the local bath is heated. Transitions are suppressed while the now-heated local bath exchanges energy and equilibrates with the thermal reservoir. However, if coupling to the thermal reservoir is ideal, this equilibration occurs on a time scale faster than that of single transitions. The system then has no persistent effect on its own thermal environment and the rate of transitions and lifetime of states does not depend upon the state of the system.

Another reason this dependence upon configurational entropy due to M may come about is if changes in M require the transfer of a conserved quantity [29]. For instance, if M is the magnetization of a cluster of spins, as it can be interpreted in the spin models presented in § 3 and 4, changes in M require the transfer of angular momentum. Considering a single spin flip, this angular momentum necessary to effect the change in M must come from the spin's local environment. This can come from either exchange between neighboring spins or collective excitations (spin waves) in the magnetization of the cluster [129]. For a cluster of spins that is small and imperfectly coupled to its environment, the availability of angular momentum on the time scale of single spin flips is limited by the cluster's magnetization. In effect, the cluster acts as its own local bath of angular momentum. In heterogeneous systems such as supercooled liquids and structural glasses [133, 19, 105, 26], the conservation

of linear momentum may similarly constrain the dynamics of independent regions [29]. In addition to the interpretation that the local bath is the locally available amount of some conserved quantity aside from energy, another interpretation is that the identity of the local bath may be the kinetic energy of the system. Indeed, neither kinetic energy nor conserved quantiites like momentum and angular momentum are accounted for by Boltzmann's factor or traditional Monte Carlo simulations. There do, however, exist a number of Monte Carlo methods that employ local and/or global conservation of energy, such as that proposed by M. Creutz [36], of other conserved quantities like angular momentum, such as Kawasaki [61] and Glauber spin dynamics [49], and combined and/or relaxed versions of these [111, 78, 20]. In the models presented here, however, it is the entropy that is being conserved, to recreate an isolated or semi-isolated system + local bath which maintains a maximum entropy state, without reference to the identity of the local bath. It is therefore appropriate to deem it a *finite entropy bath*.

The condition of equation 2.1 and 2.22, imposed upon systems with approximately Gaussian multiplicities, results in distributions of characteristic times, equation 2.10, and sojourn times, equation 2.12, which are known to yield fluctuations with a $1/f$ spectrum (see § 1.4.1 and § 1.4.2). To demonstrate this, two models are presented. The first, in § 3, consists of a small number of non-interacting, binary spins coupled to an *explicit* finite bath. This model is simulated using a simple matrix to determine transitions, which occur either in the spin system or in the explicit local bath, depending upon their relative share of their total entropy. This model has the advantage of being simple and discrete, allowing entropies and transition probabilities to be easily calculated. The model is also non-interacting so that the entropy alone governs the dynamics, allowing the effects of the condition of equation 2.1 to be studied on their own. The second model consists of interacting classical Heisenberg spins. In this

model, the condition of equation 2.1 is imposed on clusters of spins with an *implicit* local bath by accepting spin-flips with a probability determined through equation 2.22, in a manner similar to the Metropolis algorithm. This differs from the matrix model most notably in that the spins interact with one another and exchange energy with a thermal reservoir. Therefore, this model does not exactly conserve entropy for all times, simulating instead a system that is non-ideally coupled to its thermal environment. Both of these models will be seen to produce $1/f$-type fluctuations.

Chapter 3

$1/f$ NOISE FROM A SIMPLE MATRIX

To explore the effect on fluctuations of the condition in equation 2.1, a model with dynamics governed by a simple matrix was studied [25]. The physical interpretation of equation 2.1 employed here is that the system shares a constant amount of entropy with a finite bath. As will be seen, the model has the advantages (1) of being degenerate, allowing the effect of the entropy-transfer mechanism alone to be studied, (2) of having a bath that is explicit so that its size relative to the system can be set exactly, and (3) of being discrete and simple enough that exact multiplicities, the stochastic matrix, etc., can be calculated. The model also has the appeal that its simplicity allows a clear interpretation and helps to clarify the features of a constrained Heisenberg spin model including interactions and continuous degrees of freedom, based on the same principles, presented in § 4. In § 3.3, the results of simulations will be presented. Additionally, noise in this model will be compared to noise measurements in the voltage across a mesocopic metal-insulator-metal (MIM) tunnel junction [108]. Lastly, this model will be recast as a discrete Markov chain in § 3.4. This allows a stochastic matrix to be constructed, the eigenvalues of which correspond to the transition frequencies of the model. This allows an alternate route to calculating the power spectral density, and these results will be compared to the results of simulations.

Much of the work presented in this chapter was published under the title "Fluctuations theorems and $1/f$ noise from a simple matrix" in *The European Physical Journal B*. The complete citation is listed under reference [25]. The original publication was completed in collaboration with others and is included in appendix A.

3.1 Model: System and Bath States

The system is perhaps the simplest possible arrangement of spins: an even number N of non-interacting, binary spins, allowed to take values of $+1$ or -1, in 0 field. The statistics of the system is therefore governed entirely by its configurational entropy. Absent any information on the state of the system, the total multiplicity is the number of possible arrangements of the N binary spins: $\Omega_{all} = 2^N$. Given knowledge of the system's macrostate, determined by its net alignment m, the multiplicity can be found using the binomial coefficient

$$\Omega_m = \frac{N!}{\left[\frac{1}{2}(N+m)\right]!\left[\frac{1}{2}(N-m)\right]!} \tag{3.1}$$

The configurational entropy of the system, according to Boltzmann's definition, is $\mathcal{S}_m = k_B \ln(\Omega_m)$. Of course, the maximum possible value of entropy is for zero net alignment $m = 0$ with spins half-up and half-down: $\mathcal{S}_0 = k_B \ln(\Omega_0)$ with $\Omega_0 = N!/[(N/2)!]^2$. The system undergoes fluctuations about this state which reduce its configurational entropy, $\mathcal{S}_m \leq \mathcal{S}_0$. The critical assumption of this model is that the combined entropy of the system plus its bath is maximized and constant at $\mathcal{S}_0$, such that a fluctuation of the system into a macrostate with net alignment $m \neq 0$ means that the entropy of its bath has correspondingly been raised by an amount $\mathcal{S}_0 - \mathcal{S}_m > 0$. To recreate this situation, additional bath states are included in the model which modify the transition rate among macrostates of the system according to the system's net alignment. First, however, the model without bath states will be described.

The state of the system is determined by the elements of a rectangular matrix, $\mathbf{M}$. An example of this matrix for a system of $N = 4$ spins and a schematic representation of its possible microstates is shown in figure 3.1. There are $N + 1$ rows in $\mathbf{M}$, corresponding to all possible macrostates of the system, and Ω_0 columns, corresponding to

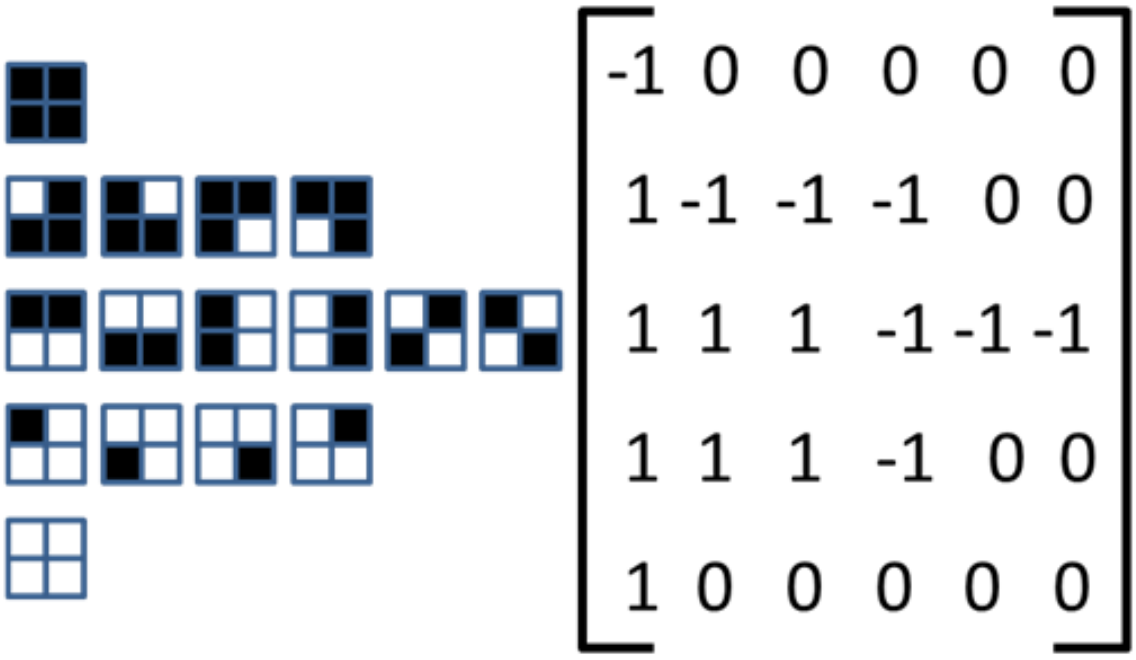

Figure 3.1: Schematic representation of all possible system states (left) and the corresponding rectangular matrix **M** (right) with bath states for an $N = 4$ spin system. Non-zero elements of the matrix **M** represent system states and the value of the element ($M_{i,j} = \pm 1$) determines how the alignment changes during a simulation step. Elements with $M_{i,j} = 0$ represent explicit bath states and do not alter the system alignment, thus slowing the dynamics for highly aligned systems.

all possible microstates of the system plus bath for a given net alignment. That is to say, **M** has elements $M_{i,j}$, with $-N/2 \leq i \leq N/2$ giving the system's net alignment $m = 2i$, and $1 \leq j \leq \Omega_0$ giving the specific microstate the system occupies for that net alignment.

Within a given row, non-zero elements of the matrix represent *system states*, while elements with $M_{i,j} = 0$, the novel feature of this model, represent *bath states* and will be discussed momentarily. So, the number of non-zero elements in a row is equal to the number of possible realizations (microstates) of that alignment (macrostate). That is, the number of non-zero elements in a row is given by the system's multiplicity Ω_m, equation 3.1. The values of the elements determine transitions of the system.

Specifically, a value of $M_{i,j} = +1$ means an increase in the alignment and a move to the next row up, whereas a value of $M_{i,j} = -1$ means a decrease in the alignment and a move to the next row down. The ratio of elements having $M_{i,j} = +1$ and -1 is such that, if bath states with $M_{i,j} = 0$ are bypassed, all microstates are equally likely and the alignment will undergo Gaussian fluctuations. That is, there are

$$\Omega_m^+ = \Omega_m \times \left[\frac{1}{2}\frac{N-m}{N}\right] = \frac{[N-1]!}{\left[\frac{1}{2}(N+m)\right]!\left[\frac{1}{2}(N-m)-1\right]!} \tag{3.2}$$

elements having $M_{i,j} = +1$, and

$$\Omega_m^- = \Omega_m \times \left[\frac{1}{2}\frac{N+m}{N}\right] = \frac{[N-1]!}{\left[\frac{1}{2}(N+m)-1\right]!\left[\frac{1}{2}(N-m)\right]!} \tag{3.3}$$

elements having $M_{i,j} = -1$. For example, the central row of $\mathbf{M}$ corresponds to zero net alignment, $m = 2i = 0$. The number of non-zero elements is Ω_0, corresponding to the number of possible configurations that give zero net alignment. $\Omega_0/2$ of these elements are $M_{0,j} = +1$ and increase the net alignment, while the remaining $\Omega_0/2$ elements are $M_{0,j} = -1$ and decrease the net alignment.

For alignments that are small compared to the number of spins, $m \ll N$, the multiplicity Ω_m can be approximated as a Gaussian. To show this, equation 3.1 for Ω_m is written as a function of the reduced alignment $\lambda \equiv m/N$:

$$\Omega_m = \frac{N!}{\left[\frac{N}{2}(1+\lambda)\right]!\left[\frac{N}{2}(1-\lambda)\right]!} \tag{3.4}$$

and its logarithm (the Boltzmann entropy) expanded using Stirling's approximation:

$$\begin{aligned}
\ln(\Omega_m) &\approx N\ln(N) - \frac{N}{2}(1+\lambda)\ln\left[\frac{N}{2}(1+\lambda)\right] - \frac{N}{2}(1-\lambda)\ln\left[\frac{N}{2}(1-\lambda)\right] \\
&= N\ln 2 - \frac{N}{2}(1+\lambda)\ln(1+\lambda) - \frac{N}{2}(1-\lambda)\ln(1-\lambda) \\
&= N\ln 2 - \frac{N}{2}(1+\lambda)\left(\lambda - \frac{\lambda^2}{2} + \frac{\lambda^3}{3} - ...\right) + \frac{N}{2}(1-\lambda)\left(\lambda + \frac{\lambda^2}{2} + \frac{\lambda^3}{3} + ...\right) \\
&= N\ln 2 - \frac{N}{2}\left(\lambda^2 + \frac{\lambda^4}{6} + ...\right) \\
&= N\ln 2 - \frac{1}{2}\frac{m^2}{N} - \mathcal{O}(m^4)
\end{aligned} \tag{3.5}$$

The first term of the last equality is recognized as the constant maximum entropy, corresponding to no knowledge of the state of the system ($\Omega_{all} = 2^N$). The next leading term is the approximate deviation from maximum entropy. It is quadratic, so that the multiplicity is Gaussian. Thus, according to the results of § 2, this system will exhibit $1/f$ fluctuations if equation 2.1 holds and the average time spent in each state is proportional to the inverse of the multiplicity, $\tau(m) \propto e^{m^2/2N}$. This condition is satisfied and $1/f$ noise accomplished through the addition of explicit *bath states*. By including the bath states explicitly, any concerns regarding the range of validity of the approximation $m \ll N$ used to show $\Omega_m \propto e^{-m^2/2N}$ are alleviated. This is important because, as has been discussed generally and will be seen for this model, a consequence of including bath states is that all macrostates are equally likely over long enough times.

The bath states are represented by the elements $M_{i,j} = 0$ in figure 3.1. For these elements, no transition is made and the system remains in its current macrostate with its current alignment while another transition is attempted. Inclusion of the bath states, then, has the effect of slowing transitions when the system is in a low-entropy, highly aligned state. The degree to which the dynamics is slowed depends

upon the number of bath states compared to the number of system states. Since inclusion of these states is meant to give the system plus bath a constant multiplicity Ω_0 for all alignments, the number of bath states for a system with alignment m is given by $\Omega_0 - \Omega_m$. So, the ratio of bath states to system states for a given alignment m of a system of N spins is

$$\frac{\Omega_0 - \Omega_m}{\Omega_m} = \frac{N-m}{N} \prod_{i=0}^{m/2} \frac{N/2+i}{N/2-i} - 1 \tag{3.6}$$

and the probability of a transition occuring when bath states are included is

$$\frac{\Omega_m}{\Omega_0} = \frac{N}{N-m} \prod_{i=0}^{m/2} \frac{N/2-i}{N/2+i} \tag{3.7}$$

The ratio of the *total* number of bath states to the *total* number of system states, using Stirling's formula, is found to be

$$\frac{\sum_{m=0}^{N}(\Omega_0 - \Omega_m)}{\sum_{m=0}^{N}(\Omega_m)} = \frac{2(N+1)}{\sqrt{2\pi N}} - 1 \tag{3.8}$$

This ratio grows slowly ($\sim \sqrt{N}$), with the number of bath states exceeding the number of system states for $N > 4$ spins. For the largest systems simulated here, $N = 24$, there are only about 3 times as many bath states as system states.

3.2 Simulation Details

To summarize the dynamics: simulations proceed by selecting an element of $\mathbf{M}$ at random from the row i corresponding to the current alignment $m = 2i$; the value of the chosen element then determines how the alignment changes. Specifically, for a time step dt, an element $M_{i,j}$ is chosen from the current row which determines the row in the next time step; if $M_{i,j} = 0$, no change is made, $i \to i$, and another transition is attempted from the same row; if $M_{i,j} = +1$, the number of the row is increased by one, $i \to i+1$; if $M_{i,j} = -1$, the number of the row is decreased

by one, $i \rightarrow i-1$. So, the alignment of the system evolves in time according to $m(t+dt) = m(t) + 2M_{i,j} = 2(i + M_{i,j})$, where $1 \leq j \leq \Omega_0$ is chosen at random at each time step.

To obtain spectra over many decades, data from simulations are collected in a manner similar to experiments by averaging the instantaneous value of alignment over a measurement time t_{av}. That is, time series are recorded of the average of $m(t)$ for averaging times separated by factors of 10, $t_{av} = 1, 10$, etc.. For the results presented here, averaging times up to $t_{av} = 10^6$ are employed, and simulations are run until 2^{17} data are collected; simulations are therefore run for as long as 1.31×10^{11} steps. Multiple simulations (~ 20) are then averaged together to obtain the values presented. To compare different sized systems, the alignment is normalized by the number of spins N to give the relative alignment $\lambda(t) = m(t)/N$.

3.3 Results and Discussion

In figure 3.2 are histograms of the relative alignment λ from simulations of $N = 24$ spins with (solid symbols) and without (open symbols) bath states. Different colors/shapes are for histograms of time series with different averaging times $t_{av} = 1,\ 10, ...,\ 10^6$. Histograms are presented on a semi-logarithmic plot, giving the Boltzmann entropy as a function of alignment for $t_{av} = 1$. Illustrating this, the black dashed curve shows the binomial distribution for $N = 24$ and, as expected, it is matched precisely by the histogram of instantaneous ($t_{av} = 1$) alignment for simulations without bath states (open squares). As t_{av} is increased, the number of possible values for alignment increases dramatically (for $t_{av} = 1$ there are, of course, only $N + 1 = 25$ possible alignments) and histograms become continuous Gaussians. The histograms become increasingly narrow, approaching a delta function for very large t_{av}. Specifically, a Gaussian fit, $\ln(\Omega) \propto \lambda^2/2\sigma^2$, to the peak of the histograms pro-

duces a variance or width that decreases as the inverse of averaging time, $\sigma^2 \propto 1/t_{av}$, giving a $\sigma^2 \approx 9.5 \times 10^{-7}$ for $t_{av} = 10^6$. Simulations without bath states therefore produce Gaussian fluctuations as expected. The inclusion of bath states produces markedly different fluctuations. The histogram of instantaneous ($t_{av} = 1$) alignment is flat, meaning that the Boltzmann entropy is constant. As averaging time t_{av} is increased, this flat distribution becomes a Gaussian for alignments close to zero, but with substantial excess wings for larger alignments. Fitting the central peak of the histogram for $t_{av} = 10^6$ to a Gaussian gives a variance $\sigma^2 \approx 7.7 \times 10^{-3}$. The heavy tails of these histograms themselves suggest the presence of slow fluctuations and $1/f$ noise, as discussed in § 1.3.1.

These two very different behaviors can be analyzed and compared in terms of their thermodynamic reversibility using a very general relationship: Crooks' fluctuation theorem [37]. Crooks' fluctuation theorem states that for a system with microscopically reversible dynamics, regardless of how far from equilibrium it may be, the ratio of the probabilities of a trajectory in time and the time-reversal of that trajectory depend exponentially on the entropy production of the forward trajectory:

$$\frac{P[\lambda_+(t)]}{P[\lambda_-(t)]} = e^{\varsigma[\lambda(t)]} \tag{3.9}$$

Where $P[\lambda_+(t)]$ denotes the probability of some trajectory $\lambda_+(t)$, $P[\lambda_-(t)]$ denotes the probability of the time-reversal $\lambda_-(t)$ of that trajectory, and $\varsigma[\lambda(t)]$ is the entropy production of the forward trajectory. From this, it can be seen that a process which increases the entropy is exponentially more likely than its reverse. Conversely, for a reversible process where the entropy remains constant, the ratio of probabilities of the forward and reverse process is exactly 1 [60]. Typically, entropy production appears as $\varsigma[\lambda(t)] = -\beta\Delta F + \beta W$ [4], where ΔF is the difference in free energy between the initial and final states of the system in the forward trajectory and W is the work done

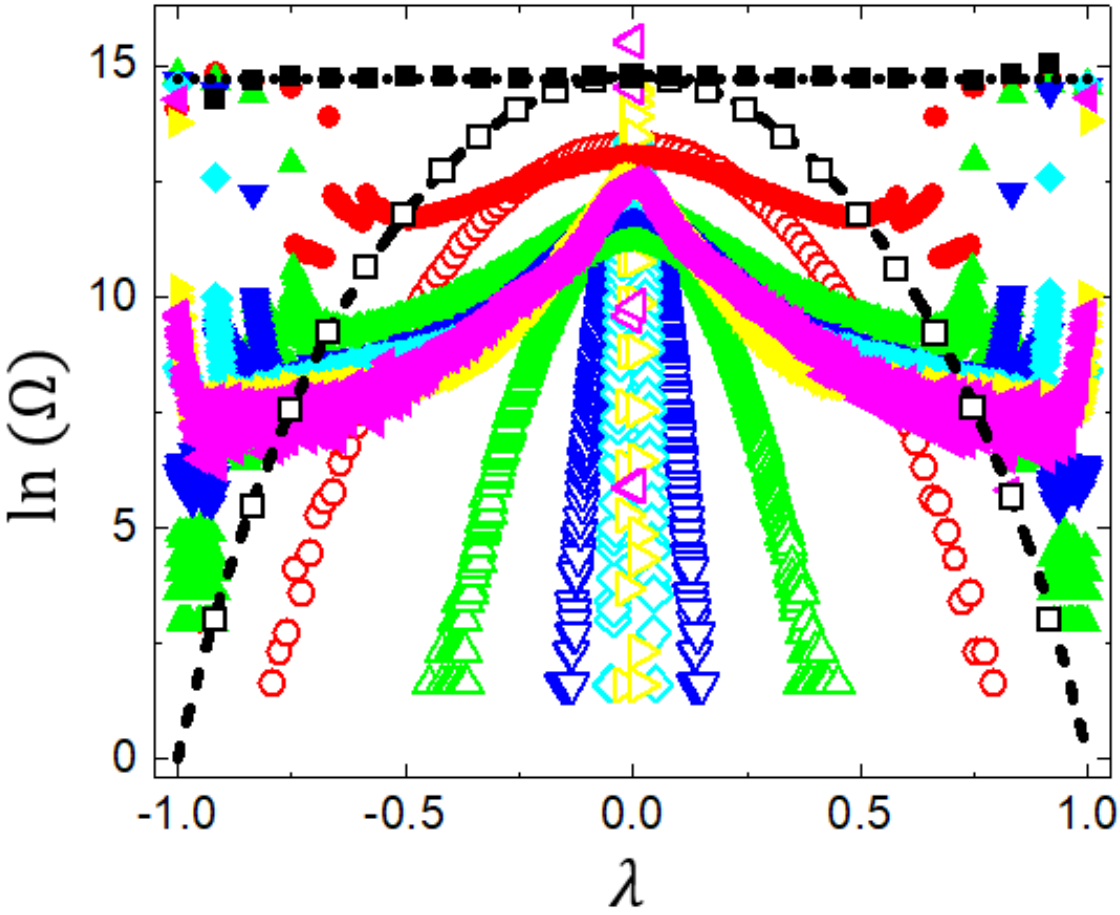

Figure 3.2: Histograms of the relative alignment for an $N = 24$ spin system, presented on a semi-logarithmic plot so that the vertical axis is proportional to the Boltzmann entropy ($\ln(\Omega)$). Different symbol shapes/colors correspond to different averaging times, from $t_{av} = 1$ to 10^6 simulation steps. Open symbols are from simulations without explicit bath states; fluctuations are clearly Gaussian and histograms narrow as t_{av} is increased. Closed symbols are from simulations with bath states; fluctuations are non-Gaussian and large values of alignment remain probable even for very large averaging times t_{av}. The heavy tails of these histograms suggest the presence of slow fluctuations and $1/f$ noise (see § 1.3.1).

on the system. In the model, however, there are no interactions between spins and no external field, so that all states are degenerate and the configurational entropy alone, easily calculated from binomial distribution, equation 3.1, determines the probability and entropy production of fluctuations.

First consider fluctuations of the system without bath states, shown in figure 3.2 as the open symbols. Consider a forward transition as one where a single spin is flipped from down to up so that $i \to i+1$ and $m \to m+2$. The reverse is of course a transition where $i+1 \to i$ and $m+2 \to m$. The probability of the forward transition is given by the ratio of system states in the row $i = m/2$ with $M_{i,j} = +1$ to total system states in the row. From equation 3.2, this probability is

$$P[m \to m+2] = \frac{1}{2}\frac{N-m}{N} \tag{3.10}$$

Similarly, for the reverse transition, the probability is given by the ratio of system states in the row $i = m/2+1$ with $M_{i,j} = -1$ to total system states in the same row. From equation 3.3,

$$P[m+2 \to m] = \frac{1}{2}\frac{N+m+2}{N} \tag{3.11}$$

And their ratio is

$$R_S = \frac{P[m \to m+2]}{P[m+2 \to m]} = \frac{N-m}{N+m+2} \tag{3.12}$$

According to Crooks' fluctuation theorem, this ratio should be equal to the exponential of the entropy production of the process. Since the system is degenerate, the entropy production is easily found from the binomial coefficient giving the configurational entropy, equation 3.1, confirming that fluctuations of the model without bath

states satisfy the Crooks' fluctuation theorem:

$$\begin{aligned} e^{\varsigma[m\to m+2]} &= e^{(\mathcal{S}_{m+2}-\mathcal{S}_m)/k_B} \\ &= \frac{\Omega_{m+2}}{\Omega_m} \\ &= \frac{N-m}{N+m+2} \end{aligned} \tag{3.13}$$

As noted, $R_S \neq 1$ means that irreversible work must be done on the system to effect this transition.

Consider next the fluctuations of the system when coupled to a finite bath with which it shares a constant entropy. The effect of this coupling is that highly aligned (low entropy) states persist for longer, *i.e.* transitions are suppressed for states with alignment m by a factor of Ω_m/Ω_0. For the same forward transition considered above ($m \to m+2$), this is given by equation 3.7:

$$\frac{\Omega_m}{\Omega_0} = \frac{N}{N-m}\prod_{i=0}^{m/2}\frac{N/2-i}{N/2+i} \tag{3.14}$$

And for the reverse transition, the probability is reduced by a factor

$$\begin{aligned} \frac{\Omega_{m+2}}{\Omega_0} &= \frac{N}{N-m-2}\prod_{i=0}^{m/2+1}\frac{N/2-i}{N/2+i} \\ &= \frac{N}{N-m-2}\times\frac{N/2-m/2-1}{N/2+m/2+1}\prod_{i=0}^{m/2}\frac{N/2-i}{N/2+i} \\ &= \frac{N-m}{N+m+2}\times\frac{\Omega_m}{\Omega_0} \end{aligned} \tag{3.15}$$

So, compared to the ratio of probabilities of the forward and reverse transitions *without* bath states R_S, equation 3.12, the new ratio is

$$R_{S+B} = \frac{\Omega_m}{\Omega_{m+2}}\times R_S = 1 \tag{3.16}$$

So, the ratio of probabilities of forward and reverse transitions is $R_{S+B} = 1$, implying that, when the system is coupled to a finite bath with which it shares a constant

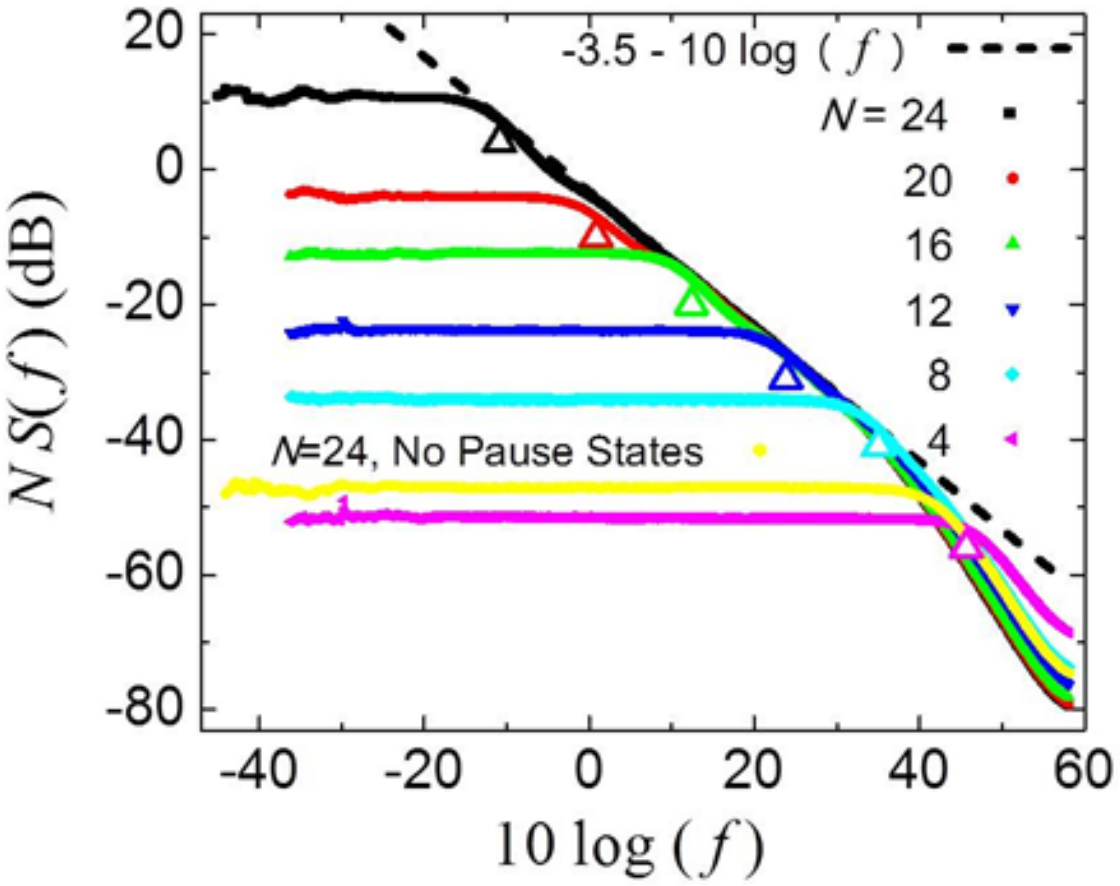

Figure 3.3: Power spectral densities of fluctuations of the relative alignment as a function of frequency from simulations of different sized (N) systems. $S_\lambda(f)$ has been normalized with a factor of N to compare spectra from different sized systems and $\log(f)$ is multiplied by 10 to put it on a decibel scale. A spectrum for a single N is composed of individual spectra from time series with 6 different averaging times from $t_{av} = 1$ to 10^6 steps. The black diagonal line shows perfect $1/f$ noise. Open triangle symbols mark the lowest frequency to exhibit $1/f$ noise, given by $10\log(f) = 53.5 - 10\log(\Omega_0)$. The yellow solid line show the power spectral density for an $N = 24$ spin system without bath states.

amount of entropy, fluctuations are slow and reversible [60]. Crooks' fluctuation theorem therefore reinforces the original demand that entropy of the system plus bath remains constant during fluctuations.

In figure 3.3 are shown power spectral densities $S_\lambda(f)$ of the relative alignment $\lambda(t)$ from 6 different system sizes $N \leq 24$. Time series of the relative alignment are

Fourier transformed and squared to find the power spectral density:

$$S_\lambda(f) = \left| \frac{1}{t_m} \sum_{t=0}^{t_m-1} \lambda(t) e^{-2\pi i f t/t_m} \right|^2 \tag{3.17}$$

Spectra are smoothed by dividing them into octaves and creating a linear least-squares fit to data contained in that octave; the value of the smoothed spectral density at the center frequency of the octave is taken to be the value of the fit at that frequency. Spectra are created for the time series of different averaging times t_{av} and these are merged together. Since each of these spectra extends over $\log_{10}(t_m) \approx 5$ decades and spectra from different averaging times are only separated by a decade, there is significant overlap of spectra from different averaging times. So, spectra with different averaging times t_{av} are merged using an average that is weighted more heavily at the center of the spectrum, where its value is less noisy.

The black dashed line in figure 3.3 shows perfect $1/f$ behavior. Without bath states, $1/f$ noise is not observed, as seen in a system of size $N = 24$ (solid yellow line). Instead, the spectrum is white for low frequencies, transitioning to a Lorentzian-like tail at the highest frequencies. Including bath states, the largest system $N = 24$ (solid black line) exhibits $1/f$ noise over approximately 4 decades in frequency f before transitioning to white noise at low frequencies. Looking at smaller systems, the range over which $1/f$ noise is observed is found to decrease with decreasing system size N. This low frequency roll-off to white noise marks the lowest frequency mode of the system and occurs when the system has had sufficient time to explore all possible macrostates. As such, it is expected that this frequency will be inversely related to the longest time scale of the system, which is the time it takes to undergo a transition in its fully aligned state, or the inverse of the probability of making a transition when fully aligned. Therefore, it is expected that the low frequency limit f_0 of the $1/f$ range to be related to system size as $f_0 \propto \Omega_N/\Omega_0 = 1/\Omega_0 = [(N/2)!]^2/N!$. This is

demonstrated by the open triangles in figure 3.3, the location of which are given by $10\log(f) = 53.5 - 10\log(\Omega_0)$. The value of 53.5 is an adjustable parameter. Since f_0 depends approximately upon the exponential of the square of the number of spins N, the range over which $1/f$ noise is observed grows very quickly with increasing system size. It should be pointed out that additional bath states ($M_{i,j} = 0$) can be added as extra columns of zero elements to the matrix $\mathbf{M}$. As might be expected, this has the effect of slowing the dynamics for all alignments by the same amount and shifts the range over which $1/f$ noise is observed.

Figure 3.4 presents the power spectral density in another way; by multiplying $S_\lambda(f)$ by frequency f, $1/f$ noise becomes constant (dashed horizontal line in the figure), allowing spectral features to be more easily resolved. Of the six spectra presented in figure 3.3, two are presented in figure 3.4, for $N = 16$ (solid green line) and $N = 24$ (solid black line) spins, showing $1/f$ noise over two and four decades of frequency, respectively. As in figure 3.3, the open triangles mark the lowest frequency mode $f_0 \propto 1/\Omega_0$ of the model. In fact, the value of 53.5 was found from the low frequency peak in $f \times S_\lambda(f)$.

Difficult to discern in figure 3.3, but clear in figure 3.4, particularly in the $N = 24$ system, are additional spectral features. These arise from higher frequency modes corresponding to less aligned states of the system. These transition frequencies of the different alignments of the system are proportional to the probability of a transition, given by equation 3.7. Specifically, they are marked by the open diamond symbols which are located at frequencies $f_1 \propto \Omega_{N-2}/\Omega_0 = f_0 \times N$, $f_2 \propto \Omega_{N-4}/\Omega_0 = f_0 \times N(N-1)/2$, $f_3 \propto \Omega_{N-6}/\Omega_0 = f_0 \times N(N-1)(N-2)/6$, etc..

$1/f$ noise in this system is an example of how a single fluctuator with a multiplicity-dependent, and therefore time-dependent, transition frequency can lead to $1/f$ noise, just as a superposition of fluctuators with the proper distribution of time-independent

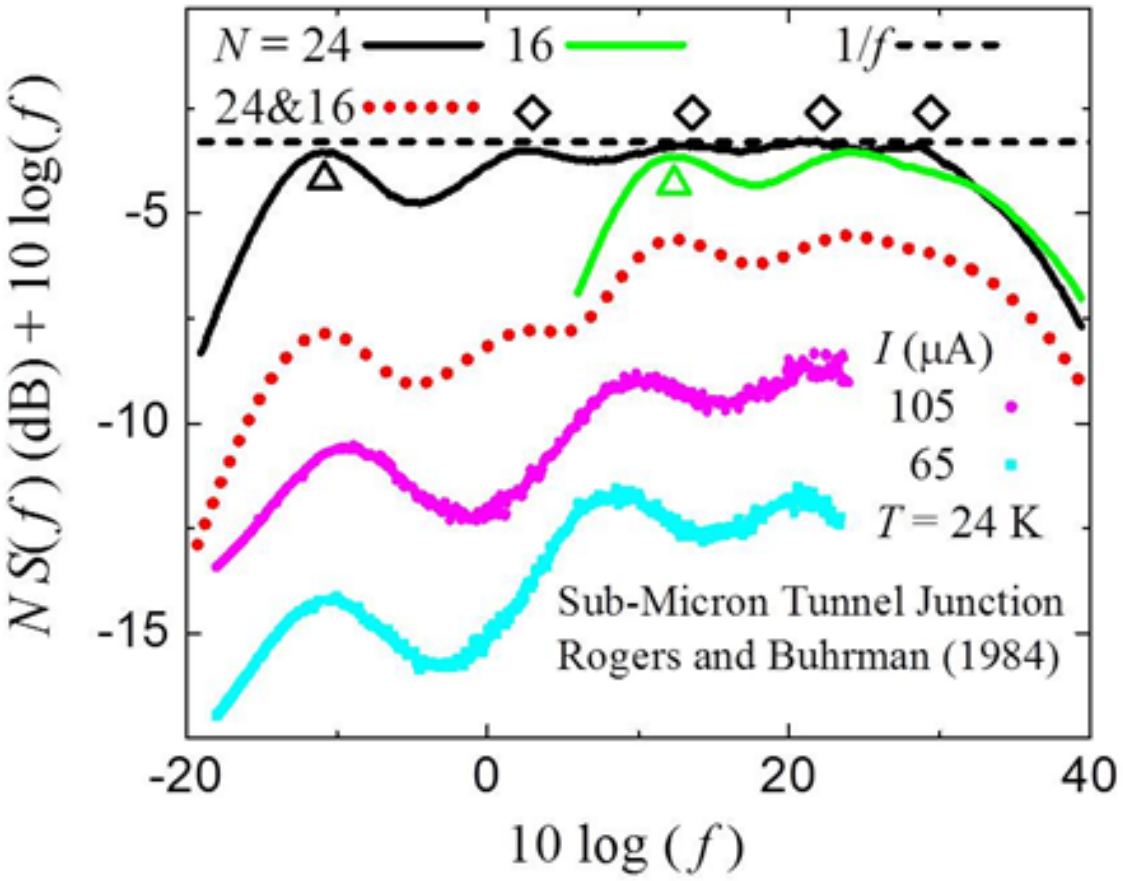

Figure 3.4: Plot of the power spectral density of fluctuations of alignment multiplied by frequency, $f \times S_\lambda(f)$, as a function of frequency f. $1/f$ behavior is now given by the horizontal dashed line (the same line as in figure 3.3). Data from simulations of an $N = 24$ spin system (solid black line) and an $N = 16$ spin system (solid green line) are shown. As in figure 3.3, open triangles depict the lowest frequency mode of the system, $f_0 \propto \Omega_N/\Omega_0 = [(N/2)!]^2/N!$. Compared to figure 3.3, multiplying $S_\lambda(f)$ by f reveals additional spectral features. These are marked by open diamonds and correspond to the transition frequency for different alignments of the system given by $f_i \propto \Omega^-_{N-2i}/\Omega_0$. The red dotted line is from a composition of $S_\lambda(f)$ for an $N = 24$ spin system and $10\times$ that of an $N = 16$ spin system, with the amplitude offset for clarity. Symbols show measurements of the voltage across a metal-insulator-metal tunnel junction for two different values of current, with amplitude and frequency offset for clarity [108].

transition frequencies can. Furthermore, as demonstrated in figure 3.4, when the possible values of the time-dependent transition frequency are discrete (corresponding here to the discrete alignments of the system), spectral features can arise, as they do for a superposition of time-independent Lorentzian spectra when a system is small enough that only a few fluctuators contribute to the observed spectrum [108, 110, 136, 92]. Of course, it is possible, even expected, that a physical system could be composed of a number of fluctuators, each coupled to their own finite bath. In such a case, both the state-dependence of each individual fluctuator's transition frequency *and* the superposition of the many fluctuators will contribute to the observed spectrum.

The first observation of features in a $1/f$ spectrum that could be tied to individual Lorentzians was reported in 1984 by C.T. Rogers and R.A. Buhrman [108]. Under investigation were voltage fluctuations of metal-insulator-metal (MIM) tunnel junctions biased with dc currents of 65 μA and 105 μA at low temperatures $T \lessapprox 80K$. These spectra are included in figure 3.4, given by the cyan ($I_b = 65\ \mu A$) and magenta ($I_b = 105\ \mu A$) symbols. Critically, they studied junctions that were small enough, with cross sectional areas of $5 \times 10^{-10}\ cm^2 < A < 10^{-8}\ cm^2$, that only a few fluctuators contributed to the the low-frequency voltage fluctuations and spectra were able to be accurately fit to a small (< 5) number of Lorentzians. Rogers and Buhrman attributed their observations to fluctuations in the conductance due to capture and release of electrons in the insulator by Arrhenius-like traps, $\tau = \tau_0 e^{-E/k_B T}$, with a broad distribution of activation energies E. This is similar to the theory developed by Dutta, Dimon, and Horn [42], using the popular two-level system formalism [3] (see § 1.4.1). Unlike Dutta, Dimon, and Horn, who used a constant attempt rate $1/\tau_0$, Rogers and Buhrman found it necessary to use at least two attempt rates for each fluctuator, corresponding to different probabilities of the capture and release of

electrons, as well as a broad distribution of attempt rates over all fluctuators. The conclusion of Rogers and Buhrman is that both the attempt rates of each fluctuator and the activation energy are distributed, leading to the observed $1/f$ spectral density.

Attempt rates in the matrix model depend upon the system state (alignment) and as a consequence distribute themselves in time in such a way as to produce $1/f$ noise. It is important to note that a $1/f$ spectrum arises naturally, without imposing or assuming an *ad hoc* distribution of time scales. In addition to the general shape, this leads to the features seen in the spectra of the $N = 24$ (solid black line) and $N = 16$ (solid green line) spin systems in figure 3.4. Furthermore, while the model does not contain any activation energies (all states are degenerate), the shape of the spectrum is determined exponentially by the size N of the system. So, the spectrum of fluctuations in net alignment of an ensemble of individual systems is expected to exhibit spectral features arising from the distribution of system sizes as well as the distribution of attempt rates. So, similar to the conclusions of Rogers and Buhrman, the model has (1) more than a single attempt rate for individual fluctuators and (2) fluctuators with different characteristic frequencies (though based on system size and not activation energy). So, with a view towards recreating some of the quailitative features of the spectra reported by Rogers and Buhrman (cyan and magenta symbols in figure 3.4), presented in figure 3.4 is also a spectrum (red dotted line) composed from the $N = 24$ spin system and $10\times$ that of the $N = 16$ spin system. Since the matrix model has no interactions, the spectrum of two systems is equivalent to the sum of their individual spectra.

Rogers and Buhrman found that a single attempt rate was not sufficient to explain the spectra they observed in their experiments. Instead, they surmised that a two-state system with two different switching rates was necessary. The two rates different

rates they attributed to the rates for the capture and the release of electrons to be different. The theory of two-rate kinetics for a simple two-state system, known as *two-state random telegraph noise*, was developed by S. Machlup [79]. Machlup framed this problem as a discrete Markov process with two possible states. Of course, a discrete Markov process can have any number of states. Since this model undergoes transitions to states which only depend upon the previous state, its dynamics is Markovian and the model can be recast as a discrete multi-state Markov process. The power spectral densities of systems of various size N will be calculated and compared to the simulated results of this section.

3.3.1 Matrix Model as a Discrete Markov Chain

To rescast this model as a discrete Markov process, the transitions and the time evolution of this system are expressed as a left stochastic matrix $\mathbf{P}$ acting on a column vector $\boldsymbol{\pi}$ of state occupancy probabilities. That is to say, π_i, the i^{th} element of the vector $\boldsymbol{\pi}$ (where $1 \leq i \leq 2N+1$), is the probability that the system has alignment $m = 2(i-1) - N$. The state occupancy probabilities $\boldsymbol{\pi}$ at time step t are found from their values one time step previous

$$\boldsymbol{\pi}(t) = \mathbf{P}\boldsymbol{\pi}(t-1) \tag{3.18}$$

The diagonal elements $P_{i,i}$ of this transition matrix are interpreted as being the probability of the system remaining in its current state (bath states). Off-diagonal elements $P_{i,j}$ represent the probability of transitions from state i to j (system states). The sum of elements of any given column is therefore 1. From equation 3.1, 3.2, and 3.3 the

matrix $\mathbf{P}$ has elements given by

$$P_{i,j} = \begin{cases} 1 - \dfrac{\Omega_m}{\Omega_0} & i = j \\ \dfrac{\Omega_m}{\Omega_0}\dfrac{N+m}{2N} & i = j-1 \\ \dfrac{\Omega_m}{\Omega_0}\dfrac{N-m}{2N} & i = j+1 \\ 0 & |i-j| > 0 \end{cases} \tag{3.19}$$

or, as a single term, by

$$\begin{aligned} P_{i,j} &= \left(1 - \frac{\Omega_m}{\Omega_0}\right)\delta_{i,j} + \frac{\Omega_m}{\Omega_0}\frac{N+m}{2N}\delta_{i,j-1} + \frac{\Omega_m}{\Omega_0}\frac{N-m}{2N}\delta_{i,j+1} \\ &= \delta_{i,j} - \frac{\Omega_m}{\Omega_0}\left[\delta_{i,j} - \delta_{i,j+1} - \frac{j-1}{N}(\delta_{i,j-1} - \delta_{i,j+1})\right] \end{aligned} \tag{3.20}$$

where $\delta_{i,j}$ is the Kronecker delta. Presented as a matrix, $\mathbf{P} =$

$$\begin{bmatrix} 1-\frac{1}{\Omega_0} & \frac{1}{N}\frac{\Omega_{N-2}}{\Omega_0} & 0 & \cdots & 0 & 0 & 0 & \cdots & 0 & 0 \\ \frac{1}{\Omega_0} & 1-\frac{\Omega_{N-2}}{\Omega_0} & \frac{2}{N}\frac{\Omega_{N-4}}{\Omega_0} & \cdots & 0 & 0 & 0 & \cdots & 0 & 0 \\ 0 & \frac{N-1}{N}\frac{\Omega_{N-2}}{\Omega_0} & 1-\frac{\Omega_{N-4}}{\Omega_0} & \cdots & 0 & 0 & 0 & \cdots & 0 & 0 \\ \vdots & \vdots & \vdots & \ddots & \vdots & \vdots & \vdots & \cdots & 0 & 0 \\ 0 & 0 & 0 & \cdots & 1-\frac{\Omega_{m-2}}{\Omega_0} & \frac{\Omega_m}{\Omega_0}\frac{N+m}{2N} & 0 & \cdots & 0 & 0 \\ 0 & 0 & 0 & \cdots & \frac{\Omega_{m-2}}{\Omega_0}\frac{N-m+2}{2N} & 1-\frac{\Omega_m}{\Omega_0} & \frac{\Omega_{m+2}}{\Omega_0}\frac{N+m+2}{2N} & \cdots & 0 & 0 \\ 0 & 0 & 0 & \cdots & 0 & \frac{\Omega_m}{\Omega_0}\frac{N-m}{2N} & 1-\frac{\Omega_{m+2}}{\Omega_0} & \cdots & 0 & 0 \\ \vdots & \vdots & \vdots & \vdots & \vdots & \vdots & \vdots & \ddots & \vdots & \vdots \\ 0 & 0 & 0 & 0 & 0 & 0 & 0 & \cdots & 1-\frac{\Omega_{N-2}}{\Omega_0} & \frac{1}{\Omega_0} \\ 0 & 0 & 0 & 0 & 0 & 0 & 0 & \cdots & \frac{1}{N}\frac{\Omega_{N-2}}{\Omega_0} & 1-\frac{1}{\Omega_0} \end{bmatrix}$$

Knowing the time-evolution of the state occupancy probabilities can provide an alternative way to find the spectral density of fluctuations other than through simulations. From equation 3.18, the occupancy probabilities after an arbitrary number of time steps t from an initial state $\boldsymbol{\pi}^{(0)}$ are

$$\boldsymbol{\pi}(t) = \mathbf{P}\boldsymbol{\pi}(t-1) = \mathbf{P}^2\boldsymbol{\pi}(t-2)... = \mathbf{P}^t\boldsymbol{\pi}(0) \tag{3.21}$$

The autocorrelation function of the relative alignment λ as a function of time t is

$$\xi_\lambda(t) = \frac{1}{N}\sum_i^{2N+1} \boldsymbol{\pi}_i\mathbf{P}^t\boldsymbol{\pi}_i \tag{3.22}$$

where $\boldsymbol{\pi}_i$ is the initial probability vector corresponding to the system being in state $i = m/2$. The power spectral density is found via the Wiener-Khinchin theorem

$$S_\lambda(f) = \frac{2}{N} \sum_{t=-\infty}^{\infty} \sum_{i}^{2N+1} \boldsymbol{\pi}_i \mathbf{P}^t \boldsymbol{\pi}_i e^{i\omega t} \tag{3.23}$$

Given the simplicity of the two state model, evaluating this by brute force was the method was employed by S. Machlup to find the spectrum of two-state random telegraph noise [79].

Another strategy allows a clearer interpretation of the power spectral density as a sum of autoregressive relaxation processes with the proper distribution of relaxation times and strengths of fluctuations. $\mathbf{P}$ can be reduced and equation 3.18 rewritten to show how the state occupancy probabilities evolve *per unit time*:

$$\begin{aligned} &\boldsymbol{\pi}(t) = \mathbf{P}\boldsymbol{\pi}(t-1) \\ &\rightarrow \frac{\boldsymbol{\pi}(t) - \boldsymbol{\pi}(t-1)}{\Delta t} = (\mathbf{P} - \mathbf{I})\boldsymbol{\pi}(t) \\ &\rightarrow \frac{d}{dt}\boldsymbol{\pi}(t) = \mathbf{Q}\boldsymbol{\pi}(t) \end{aligned} \tag{3.24}$$

where $\mathbf{I}$ is the identity matrix and the nondiagonal elements of $\mathbf{Q} \equiv \mathbf{P} - \mathbf{I}$ are transition rates from state i to j per unit time. The last of equation 3.24 are known as the *Kolmogorov equations* for a discrete Markov process. The state occupancy probabilities have the solution

$$\boldsymbol{\pi}(t) = e^{\mathbf{Q}t}\boldsymbol{\pi}(0) \tag{3.25}$$

where the exponential of $\mathbf{Q}$ is defined through the power series

$$e^{\mathbf{Q}} = \sum_{k=0}^{\infty} \frac{\mathbf{Q}^k}{k!} = \mathbf{I} + \mathbf{Q} + \frac{1}{2}\mathbf{Q}^2 + ... \tag{3.26}$$

For individual states (π_i, the components of $\boldsymbol{\pi}$) the solutions are exponentials of the form $e^{-t/\tau}$

$$\pi_i(t) = \pi_i(0)e^{-t/\tau_i} \tag{3.27}$$

where the relaxation rates τ_i^{-1} are the eigenvalues of $\mathbf{Q}$, the roots of the equation

$$\det|\mathbf{Q} - \tau^{-1} \times \mathbf{I}| = 0 \tag{3.28}$$

If a variable m (with $\langle m \rangle = 0$) in the state i has the value m_i, the autocorrelation function (defined only for $t > 0$) is found from equation 1.8:

$$\begin{aligned}
\xi_m(|t_1 - t_2|) &= \langle \delta m_i(t_1) \delta m_i(t_2) \rangle \\
&= \sum_i m_i^2 w(m_i, t_1; m_i, t_2) \\
&= \sum_i m_i^2 \pi_i(|t_1 - t_2|) \\
&= \sum_i m_i^2 \pi_i(t_1) e^{-|t_1 - t_2|/\tau_i} \\
\rightarrow \xi_m(t) &= \sum_i m_i^2 \pi_i(0) e^{-t/\tau_i}
\end{aligned} \tag{3.29}$$

where $w(m_i, t)$ is the probability density function giving the probability of m having the value of m_i at time t and $w(m_i, t_1; m_i, t_2)$ is the two-dimensional probability density function giving the probability of m having the value of m_i at time t_1 *and* t_2. In the third equality of equation 3.29, $\pi_i(|t_1 - t_2|)$ is recognized as being equivalent to $w(m_i, t_1; m_i, t_2)$. Further recognizing that $\pi_i(t_1)$ is the one-dimensional probability distribution function $w(m_i, t_1)$ giving the probability that $m = m_i$ at time t_1, it becomes clear that $e^{-|t_1 - t_2|/\tau_i}$ is the joint conditional probability that $m = m_i$ at time $t = t_2$ given that $m = m_i$ at time $t = t_1$ [65].

The power spectral density is found from equation 3.29 via the Wiener-Khinchin

theorem, equation 1.18:

$$\begin{aligned} S_m(f) &= 2\widetilde{\xi}_m(\omega) \\ &= 2\int_{-\infty}^{\infty}\left[\sum_i m_i^2\pi_i(0)e^{-t/\tau_i}\right]e^{i\omega t}dt \\ &= 4\sum_i m_i^2\pi_i(0)\left[\int_{-\infty}^{\infty}e^{-t/\tau_i}\cos(\omega t)dt\right] \\ &= \sum_i m_i^2\pi_i(0)\frac{4\tau_i}{1+\omega^2\tau_i^2} \end{aligned} \tag{3.30}$$

This can be used to find the power spectral density of the matrix model. First, relaxation times τ_i must be found using equation 3.28. Using the fact that the system is symmetric about $m = 0$, the stochastic matrix $\mathbf{P}$ can be recast as an $(N/2+1) \times (N/2+1)$ matrix, and reduced by the identity matrix $\mathbf{I}$ to give $\mathbf{Q} =$

$$\begin{bmatrix}
-\frac{1}{\Omega_0} & \frac{1}{N}\frac{\Omega_{N-2}}{\Omega_0} & 0 & \cdots & 0 & 0 & 0 & \cdots & 0 & 0 \\
\frac{1}{\Omega_0} & -\frac{\Omega_{N-2}}{\Omega_0} & \frac{2}{N}\frac{\Omega_{N-4}}{\Omega_0} & \cdots & 0 & 0 & 0 & \cdots & 0 & 0 \\
0 & \frac{N-1}{N}\frac{\Omega_{N-2}}{\Omega_0} & -\frac{\Omega_{N-4}}{\Omega_0} & \cdots & 0 & 0 & 0 & \cdots & 0 & 0 \\
\vdots & \vdots & \vdots & \ddots & \vdots & \vdots & \vdots & \cdots & 0 & 0 \\
0 & 0 & 0 & \cdots & -\frac{\Omega_{m-2}}{\Omega_0} & \frac{\Omega_m}{\Omega_0}\frac{N+m}{2N} & 0 & \cdots & 0 & 0 \\
0 & 0 & 0 & \cdots & \frac{\Omega_{m-2}}{\Omega_0}\frac{N-m+2}{2N} & -\frac{\Omega_m}{\Omega_0} & \frac{\Omega_{m+2}}{\Omega_0}\frac{N+m+2}{2N} & \cdots & 0 & 0 \\
0 & 0 & 0 & \cdots & 0 & \frac{\Omega_m}{\Omega_0}\frac{N-m}{2N} & -\frac{\Omega_{m+2}}{\Omega_0} & \cdots & 0 & 0 \\
\vdots & \vdots & \vdots & \vdots & \vdots & \vdots & \vdots & \ddots & \vdots & \vdots \\
0 & 0 & 0 & 0 & 0 & 0 & 0 & \cdots & -\frac{\Omega_2}{\Omega_0} & 1 \\
0 & 0 & 0 & 0 & 0 & 0 & 0 & \cdots & \frac{N-2}{2N}\frac{\Omega_2}{\Omega_0} & 0
\end{bmatrix}$$

The eigenvalues of this matrix, found from the solutions to equation 3.28, are the relaxation times τ_i of the system. The strength of each fluctuation, *i.e.* the square of the net alignment, is $m_i^2 = (N-2i+2)^2$. Finally, since the presence of bath states makes all states equally likely, the initial condition is simply $\pi_i(0) = (N/2+1)^{-1}$.

The results of this strategy are shown in figure 3.5. These can be compared to the results of simulations seen in FIGs. 3.3 and 3.4. Discrepancies between this method and simulations are likely due to the fact that cross-correlations between states were not included in the calculation of the correlation functions in equation 3.29. Instead,

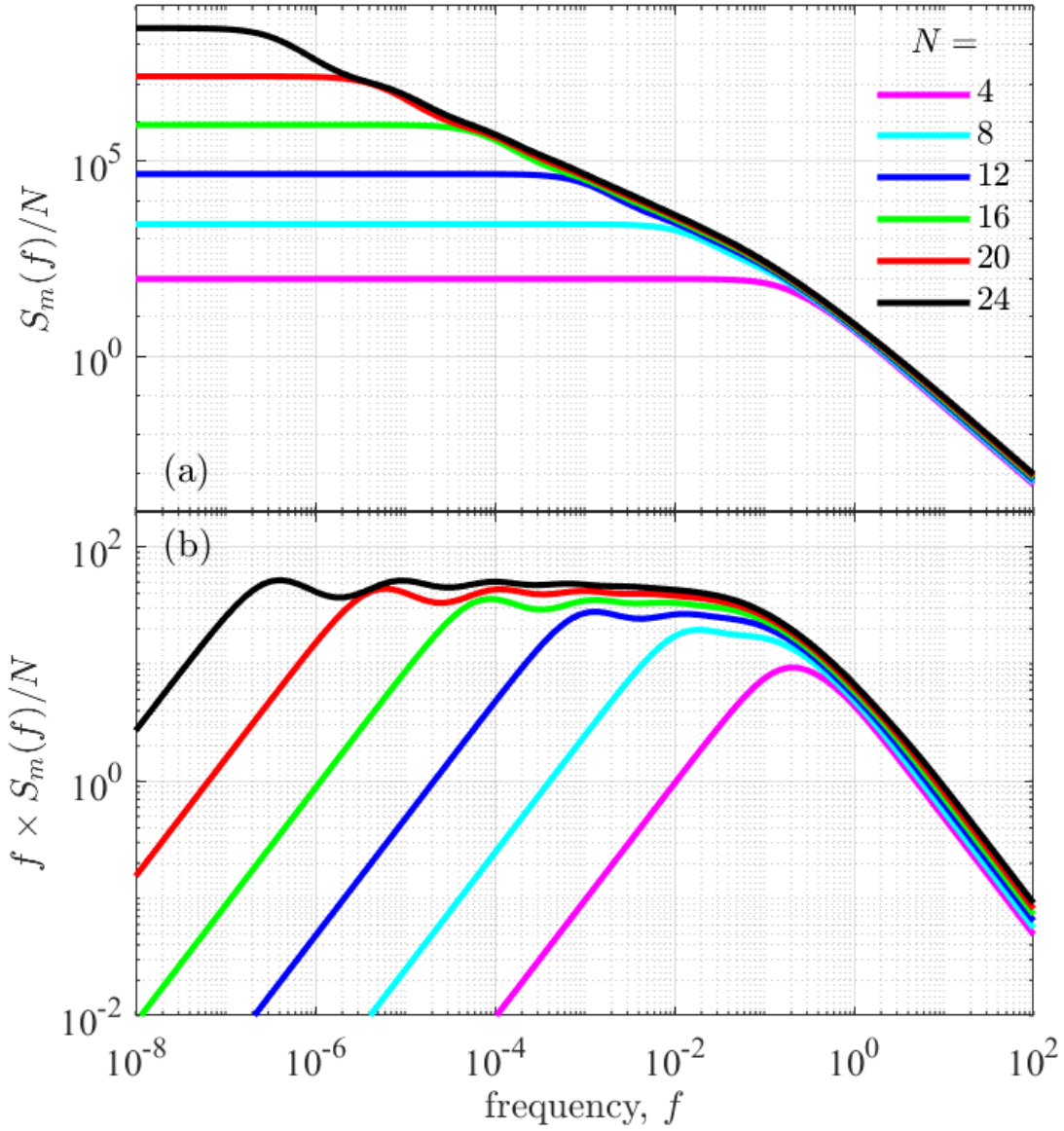

Figure 3.5: (a) Power spectral densities calculated from the stochastic matrix **Q** describing the time-evolution of the matrix model. This figure should be compared to figure 3.3. (b) The same spectra as in (a), multiplied by frequency, f. Spectral features, corresponding to the eigenvalues of **Q** are more visible. This figure should be compared to figure 3.4.

each state was taken to be an independent fluctuator with its own relaxation time. Of course, since the system only moves between adjacent states, there is a non-zero correlation between the different states. Regardless, the results presented in figure 3.5 capture the essential features of the power spectral density. Exact calculation of power spectral densities from the stochastic matrix, including cross-correlations between states, is a possible subject of future work.

3.4 Conclusions

This model, with dynamics governed by a simple matrix, has been shown to exhibit $1/f$ noise. The condition equation 2.1 is satisfied by the inclusion of explicit bath states, rendering the combined entropy of the system + bath constant during fluctuations. As shown in § 2, this is due to the Gaussian form of the system's multiplicity, equation 3.1, in terms of m. This model does not include interactions between spins, so that the multiplicity alone determines its dynamics. It is therefore a particularly revealing way to investigate multiplicity-dependent relaxation times.

With the insights gained from the matrix model, another model will be explored in the next section, based on dynamically constrained Heisenberg spins. Since this next model discussed is based on classical Heisenberg spins, continuous degrees of freedom are also introduced, a feature not seen in the matrix model. The constrained Heisenberg model will also include interactions, unlike the matrix model. In addition to constraining the Heisenberg model in a way that satisfies equation 2.1 and mimics the bath states of the matrix model, changes in the internal energy will be governed by Boltzmann's factor. The system will therefore exchange energy and entropy with a thermal reservoir, so that the entropy of the system + bath will not be constant for all time, but only approximately on the time scale of single events.

Chapter 4

$1/f$ NOISE FROM A HEISENBERG SPIN MODEL COUPLED TO A FINITE BATH

To further investigate the effects of multiplicity-dependent relaxation times, equation 2.1, a classical Heisenberg spin model is investigated. In this model, spin flips are constrained according to a spin's local configurational entropy. Unlike the previous model, a finite bath is included *implicitly* through a nonlinear dynamic constraint. In addition to this constraint, changes in the internal energy of the system, which includes spin-spin interactions, are governed by Boltzmann's factor. This is another departure from the matrix model of § 3, which did not include interactions. Since the system and its implicit local bath are coupled to a thermal reservoir, the entropy remains maximized between a system and its local bath *only on the time scale of microscopic events (single spin flips)*. Fluctuations in the alignment of this model will be compared to the $1/f$ flux noise observed in Josephson junctions, specifically in superconducting quantum interference devices (SQUIDs), reproducing the temperature dependence of noise power and spectral exponent α, as well as the relationship between α and the amplitude of the spectral density.

Much of the work presented in this chapter was published under the title "$1/f$ noise from a finite entropy bath: comparison with flux noise in SQUIDs" in *Journal of Statistical Mechanics: Theory and Experiment*. The complete citation is listed under reference [38]. The original publication was completed in collaboration with others and is included in appendix B.

4.1 Background: $1/f$ Flux Noise in SQUIDs

$1/f$ noise is present in the low-frequency fluctuations of most materials and devices, placing a limit on their functionality. As one example of concern for many modern devices, and as an example of the omnipresence of $1/f$ noise, there are at least two separate sources of $1/f$ noise in a Josephson junction. One source of noise is in the *critical current* of the Josephson junction [52]. Similar in origin to the $1/f$ noise described by McWhorter in the current through a semiconductor filament [87] or that found in the voltage across a metal-insulator-metal junction [108, 109], this noise is due to the capture and release of electrons in the tunnel barrier between superconductors having a distribution of capture/release times τ_c that varies as $1/\tau_c$. Models of this type and their application were explained in detail in § 1.4.1. However, since the amplitude of noise in the critical current linearly decreases with temperature, it is not a significant performance issue at the low temperatures where SQUIDs typically operate [100]. Instead, performance is usually limited by the second source of $1/f$ noise in a Josephson junction: *flux noise*. Discovered more than 35 years ago [64], it is this flux noise that is the primary contributor to noise in SQUIDs [138, 136] and a widely accepted explanation of its origin has yet to be found. Interest in this long-standing problem has been strengthened recently since flux noise is also the dominant cause of decoherence in flux [142, 58] and phase [11] qubits, limiting their practicality as the basic elements of quantum computers [35].

Models of $1/f$ flux noise typically involve unpaired spins residing at the superconductor-insulator interface of the Josephson junction. One of the earliest of these models assumed non-interacting spins and concluded the spins must have a surface density of $\approx 5\times10^{17}\ m^{-2}$ [64]. Measurements of paramagnetism at the superconductor-insulator interface confirmed this value [118]. However, these and further measurements showed

evidence of spins forming clusters, suggesting the presence of significant spin-spin interactions. Also observed was time-reversal symmetry breaking in the form of a correlation between surface magnetization and inductance, meaning that the spin-spin interactions are primarily ferromagnetic. Finally, correlation between the SQUID inductance and flux (related to one another through the fluctuation-dissipation relation) show that the fluctuations are non-linear, increasingly so at low temperatures [119].

Exhaustive measurements of the $1/f$ flux noise have been reported by Anton *et al.* in 10 separate dc SQUIDs [4] and by Kempf *et al.* in 84 SQUIDs and SQUID arrays [62]. For all devices, these measurements reveal not only a temperature dependence of the spectral exponent α and the overall amplitude of the flux noise, but also a consistent relationship between α and the amplitude themselves that causes the spectra of each device, measured at different temperatures, to pivot about a common crossing frequency f_c. Spectral pivoting of this kind can be expressed by the relationship

$$S_\Phi(f) = S_\Phi(f_c) \times (f_c/f)^\alpha \tag{4.1}$$

where Φ refers to the SQUID flux, and S_Φ is the spectral density of its fluctuations. Notice that this expression encodes a relationship between α and the amplitude that is independent of their individual dependences upon temperature. Taking into account that α decreases as the temperature is increased, the noise power increases for frequencies above the crossing frequency $f > f_c$, and decreases for frequencies below the crossing frequency $f < f_c$, as the temperature is increased.

Generally, unpaired spins arise on the surfaces of materials in a multitude of different ways, and a great many of these have been employed as the precise microsopic explanation of $1/f$ flux noise. These include: electronic and nuclear spins, as well as a combination of both [71]; oxygen molecules adsorbed on the superconductor surface

[134, 69]; electrons occupying localized gap states in the superconductor-insulator interface [32]; and paramagnetic dangling bonds coupling to two-level tunnelling systems in the semiconductor-oxide interface (Si/SiO_2) of some SQUIDs [123]. To describe the interaction between these unpaired spins, a number of mechanisms have been considered, including the Ruderman-Kittel-Kasuya-Yoshida (RKKY) interaction [45], dipole-dipole interactions [5], and hyperfine interactions [139]. To model $1/f$ flux noise phenomelogically, the most popular types of model are spin glasses, including disordered Ising [31, 39] and Heisenberg models [1, 5]. Models such as these have the drawback that their fluctuations are linear, showing no correlation between alignment (SQUID flux) and susceptibility (SQUID inductance), in contradiction to experiments. Furthermore, disordered spin glass models possessing an even distribution of antiferromagnetic and ferromagnetic interactions conflict with the time-reversal symmetry breaking observed at the superconductor-insulator interface [31, 119]. So, models with disorder, but a preference for ferromagnetic coupling, have been studied as well [134, 39]. As far as the spectral pivoting of equation 4.1 goes, models considered before the report of Anton *et al.* do not account for this observation. Since then, a model that modifies the RKKY interaction to produce spin diffusion with a diffusion coefficient that depends upon temperature, as well as spectral pivoting with a band of crossing frequencies, has been reported [72].

In spin glass models such as those described above, $1/f$ noise and the associated slow dynamics originate from a distribution of relaxation rates due to interaction strengths between spins with a distribution that does not change with time. While this distribution may be static in time and the interaction strengths constant, the *effective* distribution seen on short time-scales can change over longer time-scales. In the hierarchical kinetics picture of a spin glass, this occurs from the system exploring the space of possible configurations, with configurations separated by a wide distribution

of distances. In the droplet scaling picture of a spin glass, this is due to changes in spatial correlations, with the relaxation rate a droplet (or cluster) depending upon the droplet size [137].

Employed here is a Heisenberg spin model with a square lattice of spins with interactions that are not only static in time, but spatially homogeneous. The Hamiltonian therefore remains entirely homogeneous and heterogeneity instead comes from the condition equation 2.1 linking the characteristic time of spin flips to the net alignment of the clusters that contain them. The clusters distribute themselves naturally to produce $1/f$-type noise that is temperature dependent. Furthermore, since the distribution of net alignments of clusters changes with time, so does the distribution of characteristic times, yielding heterogeneity that is dynamic. Similarly, models involving a state-dependent relaxation rate have been used in models of aging and plastic flow [117, 125, 90]. Power spectral densities of this model's net alignment will be compared in § 4.4 to the $1/f$ flux noise found in SQUIDs, qualitatively reproducing the temperature dependence and the spectral pivoting of equation 4.1. Since SQUIDs operate at low temperatures, the spurious clusters of spins leading to flux noise may be non-ideally coupled to their thermal environment, leading to the condition equation 2.1 as described in § 2.2.1. Finally, imposing the condition equation 2.1 has the advantage that it links fluctuations in alignment to the magnitude of the net alignment, so that fluctuations are explicitly non-linear, similar to the flux noise of SQUIDs [119]. This model will also be contrasted with spin glass models used to recreate $1/f$ flux noise in SQUIDs.

4.2 Model: Heisenberg Spins and Nonlinear Constraint

Direct observations of magnetism at the superconductor-insulator of Josepshon junctions, including the observation of time-reversal symmetry breaking, suggest that

the $1/f$ flux noise observed in SQUIDs is due to clusters of unpaired, interacting spins [118, 119]. $1/f$ noise in general is often interpreted as being due to the superposition of fluctuators with relaxation times τ_c distributed as $p(\tau_c) \propto 1/\tau_c$. This would suggest that the relaxation times of clusters of spins at the superconductor-insulator interface are distributed in this manner. Considering the spectral pivoting expressed in equation 4.1 and observed in SQUIDs and SQUID arrays [4, 62], $p(\tau_c)$ must decrease for frequencies below the crossing frequency, $f < f_c$, and increase for frequencies above the crossing frequency, $f > f_c$, as the temperature is increased. In the droplet picture of a spin glass [137], this has a natural interpretation: as the temperature is decreased, the average size of a cluster increases, so its relaxation time (the time it takes to "flip" or reorient the entire cluster) also increases, so that the distribution $p(\tau_c)$ increases for low frequencies; in addition, as the temperature decreases and the average size of clusters increases, the number of smaller clusters with smaller relaxation times decreases, so that the distribution $p(\tau_c)$ decreases for high frequencies. Here, however, the change in $p(\tau_c)$ that leads to spectral pivoting is accomplished in a rather different way: the characteristic time of a cluster depends upon the net alignment of the cluster.

The mechanism leading to this constraint and the different interpretations of its origins were discussed in § 2, and the effects of similar nonlinear constraints have been investigated for the Ising model [29, 23, 27, 28, 24]. The constraint is interpreted as originating from maintaining a constant, maximized entropy of clusters of spins plus their local (finite) bath during fluctuations. To account completely for the entropy of a cluster, the configurational entropy is considered. In terms of energy, a finite amount of work is indeed required to change the configurational entropy of a collection of spins, and this energy is separate from that originating from spin-spin interactions, which the Boltzmann factor accounts for. In this sense, it is similar to the entropic elasticity of

the ideal, freely-jointed chain model of a polymer, which requires finite work to stretch, yet undergoes no change in internal energy [47]. As will be seen, this constraint slows the dynamics of highly aligned clusters, so that the relaxation times of clusters become distributed according to the distribution of their alignments. Of course, as the distribution of alignments evolves with time, so to does the distribution of time scales. As discussed previously, both the spatial heterogeneity of the clusters as well as their being allowed to change in time yield $1/f$ noise. Furthermore, the specific effect of the constraint as the temperature is reduced is to enhance low-frequency fluctuations of highly aligned clusters while reducing high-frequency fluctuations due to fast, single spin flips. This leads to the spectral pivoting expressed in equation 4.1.

The model is a classical Heisenberg spin system on a two-dimensional ideal square lattice with periodic boundary conditions of sizes $N \times N = 24 \times 24$ or $N \times N = 48 \times 48$, with and without varying strengths of dipolar anisotropy. The Hamiltonian is:

$$H = -J \sum_{\langle ij \rangle} \mathbf{s}_i \cdot \mathbf{s}_j - D \sum_i (s_i^z)^2 \tag{4.2}$$

Spin vectors $\mathbf{s}_i$ have a length of one, $|\mathbf{s}_i| = 1$. The first sum comes from the spin-spin interactions; it is performed over all nearest neighbor pairs of spins $\langle ij \rangle$ and the exhange constant J is set to one. This ferromagnetic coupling $J > 0$ comports with the observation of time-reversal symmetry breaking at the superconductor-insulator interface [119]. The second sum provides dipolar anisotropy in the z-direction; it is performed over all spins i and the strength D is set to $D = 0 \times J, 2 \times J$, or $4 \times J$ for the simulations presented here.

Though many of the possible physical identities of the unpaired surface spins discussed above and in the literature are electrons with a spin 1/2, including localized gap states [32] and paramagnetic dangling bonds [123], there are also indications, including the material independence of flux noise and its reduction through cycles of

heating of devices in a vacuum chamber, that spins may be due to adsorbed molecular species, specifically O_2 [134, 69]. These are better modeled using classical spins and justify using the Heisenberg Hamiltonian, equation 4.2. Density functional theory calculations of adsorbed molecular oxygen show that it retains a substantial magnetic moment when adsorbed on the surface, which is free to rotate about the O-O bond, providing physical justification for the second term in equation 4.2. In addition, a previous study of a similarly constrained discrete, two-state Ising model produced spectra with $\alpha < 1.4$ for even the lowest temperatures [28]. This is a limit that is seen in a number of physical systems, including the $1/f$ flux noise in SQUIDs discussed here. The constrained, fully isotropic, classical Heisenberg model exceeds this limit, producing $1/f$-type noise with α as high as ≈ 1.8. Including the second term in equation 4.2 restores this limit, bridging the gap between the fully discrete Ising model and the fully isotropic Heisenberg model.

To perform Monte Carlo simulations, the Metropolis algorithm [53] with Boltzmann's factor is used:

$$e^{-\Delta E/k_B T} > [0,1) \tag{4.3}$$

where $[0,1)$ is a uniformly distributed random number between zero and one, k_B is Boltzmann's constant, and T is the temperature in units of J/k_B. ΔE is the change in the internal energy (due to spin-spin interactions) from an attempted spin flip, in which new orientation for a spin is chosen at random.

In addition to Boltzmann's factor, the condition equation 2.1 described in SEC 2 is imposed upon spin flips within a given cluster. To accomplish this, the lattice is subdivided into square clusters of N_c spins and spins flips are subject to the additional, nonlinear constraint:

$$e^{-g(\mathcal{S}_c - \mathcal{S}_c^{max})/k_B} = \left[\frac{\Omega(0)}{\Omega(M_c)}\right]^g > [0,1) \tag{4.4}$$

where $\mathcal{S}_c$ is the configurational entropy of the cluster, $-N_c \leq M_c \leq N_c$ is the net alignment of the cluster, $\Omega(M_c)$ is the multiplicity of states of the cluster with alignment M_c, and the factor g is a parameter used to adjust the strength of the constraint. This nonlinear constraint arises entirely from the configurational entropy of the cluster, not the internal energy due to interactions, and does not change the Hamiltonian, equation 4.2. This is distinct from e.g. a spin glass, where heterogeneity come from non-uniform interactions [137]. Instead, the Hamitonian is kept homogeneous and heterogeneity comes from linking local dynamics in a cluster to the state of that cluster.

From the general form of equation 4.4, the specific form for the classical Heisenberg model can be found. The configurational entropy of N_c classical Heisenberg spins with net alignment M_c is given by

$$\mathcal{S}_c = \mathcal{S}_c^{max} - \int \mathcal{L}^{-1}\left(\frac{M_c}{N_c}\right) dM_c \tag{4.5}$$

where $\mathcal{L}^{-1}(x)$ is the inverse Langevin function and can be expanded as

$$\mathcal{L}^{-1}(x) = 3x + \frac{9}{5}x^3 + ... \tag{4.6}$$

so that the configurational entropy of a cluster is

$$\mathcal{S}_c = \mathcal{S}_c^{max} - N_c\left[\frac{3}{2}\left(\frac{M_c}{N_c}\right)^2 + \frac{9}{20}\left(\frac{M_c}{N_c}\right)^4 + ...\right] \tag{4.7}$$

If it is assumed that the alignment is small compared to its maximum value, $M_c \ll N_c$, the entropy can be approximated as being quadratic in M_c (in other words, M_c has a Gaussian probability distribution)

$$\mathcal{S}_c \approx \mathcal{S}_c^{max} - \frac{3}{2}\frac{M_c^2}{N_c} \tag{4.8}$$

so that the final form of the constraint is

$$e^{-g\times(3M_c^2/2N_c)} > [0, 1) \tag{4.9}$$

In order to illustrate how the use of the nonlinear constraint in this system leads to fluctuations with a $1/f$ spectrum, the high temperature limit ($T \to \infty$) with $g = 1$ is considered. In this case, the criterion set by Boltzmann's factor, equation 4.3, allows all spin flips. As a result, interactions can be ignored and the dynamics is governed solely by equation 4.9, similar to the matrix model presented in § 3. The average lifetime of a state of a cluster with alignment M_c is therefore $\tau_c(M_c) \propto 1/\Omega(M_c) = e^{3M_c^2/2N_c}$; this is inverted to obtain M_c in terms of τ_c:

$$M_c = \sqrt{\frac{2N_c \ln(\tau_c)}{3}} \tag{4.10}$$

Allowing the distribution of relaxation times to be found from equation 2.6:

$$p(\tau_c) \propto M_c^2(\tau_c) \left| \frac{dM_c}{d\tau_c} \right| \propto N_c^{3/2} \frac{\sqrt{\ln(\tau_c)}}{\tau_c} \tag{4.11}$$

As will be shown, the range of τ_c for the model considered is quite large, so that the factor $\sqrt{\ln(\tau_c)}$, growing slowly enough to be considered constant, can be neglected.

In deriving equation 4.11, it was assumed that the approximation of equation 4.8 holds, under the condition that $M_c \ll N_c$, so that the configurational entropy is quadratic in M_c. However, for small enough N_c, clusters are more likely to fluctuate into a highly aligned state and this approximation may not hold. This can be seen in figure 4.1, where power spectral densities from simulations of size $24 \times 24 = 576$ spins, at high temperature $k_B T/J = 10^9$, with no anisotropy $D = 0$, and $g = 1$ are presented for cluster sizes of $N_c = 4$ (blue curve), 9 (green), 16 (red), and 36 (black) spins. For the largest cluster size $N_c = 36$, the prediction of equation 4.11 holds and the power spectral density is very close to exact $1/f$ noise (indicated by the black dashed line) at low frequencies. For smaller N_c, where the assumption $M_c \ll N_c$ breaks down and equation 4.8 and 4.11 do not hold, spectra deviate more and more from $1/f$ behavior. The rollover to white noise is also made to be more gradual due

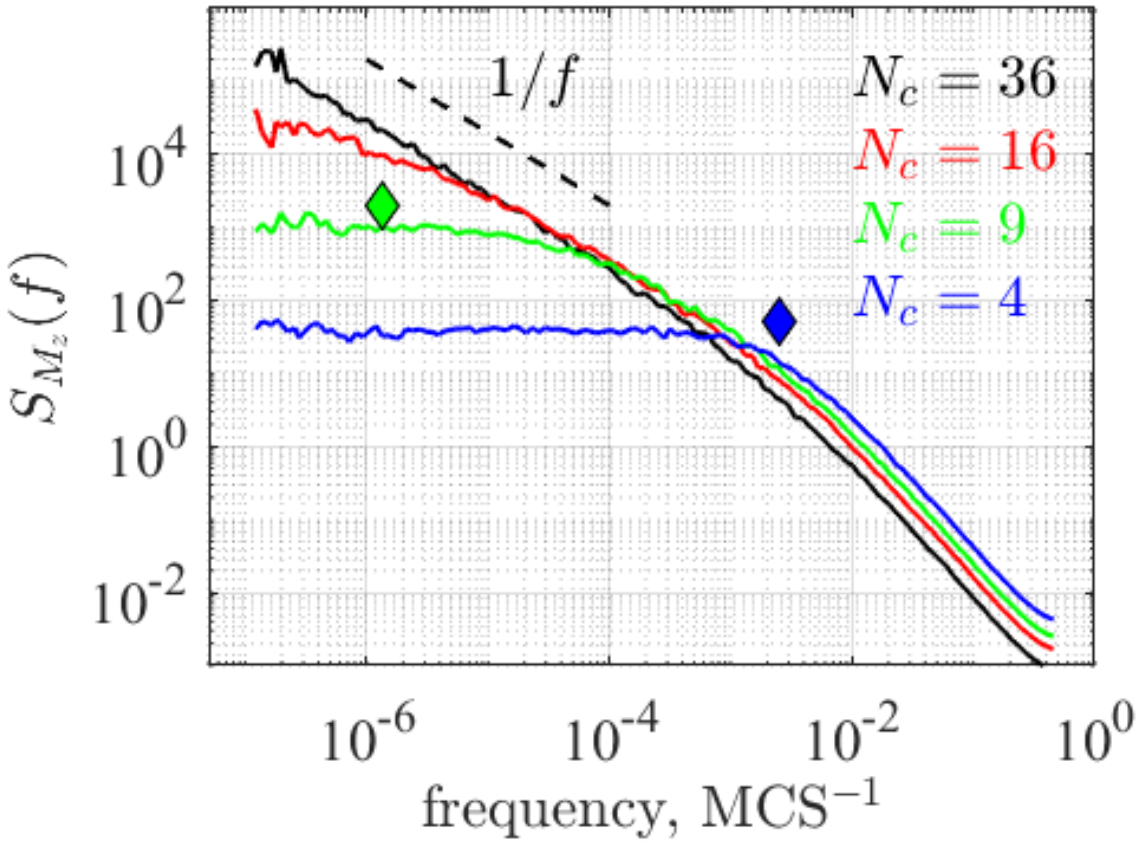

Figure 4.1: Power spectral densities from simulations of size $24 \times 24 = 576$ spins, at high temperature $k_BT/J = 10^9$, with no anisotropy $D = 0$, and $g = 1$, for cluster sizes of $N_c = 4$ (blue curve), 9 (green), 16 (red), and 36 (black) spins. Exact $1/f$ noise is indicated by the black dashed line. The lowest frequencies $f_0 = e^{-3N_c/2}$ where $1/f$ noise is expected and spectra rollover to white noise are marked by the diamond symbols for $N_c = 4$ ($f_0 \approx 2.5 \times 10^{-3}$) and 9 ($f_0 \approx 1.4 \times 10^{-6}$) spins. For increasing cluster size, these frequencies shrink exponentially, so that they are far outside the simulated range for $N_c = 16$ ($f_0 \approx 3.8 \times 10^{-11}$) and 36 ($f_0 \approx 3.5 \times 10^{-24}$) spins. For $N_c = 36$, the approximation of equation 4.8 holds in the frequency range simulated and the spectrum is exactly $1/f$ at low frequencies. For smaller N_c, $M_c \ll N_c$ breaks down and deviations from $1/f$ at low frequencies are observed.

to the breakdown of this assumption. To see this, the lowest frequencies at which $1/f$ noise is expected are marked by the diamond signals for $N_c = 4$ and 9 spins (for larger clusters, this frequency is far oustide of the simulated range). These frequencies correspond to the inverse of the longest average lifetime of the system, which is the time it takes to flip a spin in a fully aligned $M_c = N_c$ cluster:

$$f_0 = \frac{\Omega(M_c = N_c)}{\Omega(M_c = 0)} = e^{-3gN_c/2} \tag{4.12}$$

As can be seen is figure 4.1, these frequencies do mark where spectra rollover to fully white noise, but the rollover is made gradual by the failure of equation 4.8, and the spectra are far from exactly $1/f$ before this point is reached. Of course, since the frequency f_0 corresponds to a fully aligned cluster $M_c = N_c$, the assumption $M_c \ll N_c$ breaks down before this point is reached.

The exact entropy is found from the inverse Langevin function, and the next term from its expansion equation 4.7 would yield a correction to equation 4.8 of $\mathcal{O}(M_c^4)$. However, given the high density $\approx 5 \times 10^{17}\ m^{-2}$ of spins on the surface [64], clusters are expected to be quite large. In the results presented below a cluster size of $N_c = 6 \times 6 = 36$ is used, for which the rollover to white noise is far outside the simulated range, and the approximation of equation 4.8 should be sufficient. It should be pointed out that in the matrix model presented in § 3, an explicit bath was employed, so that configurational entropies are exact. As a consequence, the deviations seen in figure 4.1 are not present and the rollover to white noise is abrupt (see figure 3.3). Furthermore, in a previous study of a similarly constrained Ising model [28], exact configurational entropies from the binomial coefficient are used and the deviations and anomalous size dependence of figure 4.1 are not observed.

4.3 Simulation Details

Monte Carlo simulations were performed using the Metropolis algorithm [53] with the standard Boltzmann factor of equation 4.3, in addition to the nonlinear constraint of equation 4.4. All random numbers were generated using the Mersenne Twister pseudorandom number generator [86]. For a single spin flip, an entirely new orientation of the spin is chosen from an isotropic distribution, without regard to the spin's previous orienation. To ensure that the distribution of newly chosen orientations is isotropic, random numbers r_1 and r_2 are generated from $(-1, 1)$, are accepted only if the condition $r = (r_1)^2 + (r_2)^2 < 1$ is met, and the new spin orientation is given by $\mathbf{s}_i = (s_i^x,\ s_i^y,\ s_i^z) = (2r_1\sqrt{(1-r)},\ 2r_2\sqrt{(1-r)},\ 1-2r)$, which is then normalized to magnitude one [85]. A full Monte Carlo *sweep* (MCS) is completed after each spin has attempted a flip, at which point data are recorded; the order in which spins are flipped is randomized after each sweep.

Simulations are initialized by orienting all spin vectors in the positive z-direction, $(s_i^x,\ s_i^y,\ s_i^z) = (0,\ 0,\ 1)$, and allowing the simulation to run for 10^6 sweeps with no anisotropy and without applying the nonlinear constraint of equation 4.4. Anisotropy (if applicable) and the constraint are then applied and the simulations are run for another $2^{17} \times 10^3$ sweeps. Finally, data are collected as the simulation is run for another $t_m = 2^{17} \times 10^3$ sweeps. During these $2^{17} \times 10^3$ sweeps, four time series of the time-averaged z-component of the net alignment, $M_z(t)$, are collected, each of length 2^{17} data, averaged over averaging times of $t_{av} = 10^0,\ 10^1,\ 10^2$, or 10^3 sweeps. The Fourier transform of each of these time series is calculated and squared to estimate the power spectral density of fluctuations:

$$S_{M_z}(f) = \frac{1}{t_m}\left|\sum_{t=0}^{t_m} M_z(t) e^{2\pi i f t/t_m}\right|^2 \tag{4.13}$$

Spectra from five identical simulations are collected in such a manner and averaged

together, leaving four averaged spectra, one for each averaging time t_{av}. These spectra are then smoothed by dividing each of them into octaves, performing a linear least squares fit to the data within each octave, and taking the value of the smoothed spectrum at the center frequency of each octave to be the value of the linear fit at its octave's center frequency. Because spectra are smoothed over subsequent octaves, the resulting frequencies are evenly spaced on a logarithmic scale. Once the spectra from different averaging times are smoothed, they must be merged together. Because each spectrum covers $\mathcal{O}(\log_{10}(t_m)) \sim 5$ decades of frequency, and each spectrum is separated by a single decade, spectra from different averaging times significantly overlap each other's frequency ranges. This is useful, as it allows the spectra to be merged using an average that is weighted more heavily toward the center of each spectrum's frequency range, where the Fourier transform is less noisy; specifically, a Gaussianh distribution is used as the weighting function. This overlap can also be used to test for system equilibration and stationarity, by minimizing the integrated difference between the spectra of different averaging times in frequency range where they overlap. This process, equilibration, and stationarity in this model in general, are discussed in § 4.4.1 and in figure 4.5.

4.4 Results and Discussion

As discussed, a cluster size of $N_c = 6 \times 6 = 36$ is used for the simulations presented here. Simulations with $N_c = 36$ were found not to exhibit the deviations shown in figure 4.1 associated with the breakdown of the approximation equation 4.8. Using $g = 1$ in the nonlinear constraint, equation 4.4, the power spectral density is exactly $1/f$ ($\alpha = 1$) in the high temperature limit, $k_B T/J \to \infty$. Since α increases with decreasing temperature, for all finite temperatures, $\alpha > 1$ with $g = 1$. Thus, in order to reproduce the range $0.35 \lessapprox \alpha \lessapprox 1.40$ observed in the flux noise of SQUIDs [4, 62]

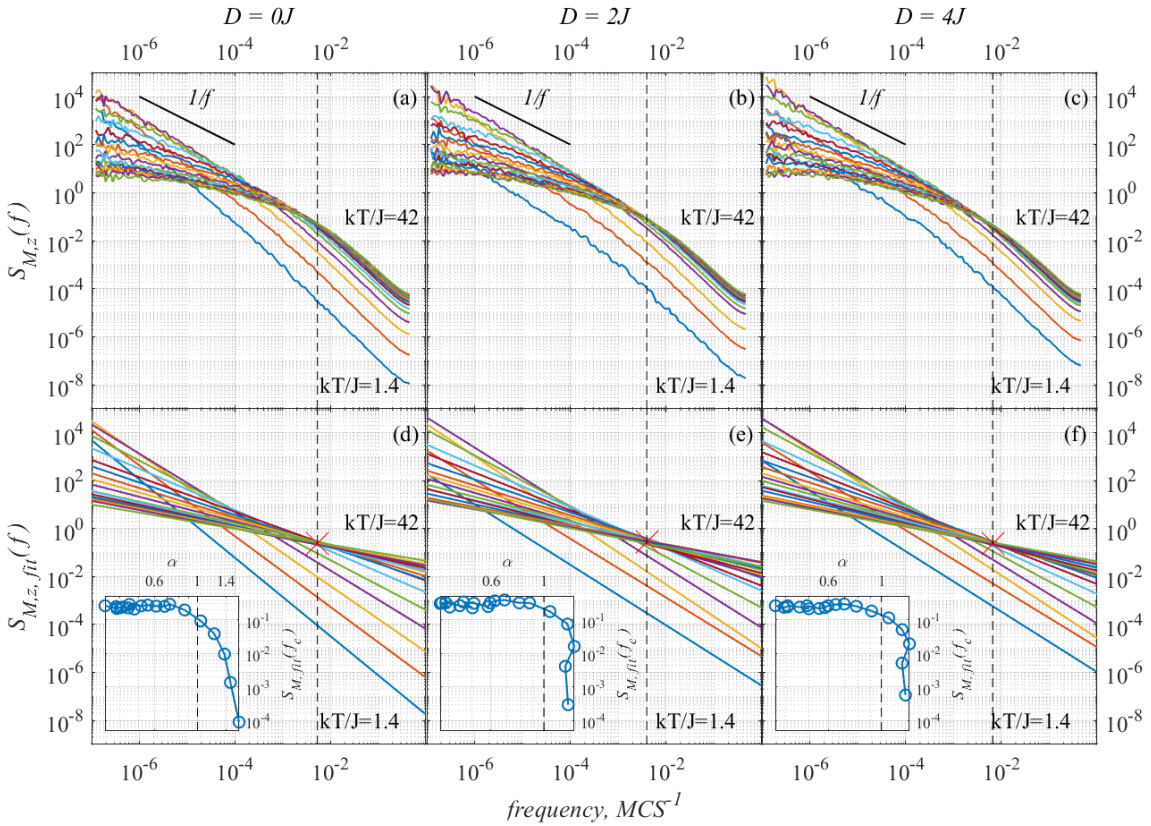

Figure 4.2: (a-c) Power spectral densities of fluctuations in the z component of net alignment for $D = 0J$ (a), $2J$ (b), and $4J$ (c) at temperatures ranging from $k_BT/J = 1.4$ to 42 (spectra of different anisotropies are not necessarily simulated at the same temperature). (d-f) Fits (equation 4.14) to the low-frequency (centered around $f = 10^{-6}$ MCS^{-1}) portion of the spectral densities in (a-c). All fits have coefficients of determination $R^2 > 0.9$. Fits to the spectra cross each other at frequencies $f_c = 5.36(+1.32/-1.06) \times 10^{-3}$ MCS^{-1}, $f_c = 3.93(+1.16/-0.90) \times 10^{-3}$ MCS^{-1} and $f_c = 6.60(+1.06/-0.91) \times 10^{-3}$ MCS^{-1} for $D = 0$, $2J$ and $4J$, respectively, as marked by the black dashed lines. Insets show the values of the fits, $S_{M_z,fit}(f_c)$, at the crossing frequency f_c, plotted against α. They are seen to depart from the otherwise common value when $\alpha \gtrapprox 1$ (marked by the black dashed line). This figure should be compared to data presented in reference [4].

a value of $g < 1$ is used. For the results presented below a value of $g = 2/3$ was used.

In figure 4.2 (a-c) are presented power spectral densities as a function of frequency from simulations with varying strengths of anisotropy: $D = 0J$ (a), $2J$ (b), and $4J$ (c). Spectra, specifically their spectral exponents α, have similar frequency dependences, consisting of a high-frequency tail where $\alpha \approx 1.8$ and is only very weakly

temperature dependent, transitioning to a low-frequency regime where $\alpha < 1.8$ and strongly depends upon temperature. In the high-frequency region, the constant shape of the spectrum is a consequence of fluctuations being dominated by single spin flips. Here, it is not expected that these Monte Carlo simulations will produce realistic fluctuations. Physically, the microscopic dynamics is expected to take over at these short time scales and fluctuations will no longer be stochastic [65]. In these simulations, single spin flips, in which spins can assume *any* new orientation, unencumbered by the underlying microscopic physics, are on the order of the highest measurable freqeuncy, 1 MCS^{-1}. Furthermore, because it decays quickly (as $\approx 1/f$, of course), this high-frequency behavior is invariably subsumed by some other source of white ($\alpha = 0$) noise in experiments, e.g. Johnson noise in the readout electronics, so that the dynamics in the observable portion of the spectrum are stochastic [40, 114, 4].

In the low-frequency regime, $0.35 \lessapprox \alpha \lessapprox 1.6$ for $D = 0$ and $0.35 \lessapprox \alpha \lessapprox 1.4$ for both $D = 2J$ and $D = 4J$, decreasing with increasing temperature. A similar range of values of α, centered on $\alpha = 1$, as well as the inverse dependence on temperature, has been reported in the literature for flux noise in SQUIDs [64, 4, 62, 40, 114]. To clarify the temperature dependence of α and of the amplitude in the low-frequency regime of the spectra, linear least squares fits to the spectra, centered around $f = 10^{-6}$ MCS^{-1}, were performed. Specifically, fits were made to the function

$$S_{M_z,fit}(f) = S_{M_z,0} \times (f/10^{-6}\ MCS^{-1})^{-\alpha} \tag{4.14}$$

where $S_{M_z,0} = S_{M_z,fit}(f = 10^{-6}\ MCS^{-1})$ was chosen for clarity of presentation and to place this fit parameter at the center of the frequency range being fit. These fits are presented in figure 4.2 (d-f). All fits have coefficients of determination $R^2 > 0.9$. From these it is clear that (1) α increases with decreasing temperature, quickly at low temperatures and much more slowly at high temperatures as interactions become

negligible and equation 4.4 dominates the dynamics instead of equation 4.3; (2) the power spectral density increases at low frequencies and decreases at high frequencies with decreasing temperature; (3) α and the power spectral density are themselves related, seemingly independent of their own dependences on temperature, in such a way that fits to the spectral densities cross each other at a common crossing frequency f_c, similar to the flux noise of SQUIDs reported by Anton *et al.* [4] and Kempf *et al.* [62]. Values of the crossing frequency are $f_c = 5.36(+1.32/-1.06) \times 10^{-3}$ MCS^{-1}, $f_c = 3.93(+1.16/-0.90) \times 10^{-3}$ MCS^{-1} and $f_c = 6.60(+1.06/-0.91) \times 10^{-3}$ MCS^{-1} for $D = 0,\ 2J$ and $4J$, respectively. These values are marked by the black dashed lines in figure 4.2 (a-f). Values of the power spectral density at the crossing frequency are $\langle S_{M_z,fit}(f_c)\rangle = 2.44(+0.27/-0.24) \times 10^{-1}\ \mathcal{M}^2\times$MCS, $\langle S_{M_z,fit}(f_c)\rangle = 2.85(+0.38/-0.33) \times 10^{-1}\ \mathcal{M}^2\times$MCS and $\langle S_{M_z,fit}(f_c)\rangle = 2.44(+0.21/-0.19) \times 10^{-1}\ \mathcal{M}^2\times$MCS for $D = 0,\ 2J$ and $4J$, respectively, where $\mathcal{M}$ is our unit of alignment, or magnetization. Crossing frequencies and the values of the fits to the power spectral density at the crossing frequency were calculated using the geometric mean of crossing frequencies of all pairs of fits; uncertainties were calculated using the geometric standard deviation. Fits to spectra for the six lowest temperatures presented in figure 4.2 are not included in these calculations, and inspecting either the spectral densities (a-c) or their fits (d-f) it can be seen why: at these temperatures, when $\alpha > 1$, spectra begin to drop substantially in amplitude, no longer preserving the relationship between α and $S_{M_z,0}$ and therefore no longer passing through a common crossing frequency f_c. This is made more clear in the insets of figure 4.2, where the values of the fits at the crossing frequency f_c, $S_{M_z,fit}(f_c)$, are plotted against α. It can be seen that $S_{M_z,fit}(f_c)$ remains approximately constant until $\alpha \approx 1$ (marked by the black dashed line), at which point it begins to drop precipitously. This behavior will be discussed in greater detail in § 4.4.1.

Examining the raw spectra of figure 4.2 (a-c) at the crossing frequency f_c (marked by the black dashed line), and comparing to the fits of figure 4.2 (d-f), it can be seen that the crossing frequency in the fits occurs approximately at the crossover from the highly temperature dependent low-frequency regime to the high-frequency tail. So, while close inspection shows that the raw spectra do in fact cross each other, it appears that they converge at high frequencies to common values of S_{M_z} and α, except for temperatures where $\alpha \gtrapprox 1$ and the spectral density at high frequencies is greatly reduced. Since this high-frequency behavior is determined by single spin flips, the convergence of the spectra of different temperatures at high frequencies suggests that this fast behavior is not strongly altered by the change in temperature or the presence of the nonlinear constraint. Again, at these high frequencies, the Monte Carlo simulations will not yield realistic dynamics. In addition to masking the high-frequency portion of the $1/f$ contribution to the spectrum, white noise in experiments give spectra a positive curvature, enhancing the appearance of a crossing frequency [4, 62, 40, 114]. Regardless of these considerations, the relationship between $S_{M_z,0}$ and α that produces the crossing frequency holds at low frequencies, $f < f_c$. Here, the effect of the nonlinear constraint is to alter the *slow* dynamics, which, as will be seen, is dominated by collective changes in the net alignment of clusters.

In figure 4.3 are shown the fit parameters of equation 4.14 as functions of temperature for strengths of anisotropy $D = 0J$ (blue curve), $2J$ (red), and $4J$ (green). Specifically, it shows spectral exponents α, figure 4.3(a), and the corresponding amplitudes $S_{M_z,0}$, figure 4.3(b). From the similarity of these curves alone it can be seen that there is a relationship between α and $S_{M_z,0}$ for spectra with $\alpha \lessapprox 1$. This is made more clear in the inset of figure 4.3(a), where the fit parameters α and $S_{M_z,0}$ are plotted against each other. The relationship between α and $S_{M_z,0}$ holds for $\alpha \lessapprox 1$ and is independent of the strength of the anisotropy, tying the relationship to the

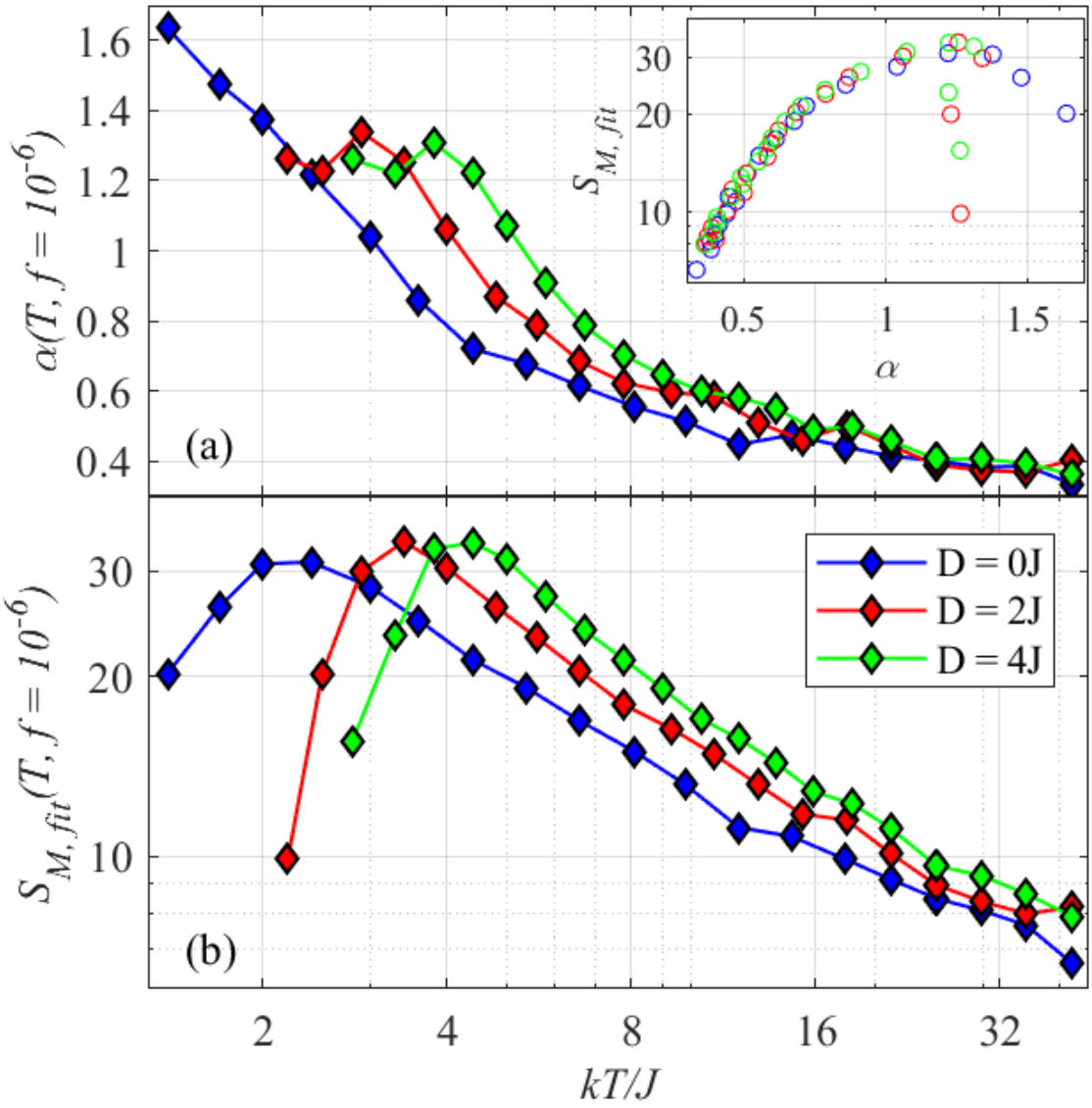

Figure 4.3: Fit parameters α (a) and $S_{M_z,0}$ (b) from fits in figure 4.2(d-f) as a function of temperature for $D = 0J$ (blue), $2J$ (red), and $4J$ (green). (Inset) The relationship between α and $S_{M_z,0}$ leading to the presence of a crossing frequency for $\alpha \lessapprox 1$ is made clearer by plotting α and $S_{M_z,0}$ against each other. The relationship is independent of D, suggesting its origin is the nonlinear constraint, equation 4.4.

constraint, the form of which, equation 4.4, depends upon the configurational entropy alone and is unaltered by the presence of anisotropy, unlike Boltzmann's factor, equation 4.3, which depends upon D through the second term in the Hamiltonian, equation 4.2. In experiments, it is reported that different SQUIDs, while possessing different dependencies of α and $S_{M_z,0}$ on temperature, show the same relationship, equation 4.1, between α and $S_{M_z,0}$, regardless of temperature [4, 62]. This is similar to the independence of the relationship on D displayed in the inset of figure 4.3(a). Generally, the temperature independence of the relationship producing a crossing frequency suggests that the origin of the relationship is independent of the internal energy of the clusters, a condition that is certainly satisfied by this model.

It was mentioned previously that the six lowest temperature spectra, for which $\alpha \gtrapprox 1$, were excluded from the calculation of the crossing frequency f_c. The reason for this is that at this point, the amplitudes of the spectra begin to drop precipitously, no longer crossing the other spectra at f_c. This is apparent from the raw spectra in figure 4.2(a) and the fits in figure 4.2(b), but is most clear in the insets, which show $S_{M_z,fit}$ dropping quickly at the crossing frequency. At lower temperatures, specifically when $\alpha \gtrapprox 1.35$, the divergence becomes even more pronounced and there is a peak in $S_{M_z,0}$, which can be seen in figure 4.3(b). It is worth noting that, since the spectra and their slopes decrease monotonically, there is similarly a peak in the total noise power $\langle M_z \rangle = \int S_{M_z}(f)df$. A similar peak in noise power has been observed in experiments on spin glasses [137, 103] and simulations of the standard Ising model [30] and the Ising model with disorder in the form of random exchange constants [31]. In these cases, the maximum in the noise power, *i.e.* the variance of the alignment, coincide with phase transitions and spin glass transitions, respectively. This is suggessted by the fluctuation-dissipation relation, relating the total noise power to the dissipative (imaginary) part of the susceptibility, which diverges at a

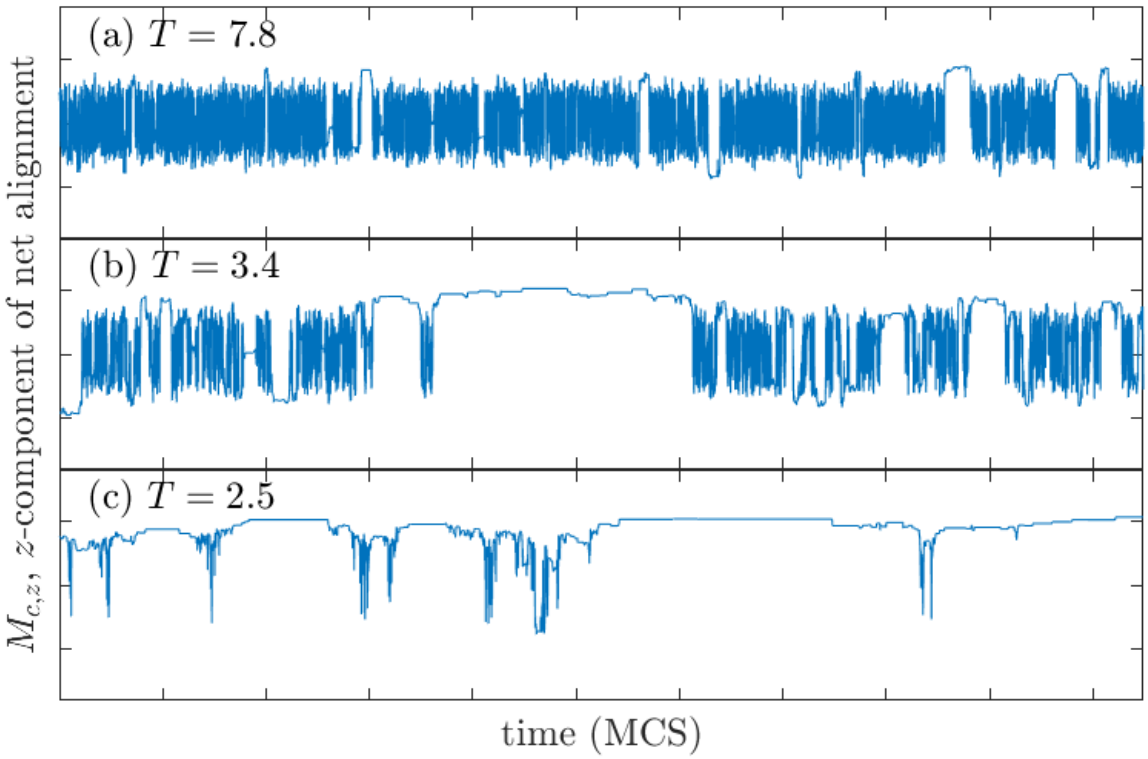

Figure 4.4: Time series of the z-component of net alignment of a *single* cluster with $D = 2J$ at $k_BT/J = 7.8$ (a), $k_BT/J = 3.4$ (b), and $k_BT/J = 2.5$ (c). The full extent of the vertical axis is fully aligned in the z-direction ($M_c = N_c = 36$) and the length of each time series is $t = 2^{19}$ MCS. (a) At $k_BT/J = 7.8$ the temperature is low enough that clusters undergo Ising-like switching. (b) As the temperature is lowered to $k_BT = 3.4$, the magnitude of fluctuations and the switching time increase. Close inspection shows that the magnitude of fluctuations and the switching time are in fact related, as in equation 4.10. (c) At $k_BT/J = 2.5$. When the temperature is low enough, the cluster no longer undergoes switching, the time-average of alignment is non-zero, and ergodicity is broken. At this temperature, $\alpha \approx 1.35$ (figure 4.3(a)) and there is a maximum in the amplitude of fluctuations (figure 4.3(b)).

phase transition temperature (for a system of infinite size) and is a maximum at the spin glass transition temperature. In this model, the maximum does not indicate a phase transition or a spin glass transition *per se*, as the classical Heisenberg in two dimensions is known not to undergo a ferromagnetic phase transition for $T > 0$ [88]. However, it does indicate a dynamical freezing and diverging time scales for reorientation of clusters, similar to that seen in the spin glass transition [137].

This can be seen in figure 4.4, which shows time series of the z-component of the

net alignment of a *single* cluster for $D = 2J$ and $k_BT/J = 7.8$ (a), 3.4 (b), and 2.5 (c). At low temperatures, clusters are found to undergo Ising like switching (figure 4.4 (a) and (b) $k_BT/J = 7.8,\ 3.4$). As the temperature is reduced, cluster become more aligned and the average amplitude of the fluctuations increase and, as a consequence of equation 4.1, the average switching times increase; this is apparent from comparing figure 4.4 (a) $k_BT/J = 7.8$ and (b) $k_BT/J = 3.4$. As suggested by equation 4.4, these switching times diverge exponentially with decreasing temperature, so that at low enough temperature the switching time is on the order of the simulation time t_m. At this point, as illustrated in figure 4.4(c) where $k_BT/J = 2.5$, clusters no longer undergo switching and the time average of alignment is non-zero over the entire simulation time ($t_m = 2^{17} \times 10^3$ MCS), meaning that ergodicity is broken on these time scales. It is at this temperature that the peak in $S_{M_z,0}$ occurs (figure 4.3(b)) and spectra begin to drop in amplitude (figure 4.2), violating the relationship equation 4.1 that yields the crossing frequency. In figure 4.3(a), it can be seen that it is also at this temperature that for simulations with anisotropy ($D = 2J,\ 4J$) the value of α levels to ≈ 1.35. An investigation of the Ising model, similarly constrained, found that simulations freeze at low temperatures when $\alpha \approx 1.4$ [28]. This is a limit seen in the resistivity fluctuations of thin metal films [44], as discussed in reference [28], as well as the flux noise of SQUIDs, discussed here. Specifically, the SQUID flux noise spectra presented by Anton *et al.* [4] show $0.35 \lessapprox \alpha \lessapprox 0.80$ for single SQUIDs and those presented by Kempf *et al.* [62] show $0.50 \leq \alpha \leq 0.82$ for single SQUIDs and $0.34 \leq \alpha \leq 1.41$ for SQUID arrays. In addition to obeying the limit of $\alpha \lessapprox 1.4$, these data are in the range of α in which no freezing occurs in our model, so that the correlation between α and $S_{M_z,0}$ is maintained, leading to the existence of a crossing frequency. This implies that the clusters of spins responsible for $1/f$ flux noise are near a transition at these temperatures, a suggestion that has been made previously

[134, 72, 39].

The form of the constraint, equation 4.9, can provide some insight into this dynamical freezing and the conditions, specifically the temperature and simulation time, when these simulations are ergodic. From equation 4.4, the constraint has the effect of extending the lifetimes of states of clusters with alignment M_c by a factor $\approx e^{g\times(3M_c^2/2N_c)} = e^{M_c^2/N_c}$, diverging rapidly as the temperature is reduced and the average net alignments M_c of clusters increase. From this, three benchmarks can be immediately established: (1) the lowest frequency at which $1/f$ noise is observed and spectra roll over to white noise, and (2) the alignment at which ergodicity is broken for a given simulation time t_m. The first of these, the white noise rolloff frequency, was discussed previously. It is the inverse of the maximum time that the constraint can slow spin flips, which is the time it takes to flip a spin in a fully aligned cluster, $f_0 = e^{-3gN_c/2}$. This was illustrated in figure 4.1 for simulations with $g = 1$, with diamond symbols marking f_0 for cluster sizes $N_c = 4$ and 9 spins. For the simulations presented in this section, with $g = 2/3$ and $N_c = 36$, $f_0 = e^{-N_c} \approx 2\times10^{-16}$ MCS^{-1}, or 9 orders of magnitude lower than the lowest simulated frequency $1/t_m \approx 10^{-7}$ MCS^{-1} presented here. Indeed, no rolloff to white noise was observed in these simulations, as seen in figure 4.2.

To establish another benchmark, it is noted that ergodicity is broken when spin flips are slowed to times comparable to the simulation time: $t_m \approx e^{g\times(3M_c^2/2N_c)}$. Inverting this equation gives the average relative (reduced by a factor of N_c) net alignment of clusters when ergodicity is broken:

$$\frac{M_c}{N_c} = \sqrt{\frac{2}{3gN_c}\ln(t_m)} \tag{4.15}$$

So, for $g = 2/3$, $N_c = 36$, and $t_m = 2^{19}\times10^3$ MCS, ergodicity is broken when clusters have relative net alignments of $M_c/N_c \approx 0.72$. Indeed, near the temperature where a

peak in noise power is observed in figure 4.3(b), relative net alignments of clusters of ≈ 0.72 are found and spin flips in these clusters are suppressed for the duration of the simulation. Under close inspection, the relationship between the lifetime of states of clusters and their net alignment can also be seen in figure 4.4, where larger values of net alignment are seen to last longer for a given temperature, and the net alignments and lifetimes of states are both generally larger at lower temperatures. This is similar to the non-linearity observed in SQUID flux noise [119].

4.4.1 Equilibration, Stationarity, and Ergodicity

As discussed in § 1.3.3, the properties of stationarity and ergodicity are intimately related. Broadly speaking, a stochastic process $x(t)$ is ergodic when ensemble averages, equation 1.7, are equal to time averages, equation 1.6: $\langle x \rangle = \overline{x}$; whereas it is stationary when its joint probability distribution is invariant under a shift in time: $w(x,t) = w(x,t+\Delta t)$ [66]. Though related, stationarity and ergodicity are not mutually inclusive. A non-stationary process cannot be ergodic; without a well-defined time average $\overline{x}$, the condition $\langle x \rangle = \overline{x}$ is meaningless. However, a process can be stationary and non-ergodic. A common example that is relevant here is the position of a classical particle trapped in a double well potential. When the particle has an energy greater than the barrier height of the well, or if its energy is taken from a canonical distribution at sufficiently high temperature, its position is ergodic: it is free to move from one well to another so that $\langle x \rangle = \overline{x}$ in a finite measurement time. It is also stationary: its position is bounded so that statistical measurements become well-defined after a finite time. However, if the energy is much less than the barrier height, or the temperature low enough, the particle will be confined to one well, for all time in the former case, and for all reasonable times in the latter. Clearly, the particle's position is no longer ergodic. However, it is stationary: being free to ex-

plore the accesible states of the single well, statistical measurements are well-defined in a reasonable and finite time. It should be noted that this system can be made ergodic if the ensemble from which averages are calculated only contains states with the particle in one well or the other.

Having considered the conditions under which this model is ergodic, it is of interest to consider when it is stationary. To initialize the model, all spins are oriented in the positive z-direction, $(s_i^x,\ s_i^y,\ s_i^z) = (0,\ 0,\ 1)$ and simulations are run without anisotropy ($D = 0$) and without the additional nonlinear constraint. Since there is no phase transition in the isotropic $2D$ Heisenberg model for $T > 0$ [88], the model at this point is both stationary and ergodic and the time-averaged net alignment becomes zero in a reasonable time ($< 10^6$ MCS). When the nonlinear constraint and (if applicable) anisotropy are applied, the system is no longer ergodic, at least not for the combination of temperatures and simulation times discussed above. What's more, for the time that the system is in transit from ergodicity and a zero time-averaged net alignment to non-ergodicity and a possibly non-zero time-averaged net alignment, it is no longer stationary. That is to say, its time-averaged net alignment, variance of net alignment, and power spectral density of fluctuations of net alignment, are all functions of time, *i.e.* they are themselves stochastic variables on these time scales. After sufficient time, clusters settle into their new equilibrium in one well or another and fluctuate about this newly established and well-defined time-averaged net alignment; stationarity is restored.

It is necessary therefore to assess how long the system takes to reach a stationary state and allow it to establish stationarity before collecting data. To do this, the power spectral densities of different averaging times are compared to one another. The raw data collected are 2^{17} values each of the z-component of net alignment averaged over four different averaging times, $t_{av} = 10^0, 10^1, 10^2$ and 10^3 MCS. Each of these time

series are Fourier transformed and squared to create four power spectral densities, each of length $\mathcal{O}(\log_{10}(t_m)) \sim 5$ decades of frequency and separated by 1 decade. This means that power spectral densities of adjacent t_{av} overlap over ≈ 4 decades of frequency. Stationarity is established by summing the difference between power spectral densities with adjacent t_{av} in this ≈ 4 decade wide range of frequencies and checking that it is sufficiently small and centered around zero for the five different simulations used to create the final spectra. An example of this process is shown in figure 4.5(a) for a simulation that was not given sufficient time to equilibrate and produced a non-stationary alignment and power spectral density. The spectra of longer t_{av} decay with time. This is because, during equilibration, clusters are settling from a state of approximately zero net alignment to a non-zero net alignment. Since the frequency of spin flips depends upon cluster net alignment M_c as $\sim e^{-M_c^2/N_c}$, fluctuations are suppressed as clusters equilibrate and M_c grows.

In § 1.3.3 it was pointed out that if the power spectral density of fluctuations of a variable $x(t)$ have the form $S_x(f) \propto 1/f^\alpha$ with $\alpha \geq 1$ all the way down to zero frequency, then the total variance $\lim_{t_m \to \infty} \int_0^{t_m} S_x(f) df = \overline{(\delta x)^2}$ of x is infinite. One possible resolution of this long-standing problem is that the power spectral density is non-stationary. Specifically, if $\overline{(\delta x)^2}$ is to remain independent of measurement time t_m, it must have the form $S(f) \propto t_m^{1-\alpha}/f^\alpha$. So, for two adjacent averaging times t_{av} separated by a decade, the spectrum will have decayed by a factor

$$\delta S(f) = \frac{S^{(t_m)}(f)}{S^{(10t_m)}(f)} = \frac{(t_m)^{1-\alpha}}{(10t_m)^{1-\alpha}} = 10^{(\alpha-1)} \tag{4.16}$$

or, converting to decibels, $\delta S(f) = 10(\alpha - 1)$.

In figure 4.5(b), $\langle \delta S(f) \rangle$ of adjacent t_{av}, averaged over their overlapping frequency range, is plotted in decibels as a function of $10(\alpha - 1)$ from multiple simulations that were not allowed sufficient time to equilibrate and were therefore non-stationary. Sim-

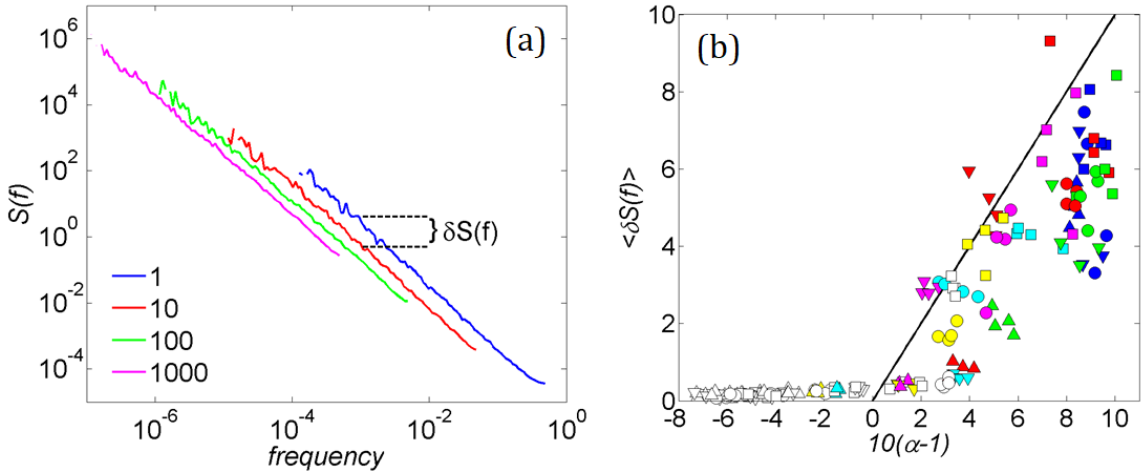

Figure 4.5: Demonstration of equilibration, aging, and non-stationary behavior in the constrained Heisenberg model. (a) Power spectral densities in the z-component of net alignment from a simulation with $D = 2J$, and averaging times $t_{av} = 10^0$ (blue curve), 10^1 (red), 10^2 (green), and 10^3 (pink) MCS. Stationarity is checked in simulations by integrating the difference $\delta S(f)$ (an example for $t_{av} = 10^0$ and 10^1 MCS is given in the figure) between spectra of adjacent t_{av} and checking that it is sufficiently small and centered around zero for different simulations. The example shown here was not allowed to equilibrate for a sufficient number of sweeps and is clearly not stationary. (b) Plot of $\langle \delta S(f) \rangle$ in decibels, averaged over the overlapping frequency range of spectra with adjacent t_{av}, as a function of $10(\alpha - 1)$, where α is the spectral exponent taken from $S(f) \propto 1/f^{\alpha}$. Different colors (symbols) correspond to different values of k_BT/J (D/J). The paradox of infinite fluctuations is avoided for non-stationary spectra if $\langle \delta S(f) \rangle = 10(\alpha - 1)$ (marked by the solid black line).

ulations were for a number of different values of temperature k_BT/J and anisotropy D/J (as indicated by different colors and symbols, respectively), but the decay of the spectrum $\langle \delta S(f) \rangle$ trends with α, independent of these. For $\alpha < 1$, $\langle \delta S(f) \rangle$ is close to zero. For $\alpha > 1$, $\langle \delta S(f) \rangle$ (which, the process being non-stationary, is a stochastic variable) roughly follows the trend necessary for the variance to remain independent of t_m in equation 1.29, thus avoiding the paradox of infinite fluctuations: $\delta S(f) = 10(\alpha - 1)$, marked by the solid black line.

Apparently, when this model is allowed to settle into equilibrium from a non-equilibrium state, the power spectral density of fluctuations decays in such a way that the total variance remains approximately constant. The reasons for this are not

clear and require further investigation. It is certain that this model does not suffer from the paradox of infinite fluctuations since, because it is bounded, its $1/f$ behavior must not continue to zero frequency. Indeed, a cutoff frequency of $f_0 = e^{-3gN_c/2}$ is predicted and has been observed (figure 4.1).

4.5 Conclusions

The classical Heisenberg spin model, with the Hamiltonian equation 4.2, constrained according to equation 4.9 to reproduce the condition of equation 2.1, has been found to exhibit fluctuations with a $1/f$-type spectrum. Unlike the matrix model of § 3, this model includes interactions and exchanges energy and entropy with a thermal reservoir, simulated using Boltzmann's factor, equation 4.3. Because of this, the constant, maximum entropy of the system + local bath is maintained only approximately on the time-scale of single spin flips. Furthermore, $1/f^{\alpha}$ behavior was found to be temperature dependent, with α increasing as the temperature was decreased, as shown in figure 4.3. In the high-temperature limit and with $g = 1$, where the criterion of equation 4.9 dominates the dynamics over equation 4.3, exact $1/f$ noise was observed, as shown in figure 4.1. Adjusting the strength of the constraint through the value of g allowed the model to reproduce the range of α reported in SQUIDs [4, 62].

Generally, the constraint produces slow dynamics and $1/f$ noise in the system by slowing transitions in more aligned regions. Therefore, the fluctuations in alignment in this model are explicitly non-linear, similar to the flux noise in SQUIDs [119]. By slowing large-sized (large alignment) fluctuations and suppressing smaller-sized, high frequency fluctuations, the constraint produces spectral pivoting of spectra at different temperatures about a common-crossing frequency f_c, equation 4.1. This behavior is a feature of the $1/f$ flux noise seen in SQUIDs, as described in § 4.1.

This model, therefore, qualitatively recreates some of the features of $1/f$ flux noise in SQUIDs. figure 4.3 shows this spectral pivoting.

At low enough temperatures, this model becomes non-ergodic for the given simulation times. The longest characteristic times of spin flips at a given temperature are related to the net alignment through the constraint. This is shown in the lowest frequency at which $1/f$ noise occurs, equation 4.12, and the net alignment corresponding to a slowing of the dynamics beyond the time of measurement, equation 4.15. Because of the exponential dependence of the characteristic time on the net alignment squared, the time-scales of this model diverge rapidly as the temperature is reduced and the average net alignment of clusters increases. This, and the ergodicity and stationarity of the model in general, were discussed in § 4.4.1.

Chapter 5

CONCLUSIONS AND POSSIBLE FUTURE WORK

In § 2, multiplicity-dependent characteristic times were discussed and shown to produce fluctuations with a $1/f$-type spectrum. The physical interpretation offered is that multiplicity-dependent characteristic times arise from coupling to a finite, local entropy bath, or from non-ideal coupling to an infinite thermal reservoir which must be mediated through a local bath. Two models employing multiplicity-dependent characteristic times were simulated and found to exhibit fluctuations with a $1/f$ spectrum in § 3 and 4. In this final chapter, the numerical results of simulations of these two models will be compared to each other and to the class of models based on a distribution of exponential relaxation processes and the class of models based on power law renewal processes. In many cases, these simlarities might not be limited to the models presented here, and may be more general. In addition to these comparisons, some unanswered questions and possible future work will be discussed.

5.1 Comparison of Numerical Results to Models Based on Distributed Exponential Relaxation Processes and Models Based on Renewal Processes

Many, though not all, models of $1/f$ noise can be placed into one of two categories: (1) those based on a spatial distribution of exponential relaxation processes with characteristic times distributed as a power law $p(\tau_c) \sim 1/\tau_c$ and (2) those based on a single relaxation processes with waiting times that are distributed as a power law $\psi(\tau) \sim 1/\tau^{-1-\theta}$ as opposed to an exponential. These two classes of models were described in detail in § 1.4.1 and 1.4.2, respectively. The relationship of these classes of models to the models based on multiplicity-dependent characteristic times presented

here was discussed in general in § 2. Here, the results of simulations of these models, presented in § 3 and 4, will be placed in the context of these classes of models. It will be seen that models based on multiplicity-dependent characteristic times possess properties of both classes of models, and that the two are not necessarily mutually exclusive.

5.1.1 Comparison of Distributed Exponential Relaxation Processes Models and Renewal Process Models

The first class of models, like that of McWhorter [87] and Dutta, Dimon, and Horn [42], are based on a random process composed of many random, uncorrelated stationary and ergodic processes, with characteristic times distributed according to a power law $p(\tau_c) \sim 1/\tau_c$. This class of models was described in § 1.4.1. The underlying processes may be modelled as two-state Poisson processes, with transition times distributed exponentially, with the mean of this distribution corresponding to the characteristic time τ_c. Processes with an exponential distribution of transition times will have an exponential autocorrelation function and a Lorentzian power spectral density. Physically, these underlying processes can be described in terms of uncorrelated transitions over classical Arrhenius-like activation barriers [10, 128, 87, 42] or, for systems at low temperatures where tunnelling dominates, two-level tunnelling systems [3, 14, 15, 16, 67, 77, 136]. Regardless of the physical origin of the underlying processes, in many of these models, the power law distribution $p(\tau_c)$ comes from assuming (1) an exponential dependence of τ_c upon some parameter, such as activation energy [42] or tunnelling distance [87], and (2) a flat distribution of that parameter in the range of interest. Because of the exponential dependence of τ_c upon the parameter, the distribution of said parameter can be flat over a relatively narrow range to accomplish a broad range over which $p(\tau_c) \sim 1/\tau_c$. Because of this, models of this

type, which rely upon spatial heterogeneity, are physically reasonable for a wide class of systems. Additionally, spatial heterogeneity is a popular explanation for a number of other physical phenomena [19, 26, 105, 133]. Finally, in recent years, with the advent of more sophisticated measurement techniques, the dimensions of samples under observation have been made small enough to resolve individual Lorentzian features in the power spectral density [92, 102, 108, 110, 136].

The second class of models, first proposed by Mandelbrot over 50 years ago [82, 81, 83, 80, 135] and now gaining renewed interest [46, 73, 76, 84, 94], is based on a single fluctuator with sojourn times that are distributed according to a power law $\psi(\tau) \sim \tau^{-1-\theta}$. These models are a class of renewal processes [50] and were discussed in § 1.4.2, specifically the simplest two-state case. An exponentially distributed two-state system, the underlying processes of the first class of models, is a special, ergodic and stationary case of a renewal process. Unlike the first class of models, these do not rely upon a spatial power law distribution of fluctuators with different characteristic times. Instead, the power law character of fluctuations comes from the distribution of sojourn times themselves, so that a *single* fluctuator will exhibit fluctuations with a $1/f$ spectrum. These models also differ from the first class of models in that they are intrinsically non-stationary and will exhibit aging like that discussed in § 1.3.3 and 1.4.2. In this way, these models resolve the paradox of infinite fluctuations, discussed in § 1.3.3. The first class of models, on the other hand, resolves the paradox with the inclusion of a maximum characteristic time τ_{max}, so that $p(\tau_c) \sim 1/\tau_c$ only for $\tau_c < \tau_{max}$.

The first and second class of models are not necessarily mutually exclusive and share a number of properties. For one thing, the concept of conditional measurements and the consequent spectra (see § 1.4.2) reconcile the stationarity and ergodicity of these two classes of models. In addition, models with sojourn times distributed as

$\psi(\tau) \sim \tau^{-1-\theta}$ can make up the underlying processes of a spatially heterogeneous system, similarly to the first class of models, resulting in a stationary $1/f$-type power spectral density [112, 73]. Also, it is possible that a process has a power law distribution of sojourn times over only a limited range, $\psi(\tau) \sim \tau^{-1-\theta} \times e^{-\tau/\tau_{max}}$. A process such as this will have a non-stationary spectrum for measurement times $t_m < \tau_{max}$ and a stationary spectrum with a cutoff frequency $f_{cutoff} \sim \tau_{max}^{-1}$ for $t_m > \tau_{max}$.

5.1.2 Matrix Model

The model based on a simple matrix, presented in § 3, does not rely upon the superposition of multiple processes, and all results presented were from simulations of a single multi-level fluctuator. In fact, since there are no interactions in this model, the superposition of multiple processes is trivial and the same spectrum can be found from adding the spectra of individual processes. This fact was used to compare the sum of spectra to the data of Rogers and Buhrman, which resolved individual Lorentzian features in the $1/f$-type spectrum of voltage fluctuations in mesoscopic MIM junctions [108].

Since the matrix model produces $1/f$ noise without the need for a superposition of processes it is, in at least one way, more similar to the class of models based on power law renewal processes. Unlike the *two-state* power law renewal processes reviewed in § 1.4.2, however, this model has multiple states, each of these having its own, well-defined characteristic time. In § 2 it was shown that models based on multiplicity-dependent sojourn times can be recast as renewal processes with a power law dependence if (1) the fluctuating variable only moves between adjacent states, equation 2.11, and (2) the difference between values of the fluctuating variable are equal for adjacent states. Both of these conditions are met in the matrix model. So, while the characteristic time of each state is well-defined, the distribution of

characteristic times follows a power law. The sum of these considerations means that the sojourn times of this model will have a power law distribution. This model therefore bears characteristics of both classes of models. These similarities, however, are not necessarily a property of this model alone, and may point to a more general similarity.

The value of the fluctuating variable in the matrix model, the net alignment m, is bounded by the number of spins: $m \leq N$. Consequently, the mean maximum sojourn time is $\tau_{max} \propto \Omega_0$. The spectrum will therefore have a cutoff frequency $f_{cutoff} \propto \Omega_0^{-1}$, as seen in figure 3.3. However, since the multiplicity Ω_m of states with m is known to be approximately Gaussian, the distribution of sojourn times will have the form $\psi(\tau) \sim \tau^{-1-\theta}$ with $\theta \gtrapprox 1$ for $\tau < \tau_{max}$. It is therefore expected that the matrix model will have the form $\psi(\tau) \sim \tau^{-1-\theta} e^{-\tau/\tau_{max}}$. As a result, for $t_m < \tau_{max}$, the power spectral density of the matrix model may be non-stationary. When in a highly aligned state, the model will undergo no fluctuations for a long period of time, depressing the value of the spectrum as described in § 1.4.2. Given this, it seems likely that the amplitude of the spectrum will vary until $t_m > \tau_{max}$ and all of phase space has been explored. The stationarity of the matrix model, however, was not investigated for $t_m < \tau_{max}$. This is a possible subject of future work.

In § 3.3.1, this model was also recast in the form of a discrete Markov process. The mathematics of discrete Markov processes, specifically the characteristic times from the system's stochastic matrix, were used to recreate the power spectral densities obtained from simulations. This process did not exactly recreate the results obtained from simulations, most likely due to the fact that correlations among different states were ignored. Calculation of these cross-correlations is a possible subject of future work. Since discrete Markov models can model diffusion processes through their generalization to continuous states [66], recasting multiplicity-dependent char-

acteristic times in this form may provide a way to generalize models of this type to microscopically realistic methods of simulation, *i.e.* molecular dynamics.

5.1.3 Constrained Heisenberg Model

Like the matrix model, the constrained Heisenberg model, presented in § 4, does not rely upon multiple processes being superposed to produce $1/f$ noise. Single clusters of spins were found to exhibit $1/f$ noise. Still, the results presented for the constrained Heisenberg model were primarily for a sample composed of many interacting clusters. These clusters arrange themselves into a distribution of different net alignments and, through the dynamic constraint, a distribution of different characteristic times. In this way, this model is similar to those based on a distribution of exponential relaxation processes. Another similarity, one shared by the matrix model, is that the broadness of the distribution of characteristic times is achieved through the exponential dependence of the characteristic time on a not-necessarily broadly distributed parameter (the square of the net alignment of a cluster). For example, in the model of Dutta, Dimon, and Horn [42], the characteristic time depends exponentially on activation energy and/or tunnelling parameter. For the matrix model and constrained Heisenberg model, it is the Gaussian dependence of the characteristic time on net alignment. To further investigate these similarities, a distribution of cluster *sizes*, either static or dynamic, might be considered. As discussed, different cluster sizes do produce differing spectra, with an increase in cluster size increasing the range over which $1/f$ noise is observed, demonstrated in figure 4.1.

At low temperatures, as seen in figure 4.4, clusters were found to undergo Ising-like switching at low enough temperatures for simulations with anisotropy ($D \neq 0$), and these single clusters did in fact exhibit $1/f$ noise on their own. These considerations suggest that at low temperatures this model for single clusters is similar to

the two-state renewal processes of § 1.4.2. Since those models are intrinsically non-stationary, the stationarity (or non-stationarity) of this model can provide insights into these similarities. At lower temperatures than which Ising-like switching occurs, no transitions often occurred over the time of measurement. Still, no aging, associated with non-stationarity, was observed in the spectra of single regions. However, as discussed in § 4.4.1, when not properly equilibrated, this model showed aging of the type discussed in § 1.4. This same behavior is expected from the model if pushed out of equilibrium, and would also be expected after a rare event, *i.e.* when a single cluster flips its orientation. In such a case, the cluster moves from its highly aligned initial state, through ≈ 0 net alignment, and to its new highly aligned state. During this time, the characteristic time of fluctuations evolve with the cluster's alignment, with fast fluctuations occuring when the cluster has ≈ 0 net alignment and slowing rapidly as the cluster settles into its new highly aligned state. In this way, the power-spectral density may actually be non-stationary at low temperatures. Methods to investigate these questions in the future might include directly measuring the distribution of waiting times of single clusters and comprehensive measurements of conditional spectra, like those discussed in § 1.4.2.

The effect of the constraint in the constrained Heisenberg model and the finite bath states of the matrix model both have the effect of equation 2.1. Given this similarity between these two models, the mechanisms by which they produce $1/f$ noise are equivalent. In fact, in the high-temperature limit, where interactions are negligible, with $g = 1$, the constrained Heisenberg model is practically equivalent to the matrix model. However, at finite temperatures the presence of interactions complicates the matter. Another difference between the two is that the matrix model is fully discrete, whereas the constrained Heisenberg model employs continuous degrees of freedom. Since the generalization of discrete Markov processes, used to analyze

the matrix model in § 3.3.1, to the continuous case provide a route to models of diffusion, this constrained Heisenberg model might be a useful point from which to consider generalizing these models to molecular dynamics. In general, modelling the constrained Heisenberg model as a diffusion process may provide insight into multiplicity-dependent characteristic times.

5.2 Final Remarks

The models considered here, based on multiplicity-dependent characteristic times, have been found to exhibit fluctuations with a $1/f$-type spectra. The physical foundation offered here of this dependence is that a system fluctuates with a characteristic time depending on its state when it is coupled to a finite, local bath, with which it shares a constant, maximimized amount of entropy. The models presented may provide insight into the origin of $1/f$ noise in heterogeneous systems and small systems which are imperfectly coupled to their larger thermal environment. The similarity of this class of models to others suggests that a universal explanation of $1/f$ noise may be able to be formulated in terms of the connectivity of a system to its thermal reservoir and how this connectivity impacts equilibrium fluctuations.

REFERENCES

[1] K. Agarwal, E. Demler, and I. Martin. $1/f^{\alpha}$ noise and generalized diffusion in random heisenberg spin systems. *Physical Review B*, 92(18):184203, 2015.

[2] A. Amir, Y. Oreg, and Y. Imry. On relaxations and aging of various glasses. *Proceedings of the National Academy of Sciences*, 109(6):18501855, 2012.

[3] P. W. Anderson, B. I. Halperin, and C. M. Varma. Anomalous low–temperature thermal properties of glasses and spin glasses. *Philosophical Magazine*, 25(1):19, 1972.

[4] S. M. Anton, J. S. Birenbaum, S. R. OKelley, V. Bolkhovsky, D. A. Braje, G. Fitch, M. Neeley, G. C. Hilton, H.-M. Cho, K. D. Irwin, and et al. Magnetic flux noise in dc squids: Temperature and geometry dependence. *Physical Review Letters*, 110(14):147002, May 2013.

[5] J. Atalaya, J. Clarke, G. Schön, and A. Shnirman. Flux $1/f^{\alpha}$ noise in two-dimensional heisenberg spin glasses: Effects of weak anisotropic interactions. *Physical Review B*, 90(1):014206, 2014.

[6] R. Baierlein. *The Canonical Probability Distribution*, chapter 5, pages 91–94. Cambridge University Press, 1999.

[7] P. Bak, C. Tang, and K. Wiesenfeld. Self-organized criticality: An explanation of $1/f$ noise. *Physical Review Letters*, 59(4):381–384, July 1987.

[8] A. Balandin, K. Wang, A. Svizhenko, and S. Bandyopadhyay. The fundamental $1/f$ noise and the hooge parameter in semiconductor quantum wires. *IEEE Transactions on Electron Devices*, 46(6):12401244, 1999.

[9] A. A. Balandin. Low–frequency $1/f$ noise in graphene devices. *Nature Nanotechnology*, 8(8):549555, 2013.

[10] J. Bernamont. Fluctuations in the resistance of thin films. *Proceedings of the Physical Society*, 49(4S):138139, 1937.

[11] R. C. Bialczak, R. McDermott, M. Ansmann, M. Hofheinz, N. Katz, E. Lucero, M. Neeley, A. D. O'Connell, H. Wang, A. N. Cleland, and et al. $1/f$ flux noise in josephson phase qubits. *Physical Review Letters*, 99:187006, 2007.

[12] A. R. Bizzarri and S. Cannistraro. $1/f^{\alpha}$ noise in the dynamic force spectroscopy curves signals the occurrence of biorecognition. *Physical Review Letters*, 110(4), 2013.

[13] A. R. Bizzarri and S. Cannistraro. Antigenantibody biorecognition events as discriminated by noise analysis of force spectroscopy curves. *Nanotechnology*, 25(33):335102, 2014.

[14] J. L. Black. Low–energy excitations in metallic glasses. *Topics in Applied Physics Glassy Metals I*, page 167190, 1981.

[15] R. D. Black, P. J. Restle, and M. B. Weissman. Hall effect, anisotropy, and temperature–dependence measurements of1fnoise in silicon on sapphire. *Physical Review B*, 28(4):19351943, 1983.

[16] R. D. Black, P. J. Restle, and M. B. Weissman. Nearly traceless $1/f$ noise in bismuth. *Physical Review Letters*, 51(16):14761479, 1983.

[17] D. D. Boehr, R. Nussinov, and P. E. Wright. The role of dynamic conformational ensembles in biomolecular recognition. *Nature Chemical Biology*, 5(11):789796, 2009.

[18] S. Bogdanovich and D. Popovi. Onset of glassy dynamics in a two–dimensional electron system in silicon. *Physical Review Letters*, 88(23), 2002.

[19] R. Böhmer, R. Chamberlin, G. Diezemann, B. Geil, A. Heuer, G. Hinze, S. Kuebler, R. Richert, B. Schiener, H. Sillescu, and et al. Nature of the non–exponential primary relaxation in structural glass–formers probed by dynamically selective experiments. *Journal of Non–Crystalline Solids*, 235–237:19, 1998.

[20] A. Bray. Theory of phase-ordering kinetics. *Advances in Physics*, 43(3):357–459, 1994.

[21] J. J. Brophy. Statistics of $1/f$ noise. *Physical Review*, 166(3):827831, 1968.

[22] M. A. Caloyannides. Microcycle spectral estimates of $1/f$ noise in semiconductors. *Journal of Applied Physics*, 45(1):307316, 1974.

[23] R. V. Chamberlin. Monte carlo simulations including energy from an entropic force. *Physica A: Statistical Mechanics and its Applications*, 391(22):53845391, 2012.

[24] R. V. Chamberlin. Reducing low-frequency noise during reversible fluctuations. *The European Physical Journal Special Topics*, 226(3):365371, 2017.

[25] R. V. Chamberlin, S. Abe, B. F. Davis, P. E. Greenwood, and A. S. Shevchuk. Fluctuation theorems and $1/f$ noise from a simple matrix. *The European Physical Journal B*, 89(9), Sep 2016.

[26] R. V. Chamberlin, R. Böhmer, E. Sanchez, and C. A. Angell. Signature of ergodicity in the dynamic response of amorphous systems. *Physical Review B*, 46(9):57875790, 1992.

[27] R. V. Chamberlin and B. F. Davis. Modified bose-einstein and fermi-dirac statistics if excitations are localized on an intermediate length scale: Applications to non-debye specific heat. *Physical Review E*, 88(4):042108, Jul 2013.

[28] R. V. Chamberlin and D. M. Nasir. $1/f$ noise from the laws of thermodynamics for finite-size fluctuations. *Physical Review E*, 90(1):012142, Jul 2014.

[29] R. V. Chamberlin, J. V. Vermaas, and G. H. Wolf. Beyond the boltzmann factor for corrections to scaling in ferromagnetic materials and critical fluids. *The European Physical Journal B*, 71(1):16, Nov 2009.

[30] Z. Chen and C. C. Yu. Measurement-noise maximum as a signature of a phase transition. *Physical Review Letters*, 98(5):057204, 2007.

[31] Z. Chen and C. C. Yu. Comparison of ising spin glass noise to flux and inductance noise in squids. *Physical Review Letters*, 104(24):247204, 2010.

[32] S. Choi, D.-H. Lee, S. G. Louie, and J. Clarke. Localization of metal-induced gap states at the metal-insulator interface: Origin of flux noise in squids and superconducting qubits. *Physical Review Letters*, 103(19):197001, Mar 2009.

[33] C. J. Christensen and G. L. Pearson. Spontaneous resistance fluctuations in carbon microphones and other granular resistances. *Bell System Technical Journal*, 15(2):197223, 1936.

[34] F. Cichos, C. von Borczyskowski, and M. Orrit. Power-law intermittency of single emitters. *Current Opinion in Colloid & Interface Science*, 12(6):272–284, Dec 2007.

[35] J. Clarke and F. K. Wilhelm. Superconducting quantum bits. *Nature*, 453(7198):10311042, 2008.

[36] M. Creutz. Microcanonical monte carlo simulation. *Physical Review Letters*, 50:1411–1414, May 1983.

[37] G. E. Crooks. Entropy production fluctuation theorem and the nonequilibrium work relation for free energy differences. *Physical Review E*, 60(3):27212726, Jan 1999.

[38] B. F. Davis and R. V. Chamberlin. $1/f$ noise from a finite entropy bath: comparison with flux noise in squids. *Journal of Statistical Mechanics: Theory and Experiment*, 2018(10):103206, 2018.

[39] A. De. Ising-glauber spin cluster model for temperature-dependent magnetization noise in squids. *Physical Review Letters*, 113(21):217002, 2014.

[40] D. Drung, J. Beyer, J.-H. Storm, M. Peters, and T. Schurig. Investigation of low-frequency excess flux noise in dc squids at mk temperatures. *IEEE Transactions on Applied Superconductivity*, 21(3):340344, 2011.

[41] F. K. Du Pré. A suggestion regarding the spectral density of flicker noise. *Physical Review*, 78(5):615615, 1950.

[42] P. Dutta, P. Dimon, and P. M. Horn. Energy scales for noise processes in metals. *Physical Review Letters*, 43(9):646649, 1979.

[43] P. Dutta and P. M. Horn. Low–frequency fluctuations in solids: $1/f$ noise. *Reviews of Modern Physics*, 53(3):497516, 1981.

[44] J. W. Eberhard and P. M. Horn. Excess $(1/f)$ noise in metals. *Physical Review B*, 18(12):66816693, 1978.

[45] L. Faoro and L. B. Ioffe. Microscopic origin of low-frequency flux noise in josephson circuits. *Physical Review Letters*, 100(22):227005, May 2008.

[46] S. Ferraro, M. Manzini, A. Masoero, and E. Scalas. A random telegraph signal of mittag-leffler type. *Physica A: Statistical Mechanics and its Applications*, 388(19):3991–3999, Oct 2009.

[47] R. P. Feynman, R. B. Leighton, and M. Sands. *The Feynmann lectures on physics*, volume 1. Addison-Wesley, 1966.

[48] P. A. Frantsuzov, S. Volkán-Kascó, and B. Jankó. Universality of the fluorescence intermittency in nanoscale systems: experiment and theory. *Nano Letters*, 13(2):402–408, Feb 2013.

[49] R. J. Glauber. Time-dependent statistics of the ising model. *Journal of Mathematical Physics*, 4(2):294–307, 1963.

[50] C. Godrèche and J. Luck. Statistics of the occupation time of renewal processes. *Journal of Statistical Physics*, 104(3/4):489–524, 2001.

[51] D. Halford. A general mechanical model for $|f|^{\alpha}$ spectral density random noise with special reference to flicker noise $1/|f|$. *Proceedings of the IEEE*, 56(3), Mar 1968.

[52] D. J. V. Harlingen, T. L. Robertson, B. L. T. Plourde, P. A. Reichardt, T. A. Crane, and J. Clarke. Decoherence in josephson-junction qubits due to critical-current fluctuations. *Physical Review B*, 70(6), Aug 2004.

[53] W. Hastings. Monte carlo sampling methods using markov chains and their applications. *Biometrika*, 57(1):97–109, Apr 1970.

[54] J. Herault, F. Pétrélis, and S. Fauve. Experimental observation of $1/f$ noise in quasi-bidimensional turbulent flows. *Europhysics Letters (EPL)*, 111(4):44002, 2015.

[55] T. L. Hill. *Statistical–mechanical ensembles*, chapter 1, pages 3–6. Dover Publications, 1986.

[56] J. B. Johnson. The schottky effect in low frequency circuits. *Physical Review*, 26(1):7185, 1925.

[57] J. B. Johnson. Thermal agitation of electricity in conductors. *Physical Review*, 32(1):97–109, 1928.

[58] K. Kakuyanagi, T. Meno, S. Saito, H. Nakano, K. Semba, H. Takayanagi, F. Deppe, and A. Shnirman. Dephasing of a superconducting flux qubit. *Physical Review Letters*, 98(4), Jan 2007.

[59] C.-C. Kalmbach, F. J. Ahlers, J. Schurr, A. Müller, J. Feilhauer, M. Kruskopf, K. Pierz, F. Hohls, and R. J. Haug. Nonequilibrium mesoscopic conductance fluctuations as the origin of $1/f$ noise in epitaxial graphene. *Physical Review B*, 94:205430, Nov 2016.

[60] R. Kawai, J. M. R. Parrondo, and C. V. D. Broeck. Dissipation: The phase-space perspective. *Physical Review Letters*, 98(8), Feb 2007.

[61] K. Kawasaki. *Phase Transitions and Critical Phenomena*, volume 2. Academic Press, 1972.

[62] S. Kempf, A. Ferring, and C. Enss. Towards noise engineering: Recent insights in low-frequency excess flux noise of superconducting quantum devices. *Applied Physics Letters*, 109(16):162601, 2016.

[63] T. Kim, R. Chamberlin, and J. Bird. Large magnetoresistance of nickel-silicide nanowires: Non-equilibrium heating of magnetically-coupled dangling bonds. *Nano Letters*, 13:1106–1110, 2013.

[64] R. Koch, J. Clarke, J. Martinis, W. Goubau, C. Pegrum, and D. Harlingen. Investigation of $1/f$ noise in tunnel junction dc squids. *IEEE Transactions on Magnetics*, 19(3):449452, May 1983.

[65] S. Kogan. $1/f$ *noise and random telegraph noise*, chapter 8, pages 203–286. Cambridge Univ. Press, 2009.

[66] S. Kogan. *Basic concepts of the theory of random processes*, chapter 1, pages 1–47. Cambridge Univ. Press, 2009.

[67] S. Kogan and K. Nagaev. On the low–frequency current noise in metals. *Solid State Communications*, 49(4):387389, 1984.

[68] D. Krapf. Nonergodicity in nanoscale electrodes. *Phys. Chem. Chem. Phys.*, 15(2):459465, 2013.

[69] P. Kumar, S. Sendelbach, M. A. Beck, J. W. Freeland, Z. Wang, H. Wang, C. C. Yu, R. Q. Wu, D. P. Pappas, R. McDermott, and et al. Origin and reduction of $1/f$ magnetic flux noise in superconducting devices. *Physical Review Applied*, 6:041001, 2016.

[70] J. Kunzler, L. Walker, and J. Galt. Adiabatic demagnetization and specific heat in ferrimagnets. *Physical Review*, 119(5):1106–1110, 1960.

[71] S. LaForest and R. D. Sousa. Flux-vector model of spin noise in superconducting circuits: Electron versus nuclear spins and role of phase transition. *Physical Review B*, 92(5):054502, Mar 2015.

[72] T. Lanting, M. H. Amin, A. J. Berkley, C. Rich, S.-F. Chen, S. Laforest, and R. D. Sousa. Evidence for temperature-dependent spin diffusion as a mechanism of intrinsic flux noise in squids. *Physical Review B*, 89(1):014503, Jul 2014.

[73] N. Leibovich and E. Barkai. Conditional $1/f^{\alpha}$ noise: From single molecules to macroscopic measurement. *Physical Review E*, 96:032132, Sep 2017.

[74] M. Li and W. Zhao. Review article: On $1/f$ noise. *Mathematical Problems in Engineering*, 2012:123, 2012.

[75] W. Li and K. Kaneko. Long–range correlation and partial $1/f^{\alpha}$ spectrum in a noncoding dna sequence. *Europhysics Letters (EPL)*, 17(7):655660, 1991.

[76] S. Lowen and M. Teich. Fractal renewal processes generate $1/f$ noise. *Physical Review E*, 47(2):992–1001, Feb 1993.

[77] A. Ludviksson, R. Kree, and A. Schmid. Low–frequency $1/f$ fluctuations of resistivity in disordered metals. *Physical Review Letters*, 52(11):950953, 1984.

[78] R. Lustig. Microcanonical monte carlo simulation of thermodynamic properties. *The Journal of Chemical Physics*, 109:8816–8828, 11 1998.

[79] S. Machlup. Noise in semiconductors: Spectrum of a twoparameter random signal. *Journal of Applied Physics*, 25(3):341343, 1954.

[80] B. Mandelbrot. Some noises with i/f spectrum, a bridge between direct current and white noise. *IEEE Transactions on Information Theory*, 13(2):289298, 1967.

[81] B. B. Mandelbrot. *The Fractal Geometry of Nature*. W. H. Freeman and Co., 1983.

[82] B. B. Mandelbrot. *Multifractals and* $1/f$ *noise: wild self-affinity in physics (1963-1976)*. Springer-Verlag, 1999.

[83] B. B. Mandelbrot and J. R. Wallis. Noah, joseph, and operational hydrology. *Water Resources Research*, 4(5):909918, 1968.

[84] G. Margolin and E. Barkai. Nonergodicity of a time series obeying lévy statistics. *Journal of Statistical Physics*, 122(1):137–167, Jan 2006.

[85] G. Marsaglia. Choosing a point from the surface of a sphere. *The Annals of Mathematical Statistics*, 43(2):645–646, 1972.

[86] M. Matsumoto and T. Nishimura. Mersenne twister: A 623-dimensionally equidistribute uniform pseudo-random number generator. *ACM Transactions on Modeling and Computer Simulation*, 8(1):3–30, Jan 1998.

[87] A. L. McWhorter. $1/f$ *Noise and germanium surface properties*, page 20728. Univ. of Philadelphia Press, 1957.

[88] N. D. Mermin and H. Wagner. Absence of ferromagnetism or antiferromagnetism in one- or two-dimensional isotropic heisenberg models. *Physical Review Letters*, 17(26):13071307, 1966.

[89] N. Metropolis, A. W. Rosenbluth, M. N. Rosenbluth, and A. H. Teller. Equation of state calculations by fast computing machines. *The Journal of Chemical Physics*, 21(6):10871092, 1953.

[90] Y. Miyamoto, K. Fukao, H. Yamao, and K. Sekimoto. Memory effect on the glass transition in vulcanized rubber. *Physical Review Letters*, 88(22):225504, Jun 2002.

[91] W. J. Moore. Statistical studies of $1/f$ noise from carbon resistors. *Journal of Applied Physics*, 45(4):18961901, 1974.

[92] J. Müller, S. Von Molnr, Y. Ohno, and H. Ohno. Decomposition of $1/f$ noise inalxga1xas/gaashall devices. *Physical Review Letters*, 96(18), 2006.

[93] M. Nelkin and A. M. S. Tremblay. Deviation of $1/f$ voltage fluctuations from scale–similar gaussian behavior. *Journal of Statistical Physics*, 25(2):253268, 1981.

[94] M. Niemann, H. Kantz, and E. Barkai. Fluctuations of $1/f$ noise and the low–frequency cutoff paradox. *Physical Review Letters*, 110(14), 2013.

[95] H. Nyquist. Thermal agitation of electric charge in conductors. *Physical Review*, 32(1):110113, 1928.

[96] E. Paladino, L. Faoro, A. D'arrigo, and G. Falci. Decoherence and $1/f$ noise in josephson qubits. *Physica E: Low–dimensional Systems and Nanostructures*, 18(1–3):2930, 2002.

[97] E. Paladino, Y. Galperin, G. Falci, and B. Altshuler. $1/f$ noise: Implications for solid–state quantum information. *Reviews of Modern Physics*, 86(2):361418, 2014.

[98] B. Pellegrini, R. Saletti, P. Terreni, and M. Prudenziati. $1/f^{\gamma}$ noise in thick–film resistors as an effect of tunnel and thermally activated emissions, from measures versus frequency and temperature. *Physical Review B*, 27(2):12331243, 1983.

[99] M. Pelton, G. Smith, N. F. Scherer, and R. A. Marcus. Evidence for a diffusion–controlled mechanism for fluorescence blinking of colloidal quantum dots. *Proceedings of the National Academy of Sciences*, 104(36):1424914254, 2007.

[100] S. Pottorf, V. Patel, and J. E. Lukens. Temperature dependence of critical current fluctuations in nb/alox/nb josephson junctions. *Applied Physics Letters*, 94(4):043501, Jan 2009.

[101] W. E. Purcell. Variance noise spectra of $1/f$ noise. *Journal of Applied Physics*, 43(6):28902895, 1972.

[102] K. S. Ralls, W. J. Skocpol, L. D. Jackel, R. E. Howard, L. A. Fetter, R. W. Epworth, and D. M. Tennant. Discrete resistance switching in submicrometer silicon inversion layers: Individual interface traps and low–frequency (1/f?) noise. *Physical Review Letters*, 52(3):228231, 1984.

[103] P. Refregier, M. Ocio, and H. Bouchiat. Equilibrium magnetic fluctuations in spin glasses: Temperature dependence and deviations from $1/f$ behaviour. *Europhysics Letters (EPL)*, 3(4):503510, 1987.

[104] S. Rice. Mathematical analysis of random noise. *The Bell System Technical Journal*, 23(3):282–332, 1944.

[105] R. Richert. Heterogeneous dynamics in liquids: fluctuations in space and time. *Journal of Physics: Condensed Matter*, 14(23), 2002.

[106] K. F. Riley, M. P. Hobson, S. J. Bence, and u. u. undefined. *Mathematical methods for physics and engineering*. Cambridge Univ. Press, 2014.

[107] M. A. Rodríguez. Class of perfect $1/f$ noise and the low–frequency cutoff paradox. *Physical Review E*, 92(1), 2015.

[108] C. T. Rogers and R. A. Buhrman. Composition of $1/f$ noise in metal-insulator-metal tunnel junctions. *Physical Review Letters*, 53(13):12721275, Sep 1984.

[109] C. T. Rogers and R. A. Buhrman. Nature of single-localized-electron states derived from tunneling measurements. *Physical Review Letters*, 55(8):859862, Aug 1985.

[110] E. V. Russell and N. E. Israeloff. Direct observation of molecular cooperativity near the glass transition. *Nature*, 408:695698, 2000.

[111] A. D. Rutenberg. Nonequilibrium phase ordering with a global conservation law. *Physical Review E*, 54:972–973, Jul 1996.

[112] S. Sadegh, E. Barkai, and D. Krapf. $1/f$ noise for intermittent quantum dots exhibits non–stationarity and critical exponents. *New Journal of Physics*, 16(11):113054, 2014.

[113] F. Schedin, A. K. Geim, S. V. Morozov, E. W. Hill, P. Blake, M. I. Katsnelson, and K. S. Novoselov. Detection of individual gas molecules adsorbed on graphene. *Nature Materials*, 6(9):652655, 2007.

[114] M. Schmelz, R. Stolz, V. Zakosarenko, S. Anders, L. Fritzsch, H. Roth, and H.-G. Meyer. Highly sensitive miniature squid magnetometer fabricated with cross-type josephson tunnel junctions. *Physica C: Superconductivity*, 476:7780, 2012.

[115] W. Schottky. Über spontane stromschwankungen in verschiedenen elektrizittsleitern. *Annalen der Physik*, 362(23):541567, 1918.

[116] W. Schottky. Small–shot effect and flicker effect. *Physical Review*, 28(1):74103, 1926.

[117] K. Sekimoto. Concept of heat on mesoscopic scales. *Stochastic Energetics Lecture Notes in Physics*, 2009.

[118] S. Sendelbach, D. Hover, A. Kittel, M. Mck, J. M. Martinis, and R. Mcdermott. Magnetism in squids at millikelvin temperatures. *Physical Review Letters*, 100(22):227006, May 2008.

[119] S. Sendelbach, D. Hover, M. Mck, and R. Mcdermott. Complex inductance, excess noise, and surface magnetism in dc squids. *Physical Review Letters*, 103(11):117001, Sep 2009.

[120] L. Silvestri, L. Fronzoni, P. Grigolini, and P. Allegrini. Event–driven power–law relaxation in weak turbulence. *Physical Review Letters*, 102(1), 2009.

[121] Z. Siwy and A. Fuliski. Origin of $1/f^{\alpha}$ noise in membrane channel currents. *Physical Review Letters*, 89(15), 2002.

[122] R. M. M. Smeets, U. F. Keyser, N. H. Dekker, and C. Dekker. Noise in solid–state nanopores. *Proceedings of the National Academy of Sciences*, 105(2):417421, 2008.

[123] R. D. Sousa. Dangling–bond spin relaxation and magnetic $1f$ noise from the amorphous–semiconductor/oxide interface: Theory. *Physical Review B*, 76(24), 2007.

[124] M. Stoisiek and D. Wolf. Recent investigations on the stationarity of $1/f$ noise. *Journal of Applied Physics*, 47(1):362364, 1976.

[125] O. Takeshi and K. Sekimoto. Internal stress in a model elastoplastic fluid. *Physical Review Letters*, 95(10):108301, Sep 2005.

[126] K. A. Takeuchi. $1/f^{\alpha}$ power spectrum in the kardar-parisi-zhang universality class. *Journal of Physics A: Mathematical and Theoretical*, 50:264006, June 2017.

[127] J. L. Tandon and H. R. Bilger. $1/f$ noise as a nonstationary process: Experimental evidence and some analytical conditions. *Journal of Applied Physics*, 47(4):16971701, 1976.

[128] A. Van Der Ziel. On the noise spectra of semi–conductor noise and of flicker effect. *Physica*, 16(4):359372, 1950.

[129] J. Van Kranendonk and J. H. Van Vleck. Spin waves. *Reviews of Modern Physics*, 30:1–23, Jan 1958.

[130] R. F. Voss. Linearity of $1/f$ noise mechanisms. *Physical Review Letters*, 40(14):913916, 1978.

[131] R. F. Voss and J. Clarke. $1/f$ noise in music and speech. *Nature*, 258(5533):317318, 1975.

[132] R. F. Voss and J. Clarke. Flicker $(1/f)$ noise: Equilibrium temperature and resistance fluctuations. *Physical Review B*, 13(2):556573, 1976.

[133] C.-Y. Wang and M. D. Ediger. Spatially heterogeneous dynamics in deeply supercooled liquids. *AIP Conference Proceedings*, 1999.

[134] H. Wang, C. Shi, J. Hu, S. Han, C. C. Yu, and R. Wu. Candidate source of flux noise in squids: Adsorbed oxygen molecules. *Physical Review Letters*, 115(7):077002, 2015.

[135] N. W. Watkins. On the continuing relevance of mandelbrot's non-ergodic fractional renewal models of 1963 to 1967. *European Physics Journal B*, 90:241–250, 2017.

[136] M. B. Weissman. $1/f$ noise and other slow, nonexponential kinetics in condensed matter. *Reviews of Modern Physics*, 60(2):537571, 1988.

[137] M. B. Weissman. What is a spin glass? a glimpse via mesoscopic noise. *Reviews of Modern Physics*, 65(3):829839, 1993.

[138] F. C. Wellstood, C. Urbina, and J. Clarke. Lowfrequency noise in dc superconducting quantum interference devices below 1 k. *Applied Physics Letters*, 50(12):772774, 1987.

[139] J. Wu and C. C. Yu. Modeling flux noise in squids due to hyperfine interactions. *Physical Review Letters*, 108(24):247001, Nov 2012.

[140] E. Yamamoto, T. Akimoto, Y. Hirano, M. Yasui, and K. Yasuoka. $1/f$ fluctuations of amino acids regulate water transportation in aquaporin 1. *Physical Review E*, 89(2), 2014.

[141] E. Yamamoto, T. Akimoto, M. Yasui, and K. Yasuoka. Origin of $1/f$ noise in hydration dynamics on lipid membrane surfaces. *Scientific Reports*, 5(1), 2015.

[142] F. Yoshihara, K. Harrabi, A. O. Niskanen, Y. Nakamura, and J. S. Tsai. Decoherence of flux qubits due to $1/f$ flux noise. *Physical Review Letters*, 97(16), 2006.

[143] C. C. Yu. Why study noise due to two level systems: A suggestion for experimentalists. *Journal of Low Temperature Physics*, 137(3/4):251265, 2004.

APPENDIX A

ORIGINAL PUBLICATION: FLUCTUATION THEOREMS AND $1/F$ NOISE FROM A SIMPLE MATRIX

A.1 Introduction

Much of the work presented in § 3 was published under the title "Fluctuations theorems and $1/f$ noise from a simple matrix" in *The European Physical Journal B*. The complete citation is listed under reference [25]. This work was completed in collaboration, in the order appearing in the original publication, by Ralph V. Chamberlin, Sumiyoshi Abe, Bryce F. Davis (myself), Priscilla E. Greenwood, and Andrew S.H. Shevchuk. The coauthors have granted their permission to have this work included in this dissertation.

Simulations, the creation of figures, and writing were primarily done by Ralph Chamberlin. Priscilla Greenwood provided the initial inspiration to cast the model in the form of a simple matrix. Priscilla Greenwood and Sumiyoshi Abe aided in the language and interpretation involving Markov processes and information theory. Algorithms for simulating the model and the structure of the simulation matrix were developed by Ralph Chamberlin and myself. Ralph Chamberlin, Andrew Shevchuk, and myself contributed to the physical interpretation of the results of simulations.

Specifically, my contribution was in the development of the simulation algorithm and structure of the simulation matrix, allowing a system which conserves entropy at each step to be simulated explicitly. This was done through discussions and code testing with Ralph Chamberlin. I also contributed to the physical interpretation of the results, most notably the distribution of transition frequencies and the identity of the cutoff frequency of $1/f$ noise. This was done by recasting the model as a discrete Markov process, developing the stochastic matrix, finding its eigenvalues, relating them to the transition frequencies of the model, and relating these to spectral features seen in the power spectral densities obtained from simulations.

The original publication is included below.

Eur. Phys. J. B (2016) 89: 185
DOI: 10.1140/epjb/e2016-70242-0

THE EUROPEAN PHYSICAL JOURNAL B

Regular Article

Fluctuation theorems and 1/f noise from a simple matrix

Ralph V. Chamberlin[1,a], Sumiyoshi Abe[2,3], Bryce F. Davis[1], Priscilla E. Greenwood[4], and Andrew S.H. Shevchuk[1]

[1] Department of Physics, Arizona State University, Tempe, AZ 85287-1504, USA
[2] Department of Physical Engineering, Mie University, 514-8507 Mie, Japan
[3] Institute of Physics, Kazan Federal University, 420008 Kazan, Russia
[4] Department of Mathematics, University of British Columbia, Vancouver, BC V6T 1Z2, Canada

Received 21 April 2016 / Received in final form 25 May 2016
Published online 5 September 2016 – © EDP Sciences, Società Italiana di Fisica, Springer-Verlag 2016

Abstract. Here we present a model for a small system combined with an explicit entropy bath that is comparably small. The dynamics of the model is defined by a simple matrix, M. Each row of M corresponds to a macrostate of the system, e.g. net alignment, while the elements in the row represent microstates. The constant number of elements in each row ensures constant entropy, which allows reversible fluctuations, similar to information theory where a constant number of bits allows reversible computations. Many elements in M come from the microstates of the system, but many others come from the bath. Bypassing the bath states yields fluctuations that exhibit standard white noise; whereas with bath states the power spectral density varies as $S(f) \propto 1/f$ over a wide range of frequencies, f. Thus, the explicit entropy bath is the mechanism of $1/f$ noise in this model. Both forms of the model match Crooks' fluctuation theorem exactly, indicating that the theorem applies not only to infinite reservoirs, but also to finite-sized baths. The model is used to analyze measurements of $1/f$-like noise from a sub-micron tunnel junction.

Fluctuation theorems [1–5] provide fundamental formulas that have been used to describe the thermal properties of small systems that may be far from equilibrium. These formulas have been applied to the out-of-equilibrium behavior of several small systems including: stretching of RNA molecules [6], information-to-energy conversion [7–9], and particles driven by an external field [10,11]. Of course the theorems should also apply to fluctuations of small systems around equilibrium, but what if the thermal bath is similarly small? Nanothermodynamics was originally developed to describe the thermal properties of a large ensemble of small systems [12,13], which has been extended to treat the dynamics of individual small systems with their own local bath [14,15]. Here we describe a model based on a single matrix M that contains a maximum number of system states Ω_0, with a comparable number of bath states. We show that if the bath states are bypassed, the matrix model yields a power spectral density that exhibits standard white noise and agrees with one value from the Crooks fluctuation theorem [1]. However if the explicit bath states are included, the matrix model yields $1/f$-like noise and agrees with a different value from the Crooks theorem. Finally, the matrix model is used to analyze measurements of voltage noise from a sub-micron-sized tunnel junction [16].

The matrix model is based on information theory [17], adapted to treat thermal fluctuations. The matrix model includes bath states that maintain maximum entropy during fluctuations of a binary system, similar to "garbage" states in information theory. Neighboring rows of M are connected by an Ω_0-to-Ω_0 map that yields reversible fluctuations, similar to the one-to-one map that yields reversible computations (e.g. Fig. 3a of Ref. [17]). Specific Hamiltonians that may accomplish the transfer of information are discussed in references [17,18], but here we focus on the general principle that entropy must remain maximized if fluctuations are to be reversible. Experimental evidence establishing that information is a physical quantity comes from the minimum work necessary to erase a single bit [9].

All system states in the matrix model are degenerate, with an explicit local bath that is comparable to system size and depends on system entropy, thereby violating multiple assumptions required for thermal properties to be governed solely by Boltzmann's factor [19]. Thus, the resulting thermal fluctuations differ from those found from standard statistical mechanics and stochastic thermodynamics [20], which are based on Boltzmann's factor alone. Indeed, because all system states are degenerate, the thermal properties are governed entirely by entropy, similar to microcanonical behavior. And as expected, finite-sized fluctuations depend on the ensemble. To compare: Boltzmann's factor favors low *energy* states of the system when *energy* is transferred to an infinite heat reservoir; whereas the matrix model favors low *entropy* states of the system when *entropy* is transferred to the finite

[a] e-mail: ralph.chamberlin@asu.edu

entropy bath. Non-degenerate states in the system can be accommodated by combining Boltzmann's factor from energy transfer with a nonlinear correction from entropy transfer [14,15], but here we emphasize that the entropy-transfer mechanism is the crucial ingredient for $1/f$-like noise. Using Boltzmann's factor for energy transfer generally yields deviations from pure $1/f$ behavior [21].

Thermal fluctuations exhibiting $1/f$-like noise were first reported in 1925 [22,23]. Similar $1/f$-like noise has since been found in virtually all types of materials, as well as in electronic, magnetic, and quantum devices [24–26], and even in biological systems [27,28] and human preferences [29,30]. No single mechanism can explain all details in the dynamics of such diverse systems. Nevertheless, an Ising-like model has been found to simulate measured $1/f$-like noise, including temperature-dependent slopes shown by various metal films, and tri-modal histograms exhibited by spin glasses and nanopore systems [21]. Here we study the basic cause of $1/f$ noise in the Ising-like model. The key ingredient is a nonlinear correction to Boltzmann's factor that can be justified in several ways [14,15,31,32]. One mechanism comes from conservation of energy by including Hill's subdivision potential to treat non-extensive contributions from finite-sized fluctuations. Another comes from the statistics of indistinguishable particles. Here we focus on a third mechanism, where maximum entropy is maintained by transferring entropy between the system and its bath.

Consider an isolated small system that fluctuates into a low-entropy state. Although seeming to violate the 2nd law of thermodynamics, at least three possible explanations have been proposed. Total entropy may decrease temporarily if the system is small enough [2,33]. The time-averaged Gibbs entropy should be used instead of the time-dependent Boltzmann expression [34,35]. Alternatively, because information theory [7,8] requires a transfer of entropy when knowledge about the system changes, a decrease in entropy of the system implies an increase in entropy elsewhere, consistent with measurements of bit erasure [9]. Information theory is also consistent with using Lagrange multipliers for higher moments that maximize the total entropy of a fluctuating system and its environment. Here we treat the transferred entropy exactly by including explicit bath states that slow down the dynamics of the system.

For simplicity, assume that the system contains an even number (N) of binary degrees of freedom ("spins"), so that each spin may be up (+1) or down (–1). If the alignment of the system is unknown, then the total multiplicity is always $\Omega_{All} = 2^N$. Whereas if the net alignment (m) is known, then the multiplicity of each macrostate is given by the binomial coefficient $\Omega_m = N!/\{[1/2(N+m)]![1/2(N-m)]!\}$. Using Boltzmann's definition, the alignment entropy of the system is $S_m = k_B \ln(\Omega_m)$. The maximum multiplicity occurs when spins are half-up and half-down: $\Omega_0 = N!/[(1/2N)!]^2$, yielding the maximum entropy $S_0 = k_B \ln(\Omega_0)$. Fluctuations reduce this alignment entropy, $S_m \leqslant S_0$. The matrix model is based on the assumption that if $S_m < S_0$ because

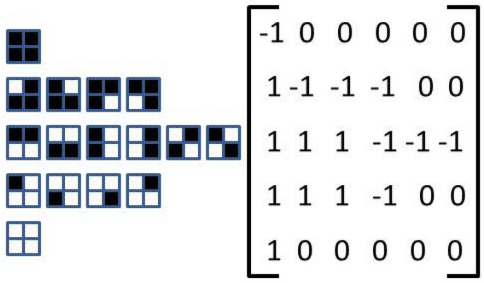

Fig. 1. System states (left) and rectangular matrix M (right) for an $N = 4$ spin system. Non-zero elements in M correspond to system states, with the fraction of $M_{ij} = +1$ or –1 from the probability that inverting a spin at random will increase or decrease the alignment, respectively. Elements with $M_{ij} = 0$ are explicit bath states that pause the dynamics of the system.

$m \neq 0$, an amount of entropy $S_0 - S_m$ must have been transferred from the system to its bath. Thus, the total entropy of the system plus bath remains maximized at S_0, which never decreases.

The dynamics of the system is governed by a rectangular matrix, M (see Fig. 1). (Note that the standard transition matrix of the alignment process is easily obtained from M). The elements of M are M_{ij}, with $N+1$ rows ($-N/2 \leqslant i \leqslant N/2$) from the net alignments of the system $m = 2i$, and Ω_0 columns ($1 \leqslant j \leqslant \Omega_0$) from all microstates of the system plus bath. The middle row of M contains Ω_0 non-zero elements ($M_{0j} = \pm 1$), one for each configuration of the unaligned system, with no states for the bath. The sign of the element governs how the alignment of the system will change: $M_{0j} = +1$ if m is to increase and $M_{0j} = -1$ if m is to decrease. Thus, in the middle row there are $\Omega_0/2$ elements having $M_{0j} = +1$, and an equal number having $M_{0j} = -1$. Other rows have $\Omega_m < \Omega_0$ non-zero elements, from the number of system states for $m \neq 0$. The remaining $\Omega_0 - \Omega_m$ elements in each row have $M_{ij} = 0$, representing bath states. The system states in each row, $M_{ij} = +1$ or –1, have the appropriate ratio for the probability that the alignment will increase or decrease, respectively. Specifically, there are $\Omega_m[1/2(N-m)/N] = (N-1)!/\{[1/2(N+m)]![1/2(N-m)-1]!\}$ elements having $M_{ij} = +1$; and $\Omega_m[1/2(N+m)/N] = (N-1)!/\{[1/2(N+m)-1]![1/2(N-m)]!\}$ elements having $M_{ij} = -1$. Adding extra 0 elements, as might be expected for large baths in contact with small systems, lowers the frequency where the system starts $1/f$-like behavior, but does not alter the general features of the $1/f$ regime. Using Stirling's formula, the ratio of bath states to system states is: $\frac{2(N+1)}{\sqrt{2\pi N}} - 1$. Thus, for $N \geqslant 6$ there are more bath states than system states; but the square-root dependence keeps the ratio relatively small, so that even for $N = 24$ there are only about 3 times as many bath states as system states. Because the number of bath states depends on system entropy, our model yields fluctuations that differ from most other treatments that are based solely on Boltzmann's factor that assumes an infinite heat reservoir.

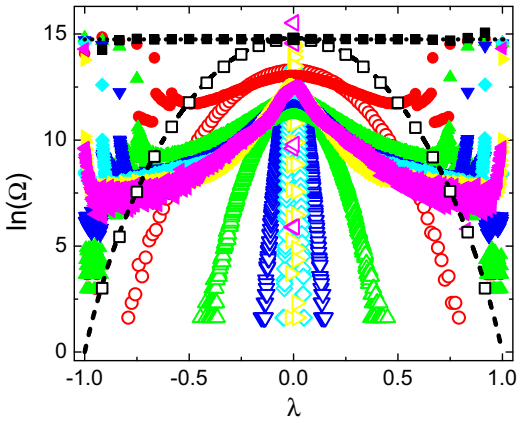

Fig. 2. Histograms, converted to the logarithm of multiplicity, from the dynamics of the $N = 24$ matrix. Solid (open) symbols are from simulations with (without) explicit bath states. Different shapes come from different averaging times, from $\tau = 1$ to 10^6 steps. The most-probable values in the wings come from the allowed alignments, with lower values from averaging between them.

The dynamics of the model involves a time step (dt) that has two parts. In part one, an element is chosen at random from the current row of M. In part two, this element is used to determine how the row might change: if $M_{ij} = 0$ there is no change $j \to j$; if $M_{ij} = +1$ the row increases by one $j \to j+1$; if $M_{ij} = -1$ the row decreases by one $j \to j-1$. In other words, all possible changes in alignment are determined by $m(t+dt) = m(t)+2M_{ij}$. The dynamics continues by repeating parts one and two. For standard Monte-Carlo simulations without explicit bath states, part one is modified by choosing only non-zero elements (states with $M_{ij} = 0$ are bypassed), so that $m(t)$ changes every step. To realistically simulate measurements over a wide dynamic range we use an averaging time τ. Specifically if $\tau = 1$, $m(t)$ is recorded every step, if $\tau = 10$, $m(t)$ is averaged over 10 steps before recording, etc. We use averaging times up to $\tau = 10^6$ steps, with 2^{17} data points per simulation, yielding up to 1.31×10^{11} steps per simulation. Smoother curves are obtained by simulating the system ∼20 times using different initial conditions, but intrinsic noise is retained by analyzing each simulation separately before averaging. To compare systems of different size we use relative alignment, $\lambda(t) = m(t)/N$.

The solid (open) symbols in Figure 2 come from histograms of $\lambda(t)$ with (without) bath states, from the matrix having $N = 24$. Each point in the histogram gives the likelihood of the alignment. Thus, when $\tau = 1$ (to avoid averaging between alignments) a logarithmic plot (Fig. 2) yields the entropy as a function of alignment. Without explicit bath states (open squares), the $\tau = 1$ histogram matches the binomial distribution (dashed curve), as expected for non-interacting binary degrees of freedom with no local bath. For $\tau \gg 1$ this discrete binomial evolves to a continuous Gaussian, as expected from the central-limit theorem. The width of the Gaussian decreases with increasing τ, and approaches a delta function for very large τ, as expected from the law of large numbers. Indeed, after the system has had time to explore all states, $\tau \gg N$, a Gaussian fit $[\ln(\Omega) \sim -\lambda^2/2\sigma^2]$ to the central part of the peak yields a variance of $\sigma^2 \approx 0.95/\tau$, so that $\sigma^2 \approx 9.5 \times 10^{-7}$ for $\tau = 10^6$. Such inverse-τ dependence is expected for long-time averaging of normal fluctuations. In contrast, simulations with explicit bath states yield constant entropy for $\tau = 1$ (horizontal dotted line), evolving into a broad Gaussian with excess wings for $\tau \gg 1$. Again fitting the central part of the peak to a Gaussian, the variance is $\sigma^2 \approx 7.7 \times 10^{-3}$ for $\tau = 10^6$, which extrapolates towards $\sigma^2 \sim 3.2 \times 10^{-3}$ as $\tau \to \infty$. However, because the range of alignments is limited ($-1 \leqslant \lambda \leqslant +1$), this central Gaussian must also eventually approach a delta function for $\tau \gg 2^N = 1.67 \times 10^7$.

Crooks' fluctuation theorem is consistent with both forms of behavior shown in Figure 2. Furthermore, since both forms involve all states explicitly, Crooks' fluctuation theorem is a consequence of detailed balance. First consider the open squares for fluctuations of the system without explicit bath states. Note that because the states of the system are degenerate, entropy alone governs all thermal properties, so that fluctuations are identical in the microcanonical ensemble with no bath, and canonical ensemble with infinite heat reservoir. Let the "forward" step change the alignment from m to $m+2$, and the "reverse" step change $m+2$ to m. From the fraction of non-zero elements in row $i = m/2$ having $M_{ij} = +1$, the forward step has probability $P_m(+2) = {}^1\!/\!_2(N-m)/N$, the reverse step has $P_{m+2}(-2) = {}^1\!/\!_2(N+m+2)/N$, and their ratio is $R_S = P_m(+2)/P_{m+2}(-2) = (N-m)/(N+m+2)$. The Crooks' fluctuation theorem states that this ratio should come from the difference in entropy: $R_S = \exp[(S_{m+2} - S_m)/k_B]$. Indeed, using the entropy of the system from the binomial coefficient yields $\exp[(S_{m+2} - S_m)/k_B] = (N-m)/(N+m+2)$, matching the ratio R_S as expected from the fluctuation theorem. Here $R_S \neq 1$ implies irreversible work must be done to change the net alignment of the system [4].

Now consider fluctuations of the system plus explicit entropy bath. For large systems with $m \approx \pm N$ the dynamics is very slow because the system plus bath spends most of its time exploring bath states that do not change m. Specifically, the probability of a forward step is reduced by a factor $\Omega_m/\Omega_0 = [({}^1\!/\!_2N)!]^2/\{[{}^1\!/\!_2(N+m)]![{}^1\!/\!_2(N-m)]!\}$, with the reverse step similarly reduced $\Omega_{m+2}/\Omega_0 = [({}^1\!/\!_2N)!]^2/\{[{}^1\!/\!_2(N+m)+1]![{}^1\!/\!_2(N-m)-1]!\}$. Note that the ratio of these factors is $\Omega_m/\Omega_{m+2} = (N+m+2)/(N-m)$, so that the ratio of forward to reverse steps is simply $R_{S+B} = R_S\Omega_m/\Omega_{m+2} = 1$. Here $R_{S+B} = 1$ implies that the system may change its net alignment reversibly [4]. Thus, from Crooks' fluctuation theorem the total entropy of the system plus bath should be constant, as ensured by the constant number of elements in each row and shown by the solid squares in Figure 2.

The solid symbols in Figure 3 show the power spectral density of the alignment process, $S(f)$. The data come

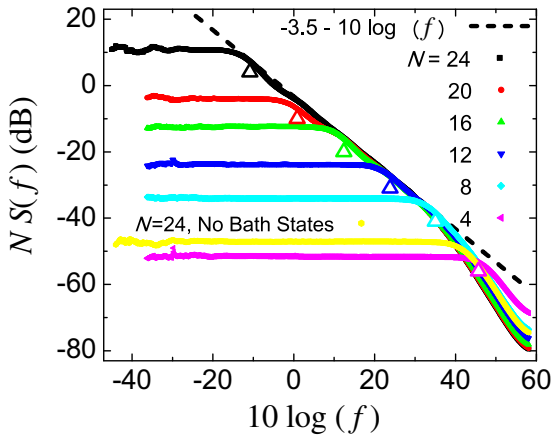

Fig. 3. Power spectral density of noise as a function of frequency. Solid symbols are from simulations of systems with several sizes (N). Note that $S(f)$ is multiplied by N to scale the power from normal fluctuations, and $\log(f)$ is multiplied by 10 to match the dB scale. The wide frequency range is obtained by averaging the Fourier transform from several time-series sequences, with averaging times of τ =1 to 10^6 steps. The diagonal dashed line shows exact $1/f$ behavior. The open triangles identify the frequency of the slowest response rate, from $10\log(f) = 53.5 - 10\log(\Omega_0)$. The hexagonal symbols are from the $N = 24$ matrix, but with all bath states bypassed.

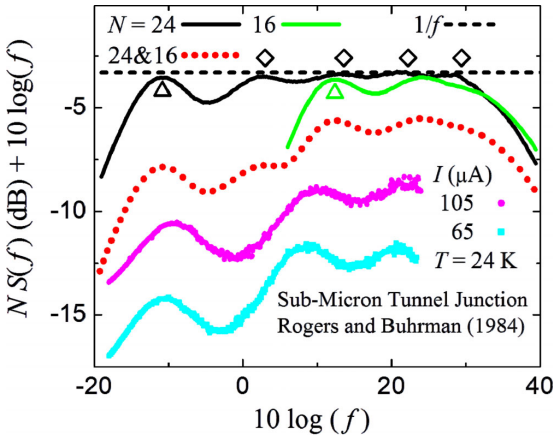

Fig. 4. Log-log plot of noise power spectral density multiplied by frequency. The dashed line (from the same equation as the dashed line in Fig. 3) shows exact $1/f$ noise. Solid lines, from the $N = 24$ and 16 matrices M with explicit bath states, show a $1/f$-like regime with distinct oscillations. Triangles mark the lowest frequency for transitions out of the fully-aligned state: $f_0 \propto 1/\Omega_0 = [(1/2N)!]^2/N!$. Diamonds mark progressively higher frequencies expected for the less-aligned states of the $N = 24$ system. The dotted line comes from the response of one $N = 24$ matrix added to ten times the N =16 matrix, with the amplitude offset for clarity. Symbols are from measurements of voltage noise across a submicron tunnel junction [16], with the amplitude and frequency offset for clarity.

from the same simulations used for Figure 2, and from 5 other systems with sizes $N < 24$. The relative alignment as a function of discrete time is converted to the power spectral density using a discrete Fourier transform:

$$S(f) = \left| \frac{1}{j} \sum_{t=0}^{j-1} \lambda(t) \exp(-2\pi i f t/j) \right|^2 .$$

The spectra are smoothed by linear regression using a sliding frequency range; then spectra with different τ are matched using a weighted average [21]. The diagonal dashed line indicates exact $1/f$ noise. The single system with $N = 24$ shows $1/f$-like behavior over at least 4 orders of magnitude in f, but the frequency range decreases with decreasing N. Open triangles show the lowest-frequency mode of each system, given by the single fully-aligned state divided by the total number of all states, $f_0 \propto 1/\Omega_0 = [(1/2N)!]^2/N!$, which includes $\Omega_0 - 1$ bath states. Without explicit bath states, the symbols near the bottom of Figure 3 exhibit white noise over at least 8 orders of magnitude in f, with no $1/f$ regime.

Figure 4 presents a useful way to focus on the $1/f$-like behavior, where $S(f)$ is multiplied by frequency so that $1/f$ noise becomes horizontal. Indeed, the horizontal dashed line is the same equation as the diagonal dashed line in Figure 3 showing $1/f$ noise. The solid lines showing $1/f$-like behavior over 4 and 2 orders of magnitude in frequency come from the matrix model with $N = 24$ and $N = 16$, respectively. Triangles mark the lowest-frequency modes from the fully-aligned states $f_0 \propto 1/\Omega_0$ (as in Fig. 3). Diamonds mark the expected higher-frequency modes from progressively less-aligned states of the $N = 24$ matrix: $f_1 = f_0 N$, $f_2 = f_0 N(N-1)/2$, $f_3 = f_0 N(N-1)(N-2)/6$, etc.

We compare the matrix model to measurements of voltage noise from a submicron metal-insulating-metal (MIM) tunnel junction [16]. In general, $1/f$ noise in tunnel junctions is attributed to two-level systems (TLS) with exponentially-broad time scales [26]. Specific mechanisms that have been proposed for these TLS include: disordered atomic positions, charge traps, electrons with random spin orientations [36], and diffusion of independent spins [37]. The Ising model is useful for treating such binary degrees of freedom because it maps directly to several scenarios, including binary alloys having random atomic positions, lattice gases with random particle traps, and simplified electron spins. A common challenge is to explain the exponentially broad distribution of relaxation times for $1/f$ noise, often attributed to a broad range of local environments or interaction strengths. The matrix model, which comes from the degenerate Ising model for non-interacting TLS, achieves $1/f$-like noise by including bath states that ensure thermodynamically-reversible equilibrium fluctuations.

The symbols in Figure 4 are from measurements of voltage noise across a MIM tunnel junction measured at constant currents of (A) 65 and (B) 105 μA. This junction is small enough (0.3 μm on both sides) that deviations

from pure $1/f$ noise can be seen. The dominant features are three distinct maxima. We chose to compare the matrix model to these measurements because they cover more than four orders of magnitude in frequency, and were the first to show finite-size effects in $1/f$ noise. Although qualitatively similar to the oscillations in the simulations, a quantitative analysis yields unrealistic values for the frequencies, as follows. From the published measurements we find characteristic frequencies of $f_{A0} = 7.2$ Hz, $f_{A1} = 585$ Hz, $f_{A2} = 9.52$ kHz and $f_{B0} = 10.1$ Hz, $f_{B1} = 865$ Hz, $f_{B2} = 12.9$ kHz. Averaging the ratio of the lowest two frequencies yields $f_1/f_0 = 84 \pm 2$, implying that the MIM junction would need $N \approx 84$ binary degrees of freedom if these peaks were to come from the two lowest frequencies of a single matrix. This N yields $f_0 \sim [(1/2N)!]^2/N! \sim 1.68 \times 10^{-24}$, which would require that the microscopic dynamics be an unphysical 24 orders of magnitude faster than the measured f_0. More likely the distinct maxima come from independent subsystems inside the sample, supporting the original interpretation of the measurements. The dotted line in Figure 4 comes from the sum of responses from one $N = 24$ matrix plus ten times the $N = 16$ matrix. The sizes and weights of these simulations are chosen to give qualitative similarity between the model and experimental data, including the net slope when plotted as in Figure 4 showing deviations from pure $1/f$ noise. Quantitative values can be obtained by assuming microscopic dynamics at a frequency of $f_{max} \sim 10^{10}$ Hz. Then, using $f_0 = f_{max}/\Omega_0$ for the characteristic frequency, the published data yield $N \sim 33$, 26, and 22 for the effective number of binary degrees of freedom causing the three measured peaks. The matrix model is too simplistic to reproduce all details in these spectra, but the similarity indicates that it is possible to capture the general features in such $1/f$-like noise measurements by combining binary degrees of freedom with explicit bath states.

We have shown that a simple system with explicit bath states fluctuates differently than the isolated system, and also differently from the system coupled to an infinite reservoir. Without explicit bath states the fluctuations yield well-known white noise. With explicit bath states the fluctuations yield $1/f$-like noise, which is measured universally at lower frequencies, signifying the final approach to thermal equilibrium. Having explicit bath states also maintains maximum entropy. Thus, at least if the fluctuations are slow enough, the 2nd law of thermodynamics may be a fundamental physical law, not just a statistical rule-of-thumb. Additional tests of the matrix model will come from measuring systems with small enough baths that they exhibit the return to white noise at ultra-low frequencies, as shown in Figure 3. From Stirling's approximation of the multiplicities, the model predicts that the minimum frequency for $1/f$-like noise should decrease exponentially with increasing number of degrees of freedom. At these ultra-low frequencies, the system has time to explore all states of the system and its bath, thereby achieving the true thermal equilibrium. Because it is usually difficult to calculate all contributions to entropy exactly, the matrix model provides a simplistic way to simulate how strict adherence to the 2nd law of thermodynamics yields a basic mechanism for $1/f$-like noise.

We thank S. Deffner and G.H. Wolf for helpful comments. Most of the simulations utilized the A2C2 computing facility at Arizona State University. RVC, BFD, and ASHS are grateful for financial support from the ARO via W911NF-11-1-0419. SA was supported in part by JSPS and the Ministry of Education and Science of the Russian Federation (the program of competitive growth of Kazan Federal University).

References

1. G.E. Crooks, Phys. Rev. E **60**, 2721 (1999)
2. D.J. Evans, E.G.D. Cohen, G.P. Morriss, Phys. Rev. Lett. **71**, 2401 (1993)
3. G. Gallavotti, E.G.D. Cohen, Phys. Rev. Lett. **74**, 2694 (1995)
4. R. Kawai, J.M.R. Parrondo, C. Van den Broek, Phys. Rev. Lett. **98**, 080602 (2007)
5. S. Pressé, K. Ghosh, J. Lee, K.A. Dill, Rev. Mod. Phys. **85**, 1115 (2013)
6. D. Collin, F. Ritort, C. Jarzynski, S.B. Smith, I. Tinoco Jr., C. Bustamante, Nature **437**, 231 (2005)
7. S. Toyabe, T. Sagawa, M. Ueda, E. Muneyuki, M. Sano, Nat. Phys. **6**, 988 (2010)
8. G. Verley, M. Esposito, T. Willaert, C. Van den Broeck, Nat. Commun. **5**, 1 (2014)
9. A. Berut, A. Arkakelyan, A. Petrosyan, S. Ciliberto, R. Dillenschneider, E. Lutz, Nature **483**, 187 (2012)
10. J.V. Koski, T. Sagawa, O.P. Saira, Y. Yoon, A. Kutvonen, P. Solinas, M. Möttönen, T. Ala-Nissila, J.P. Pekola, Nat. Phys. **9**, 644 (2013)
11. J. Mehl, B. Lander, C. Bechinger, V. Blickle, U. Seifert, Phys. Rev. Lett. **108**, 220601 (2012)
12. T.L. Hill, *Thermodynamics of Small Systems (Parts I and II)* (Dover, Mineola NY, 1994)
13. R.V. Chamberlin, Nature **408**, 337 (2000)
14. R.V. Chamberlin, J.V. Vermaas, G.H. Wolf, Eur. Phys. J. B **71**, 1 (2009)
15. R.V. Chamberlin, Entropy **17**, 52 (2015)
16. C.T. Rogers, R.A. Buhrman, Phys. Rev. Lett. **53**, 1272 (1984)
17. R. Landauer, Phys. Today **44**, 23 (1991)
18. R.P. Feynman, Found. Phys. **16**, 507 (1986)
19. R.P. Feynman, *Statistical Mechanics* (Perseus Books, Reading, 1998)
20. U. Seifert, Rep. Prog. Phys. **75**, 1 (2012)
21. R.V. Chamberlin, D.M. Nasir, Phys. Rev. E **90**, 012142 (2014)
22. S. Kogan, *Electronic Noise and Fluctuations in Solids* (Cambridge University Press, Cambridge, 2008)
23. E. Vidal Russell, N.E. Israeloff, Nature **408**, 695 (2000)
24. F. Yoshihara, K. Harrabi, A.O. Niskanen, Y. Nakamura, J.S. Tsai, Phys. Rev. Lett. **97**, 167001 (2006)
25. A.A. Balandin, Nat. Nanotechnol. **8**, 549 (2013)
26. E. Paladino, Y.M. Galperin, G. Falci, B.L. Altshuler, Rev. Mod. Phys. **86**, 361 (2014)

27. K.S. Nagapriya, A.K. Raychaudhuri, Phys. Rev. Lett. **96**, 038102 (2006)
28. R.M.M. Smeets, U.F. Keyser, N.H. Dekker, C. Dekker, Proc. Natl. Acad. Sci. USA **105**, 417 (2008)
29. J.P. Boon, Adv. Complex Syst. **13**, 155 (2010)
30. L.M. Ward, P.E. Greenwood, http://www.scholarpedia.org/article/1/f_noise
31. R.V. Chamberlin, G.H. Wolf, Eur. Phys. J. B **67**, 495 (2009)
32. R.V. Chamberlin, Physica A **391**, 5384 (2012)
33. G.M. Wang, E.M. Sevick, E. Mittag, D.J. Searles, D.J. Evans, Phys. Rev. Lett. **89**, 050601 (2002)
34. J.L. Lebowitz, Phys. Today **46**, 32 (1993)
35. D.A. Lavis, Phil. Sci. **75**, 682 (2008)
36. R.H. Koch, D.P. DiVincenzo, J. Clarke, Phys. Rev. Lett. **98**, 267003 (2007)
37. L. Faoro, L.B. Ioffe, Phys. Rev. Lett. **100**, 227005 (2008)

European Physical Journal B -- Condensed Matter is a copyright of Springer, 2016. All Rights Reserved.

A.2 Remarks

This model was useful for understanding the role of finite entropy baths in that it involves no interactions or internal energy, meaning the dynamics is determined entirely by the system's entropy. This allows the effects of multiplicity-dependent characteristic times to be studied entirely on their own. The simplicity of the model allowed the stochastic matrix to be written explicitly and from this the transition frequencies to be calculated exactly.

All of these properties proved useful for comparison purposes when applying the same concepts to the constrained Heisenberg model, which *does* involves interactions, exchanges energy with an infinite reservoir through the application of Boltzmann's factor, and involves continuous degrees of freedom

APPENDIX B

ORIGINAL PUBLICATION: $1/f$ NOISE FROM A FINITE ENTROPY BATH: COMPARISON WITH FLUX NOISE IN SQUIDS

B.1 Introduction

Much of the work presented in § 3 was published under the title "$1/f$ noise from a finite entropy bath: comparison with flux noise in SQUIDs" in *Journal of Statistical Mechanics: Theory and Experiment*. The complete citation is listed under reference [38]. This work was completed in collaboration, in the order listed in the original publication, by Bryce F. Davis (myself) and Ralph V. Chamberlin. The coauthor (Ralph Chamberlin) has granted his permission to have this work included in this dissertation.

Simulations, the creation of figures, writing of code, and writing of the article were primarily done by myself. Algorithms for simulating the model, most notably the form of the dynamic constraint, were developed by Ralph Chamberlin and myself. Physical interpretation of the results was done by Ralph Chamberlin and myself.

The original publication is included below.

Journal of Statistical Mechanics:
Theory and Experiment

PAPER: CLASSICAL STATISTICAL MECHANICS, EQUILIBRIUM AND NON-EQUILIBRIUM

1/*f* noise from a finite entropy bath: comparison with flux noise in SQUIDs

To cite this article: Bryce F Davis and Ralph V Chamberlin *J. Stat. Mech.* (2018) 103206

View the article online for updates and enhancements.

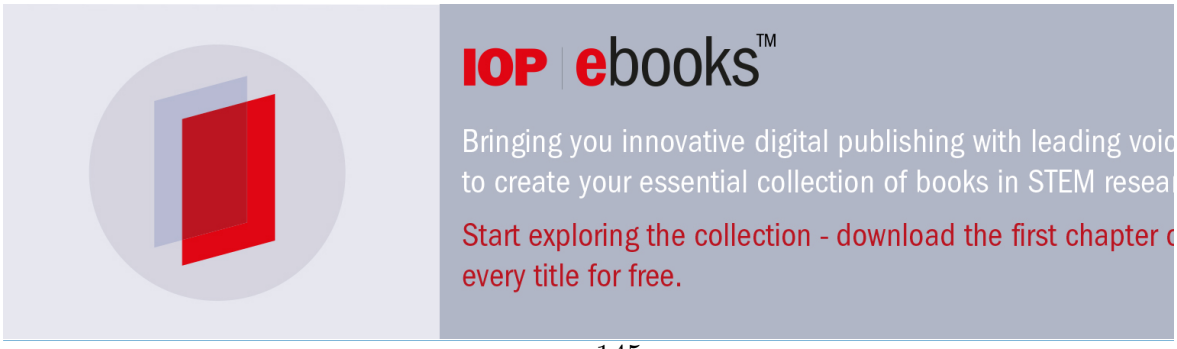

Journal of Statistical Mechanics: Theory and Experiment
An IOP and SISSA journal

PAPER: Classical statistical mechanics, equilibrium and non-equilibrium

1/*f* noise from a finite entropy bath: comparison with flux noise in SQUIDs

Bryce F Davis and Ralph V Chamberlin

Department of Physics, Arizona State University, Tempe, AZ 85287-1504, United States of America
E-mail: Bryce.F.Davis@asu.edu

Received 26 June 2018
Accepted for publication 16 September 2018
Published 23 October 2018

Online at stacks.iop.org/JSTAT/2018/103206
https://doi.org/10.1088/1742-5468/aae2df

Abstract. The primary low-frequency noise in superconducting quantum interference devices (SQUIDs) at low temperature is flux noise with a power spectral density of the form $S(f) \propto 1/f^{\alpha}$ with $\alpha \approx 1$. Experiments show this noise is due to independent clusters of interacting spins at the metal-insulator interface of the Josephson junction. The temperature dependences of the amplitude and the spectral exponent α are such that the noise spectra $S(f)$ of devices taken at different temperatures cross each other at a common crossing frequency f_c, so that $S(f_c)$ is constant over a wide range of temperatures. Presented here are Monte Carlo simulations of a Heisenberg spin model modified with a type of dynamic constraint that depends on the configurational entropy of clusters of spins. The constraint arises from assuming that coupling between clusters of spins and the thermal reservoir is mediated by a local bath. Noise in the alignment of this model shows similarities to the temperature-dependent flux noise of SQUIDs, reproducing the relationship between α and the amplitude that leads to the existence of a crossing frequency f_c of spectra at different temperatures.

Keywords: noise models, fluctuation phenomena, mesoscopic systems, slow relaxation, glassy dynamics, aging

© 2018 IOP Publishing Ltd and SISSA Medialab srl

Contents

1. Introduction

Standard statistical mechanics in the canonical ensemble assumes systems are ideally coupled to an effectively infinite heat reservoir. Specifically, the reservoir is taken to be large enough and the coupling fast enough that the local thermal environment of the system is unaltered by the state of the system. However, when the length and time scales of events are small enough, or when a system is not ideally connected to a larger thermal environment, as may be the case when the system is at low temperatures, these assumptions break down. An immediate example in classical systems is the limitation imposed by the speed of sound. At the mesoscopic scale, evidence of imperfect coupling to the thermal environment is found in the observation of dynamically independent, nanometer-sized regions. Spatial heterogeneity of this type has been inferred from the stretched exponential primary response of materials as well as directly observed using techniques such as nuclear magnetic resonance, non-resonant spectral hole burning, and neutron scattering [1–3]. Theoretical strategies to address these questions include rigorous modifications of thermodynamics, stochastic equations of motion for systems that alter their own environment and possess a memory, and the marriage of these two in form of stochastic thermodynamics [4–7].

Here, we consider a simple modification to Monte Carlo simulations by way of a nonlinear constraint that recreates the dynamic heterogeneity seen in many physical systems. The constraint originates from assuming that the system, in addition to being coupled to the larger thermal reservoir, is in contact with a finite, local bath. On the time scale of microscopic events, the combined entropy of the system and its local bath is maintained at a maximum. The addition of this constraint is found to produce $1/f$-type noise, ubiquitous in nature, in systems that otherwise exhibit white noise. Simulations of various models using a similar constraint have been reported in previous publications [8–12]. Here, we constrain the classical Heisenberg spin model, with and without dipolar anisotropy, and focus on $1/f$ noise in the net alignment. The results of simulations are compared to a long-standing problem: the origin of low-frequency $1/f$ flux noise found in superconducting quantum interference devices (SQUIDs). The model is also compared to models of spin glasses with disordered Hamiltonians, previously

used for explaining $1/f$ flux noise in SQUIDs, which produce slow dynamics and heterogeneity in a notably different fashion.

1.1. Flux noise in SQUIDs

Low frequency noise with a power spectral density (PSD) of the form $S(f) \propto 1/f^{\alpha}$ with $\alpha \approx 1$ (referred to as $1/f$ noise) is found virtually everywhere in nature. First observed in the current through resistors [13], it has since been found in most types of materials and devices. $1/f$ noise often limits the performance of traditional electronic systems as well as that of more modern devices. Specifically, $1/f$ noise has been known for some time to be the dominant form of noise at low temperature in SQUIDs [14–16], and more recently has been found to be the primary cause of decoherence in flux [17, 18] and phase [19] qubits. In a testament to its ubiquity, there are at least two sources of $1/f$ noise in a Josephson junction (the essential component of all SQUIDs and many qubits). One source of noise is in the critical current, caused by the capture and release of electrons at sites in the tunnel barrier between superconductors, with a static density of release times τ that varies as $1/\tau$ [20, 21]. Models such as these, based on a distribution of relaxation times, are probably the most widely-known and frequently-invoked explanation for $1/f$ noise [22]. However, since the amplitude of this critical current noise decreases linearly with temperature [23], device performance at low temperatures is instead limited by $1/f$ *flux noise*. In the more than 30 years since its discovery [14–16] a satisfactory explanation of $1/f$ flux noise in Josephson junctions has yet to be provided. Interest in the problem has been strengthened in recent years since flux noise is the primary cause of dephasing in qubits [17–19], limiting their viability as the components of quantum computers [24].

Most models for flux noise are based upon unpaired spins at the metal-insulator interface of the SQUID. An early such model [16], based on non-interacting spins, predicted an areal density of spins of 5×10^{17} m^{-2}, and this value comports with direct measurements of paramagnetism at the superconductor surface [25]. However, further measurements indicate that spin-spin interactions are significant, causing the spins to form clusters. These measurements also show evidence of time-reversal symmetry breaking, indicating that interactions are ferromagnetic [26]. Comprehensive flux noise measurements have been reported of 10 different dc SQUIDs by Anton *et al* [27] and 84 different SQUIDs and SQUID arrays by Kempf *et al* [28]. These measurements show a dependence upon temperature of both the flux noise amplitude and spectral exponent α, as well as a relationship between the two that leads to the spectra of individual devices at different temperatures coinciding at a crossing frequency f_c. This spectral pivoting can be expressed by the relationship

$$S_{\Phi}(f) = S_{\Phi}(f_c) \times (f_c/f)^{\alpha}. \tag{1}$$

Where S_{Φ} denotes the power spectral density of flux noise. Since α is found to increase with decreasing temperature, this functional form of the power spectral density means that with decreasing temperature, the noise power decreases for $f > f_c$, and increases for $f < f_c$.

Contenders for the microscopic physical origin of the surface spins include nuclear or electron spins, or a combination of the two [29]; adsorbed oxygen molecules [30,

31]; electrons in localized gap states at the metal/insulator interface [32]; and paramagnetic dangling bonds coupled to two-level tunneling systems at the amorphous-semiconductor/oxide interface [33]. Mechanisms of spin interactions that have been considered include the Ruderman–Kittel–Kasuya–Yoshida (RKKY) interaction [34], anisotropic dipole–dipole interactions [35], or hyperfine interactions [36]. Various spin glass models, including disordered Heisenberg [35, 37] and Ising [38, 39] models, have been employed to test these mechanisms. Spin glass models with a distribution of ferromagnetic and antiferromagnetic interactions may be incompatible with observations of time-reversal symmetry breaking [26, 38], but disordered models with preferentially ferromagnetic interactions, more compatible with observations of time-reversal symmetry breaking, have also been explored [30, 39]. Furthermore, models previous to the report of Anton *et al* [27] do not account for the observed spectral pivoting. A subsequent modification of a spin diffusion model involving the RKKY interaction has since been presented which yields a temperature dependent diffusion coefficient and a band of crossing frequencies [40].

Slow dynamics and $1/f$ noise in these spin glass models are attributed to static disorder in the form of non-uniform interaction strengths. While the distribution of interaction strengths is indeed constant, what does change with time is the subsequent distribution of relaxation times, either by exploring configurations with a distribution of separations in the space of states, as in models based on hierarchical kinetics, or by changing spatial correlations, as in the droplet scaling picture [41]. Here, however, we describe a Heisenberg model for spins with *uniform* interactions on an ideal square lattice, but with the relaxation time of spins in a cluster dependent upon the net alignment of the cluster. The Hamiltonian in this model remains homogeneous and the heterogeneity comes instead from the distribution of net alignments of clusters, yielding a time-dependent distribution of relaxation times so that the hetergeneity is dynamic. Dependence of the relaxation time upon the system state has been employed to describe slow dynamics in models of plastic flow and aging [7, 42, 43]. Noise spectra of the net alignment of this model will be compared with $1/f$ flux noise observed in SQUIDs, specifically the observed spectral pivoting, equation (1) [27, 28]. Our model will also be compared to spin glass models for $1/f$ flux noise in SQUIDs.

1.2. Model and nonlinear constraint

There is direct evidence that $1/f$ flux noise in SQUIDs is the result of unpaired, interacting spins which form into clusters [25, 26]. The common interpretation of $1/f$ noise as arising from a $1/\tau$ distribution of relaxation times suggests that the relaxation times of these clusters is distributed in just such a way. The spectral pivoting, equation (1), observed by Anton *et al* [27] and Kempf *et al* [28] further suggests that, as the temperature is decreased, this distribution increases for frequencies below f_c and decreases for frequencies above f_c. One explanation is that the relaxation time of a cluster increases as the cluster grows, so that the change in the distribution of relaxation times is due to an increase in the average size of clusters and a reduction of the number of smaller clusters with decreasing temperature, as in the droplet picture of a spin glass [41]. In this paper, however, we explore the possibility that the relaxation time of a cluster is connected to its net alignment through its local configurational entropy. To test this picture, we

performed computer simulations of the standard Heisenberg spin model with dynamics modified by a constraint due to the configurational entropy of clusters. Clusters are obtained by explicitly subdividing the entire lattice into local regions. To demonstrate that a distribution of cluster sizes is not needed in our model to produce the necessary distribution of relaxation times, all clusters are given the same fixed size. In our case, the dynamics of each spin is constrained according to the configurational entropy of all spins within the cluster that contains that spin. Our model has the advantage that neither a specific distribution of cluster sizes nor an explicit temperature dependence are needed to obtain the distribution of relaxation times that produces $1/f$ noise.

Various mechanisms for similar nonlinear constraints have been considered elsewhere for the Ising model [8–12]. Here, for the Heisenberg model, we attribute the constraint to the additional heat transfer required to change the local configurational entropy within a cluster of spins. This heat, arising purely from a change in entropy, is distinct from the fluctuations in internal energy due to spin-spin interactions accounted for by the Boltzmann factor. Well-known examples of heat/work with a purely entropic origin include the work required to stretch an ideal, freely-jointed chain [44], and the cooling afforded by adiabatic demagnetization [45, 46]. The constraint suppresses spin-flips in highly aligned clusters, creating a distribution of relaxation times that evolve with the cluster's configuration, yielding $1/f$ noise. The constraint also suppresses high-frequency single spin-flips while enhancing low-frequency reorientations of whole clusters, which yields spectral pivoting, equation (1).

We start with a classical Heisenberg spin model with and without dipolar anisotropy. While many candidates for the physical identity of the unpaired surface spins are electrons with spin 1/2, such as dangling bonds [33] and localized gap states [32], there are also explanations better modeled by classical spins, e.g. adsorbed molecular oxygen [30, 31]. Density functional theory calculations of adsorbed O_2 have shown that the molecule retains a large magnetic moment while adsorbed on the surface, which is able to rotate freely about the O–O bond [30], providing physical justification for the use of classical, anisotropic spins. We use a two-dimensional square lattice with periodic boundary conditions and a total number of spins $N = 24 \times 24$ or 48×48. The Hamiltonian is:

$$H = -J \sum_{\langle ij \rangle} \mathbf{s}_i \cdot \mathbf{s}_j - D \sum_i (s_i^z)^2. \tag{2}$$

The spin vectors $\mathbf{s}_i$ are of magnitude 1, and the first sum is taken over all nearest-neighbor pairs $\langle ij \rangle$. The exchange constant J is set to 1 for results presented here, and this ferromagnetic coupling is consistent with observations of time-reversal symmetry breaking [26]. The second term introduces anisotropy in the z-direction and the strength D is set to $0J$, $2J$, or $4J$. As will be seen, without anisotropy ($D = 0$), our dynamically constrained Heisenberg model produces noise spectra with $\alpha > 1.4$ at low temperatures, exceeding a limit on α seen in some systems, including the flux noise in SQUIDs [27, 28]. On the other hand, an investigation [11] of the Ising model with a dynamic constraint similar to that used here (detailed below, see equation (4)) found that the discrete, two-state Ising model obeys this limit and produces noise spectra $S(f) \propto 1/f^{\alpha}$ with $\alpha < 1.4$ even at the lowest temperatures. Thus, inclusion of the second term in equation (2) is meant to bridge the gap between the discrete, two-state

Ising model and the fully isotropic Heisenberg model, and allows α to assume the range of values $0.35 \lessapprox \alpha \lessapprox 1.40$ observed in the flux noise in SQUIDs [27, 28].

The model is simulated using a Metropolis algorithm with Boltzmann's factor:

$$e^{-\Delta E/k_B T} > [0,1). \tag{3}$$

Where k_B denotes Boltzmann's constant, T the temperature, and $[0,1)$ is a random number uniformly distributed between zero and one. ΔE is the change in energy from an attempted spin flip, in which a single spin is given a new orientation chosen from an isotropic distribution.

The novel feature in our model is to subdivide the lattice into $N_c = 6 \times 6 = 36$ spin clusters and subject spin flips within each cluster to the additional constraint:

$$e^{g(S_c - S_c^{\max})/k_B} = \left[\frac{\Omega(0)}{\Omega(M_c)}\right]^g > [0,1). \tag{4}$$

Here S_c denotes the configurational entropy of the cluster, M_c is the cluster's net alignment, $\Omega(M_c)$ is the multiplicity of a cluster with alignment M_c, and g is a parameter used to control the strength of the constraint. For a cluster of N_c classical Heisenberg spins of length 1, with net alignment M_c, the configurational entropy is $(S_c - S_c^{\max})/k_B \approx -3M_c^2/2N_c$ (for $M_c \ll N_c$) [47]. So, for our model, the constraint, equation (4), becomes

$$e^{-g\times(3M_c^2/2N_c)} > [0,1). \tag{5}$$

To better understand how this constraint modifies the dynamics of our model, it is useful to consider the high temperature limit, $k_B T \to \infty$, with $g = 1$. In this limit, all spin flips are accepted according to the criterion set by Boltzmann's factor, equation (3). Therefore, spin-spin interactions may be ignored and the dynamics are determined entirely by the nonlinear constraint, equation (4). Specifically, at infinite temperature and with $g = 1$, the constraint causes states of the cluster with alignment M_c to persist for an average lifetime of $\tau = \Omega(0)/\Omega(M_c)$. To find the power spectrum of fluctuations in alignment, we note that a distribution $F(\tau)$ of fluctuations, each having a Lorentzian spectrum of characteristic time τ, yields a total power spectrum:

$$S_{M_c}(f) = \int_0^\infty F(\tau)\frac{4\tau}{1+\omega^2\tau^2}\mathrm{d}\tau. \tag{6}$$

With $F(\tau) \propto 1/\tau$ in the interval $\tau_1 < \tau < \tau_2$, the spectrum has the form $S_{M_c}(f) \propto 1/f$ in the interval $1/\tau_2 < f < 1/\tau_1$. Since the total integral of the power spectrum gives the total variance, $\int S(f)\mathrm{d}f = \int F(\tau)\mathrm{d}\tau = \overline{(\delta x)^2}$, we recognize $F(\tau)\mathrm{d}\tau$ as the variance from fluctuators with characteristic times between τ and $\tau + \mathrm{d}\tau$ [22]. As such, $F(\tau)$ must contain the density $\Omega(\tau)$ of fluctuators with characteristic time τ as well as the contribution $A^2(\tau)$ of a single fluctuation, so that $F(\tau) = A^2(\tau) \times \Omega(\tau)$ [48]. First, $\Omega(\tau)$ can be found from the relationship $\tau \propto 1/\Omega(M_c)$:

$$\Omega(\tau) = \Omega(M_c)\left|\frac{\mathrm{d}M_c}{\mathrm{d}\tau}\right| = \frac{1}{\tau}\left|\frac{\mathrm{d}M_c}{\mathrm{d}\tau}\right|. \tag{7}$$

Turning to $A^2(\tau)$, the average contribution to the variance from a fluctuation of size M_c and average lifetime τ is $A^2 \sim M_c^2 \times \tau$. Finally, for our constrained Heisenberg model $\tau \propto 1/\Omega(M_c) = \mathrm{e}^{3M_c^2/2N}$ so that $M_c \propto \sqrt{2N\ln(\tau)/3}$. So, the distribution of fluctuators with characteristic time τ is

$$F(\tau) = M_c^2 \left| \frac{\mathrm{d}M_c}{\mathrm{d}\tau} \right| \propto N^{3/2} \frac{\sqrt{\ln(\tau)}}{\tau}. \tag{8}$$

Which, over the range of τ considered here is very nearly $1/\tau$. Indeed, for $g = 1$, it was found that simulations produce exact $1/f$ noise in the high temperature limit, with α increasing with decreasing temperature. The high temperature limit of the Ising model, similarly constrained with $g = 1$, was also found to be an exact $1/f$ spectrum [11]. Finally, a similar model employing binary spins *without* interactions, coupled to an *explicit* local bath in lieu of a nonlinear constraint (equation (4) also produced fluctuations in alignment with an exact $1/f$ spectrum [49]. These considerations indicate that the alignment fluctuates with an exact $1/f$ spectrum when the average lifetime of states $\tau(M_c) \propto 1/\Omega(M_c)$. For $g = 1$ this occurs at infinite temperature, when spin-spin interactions can be neglected and the dynamics are controlled by the nonlinear constraint alone.

In deriving equations (5) and (8), the approximation $(S_c - S_c^{\max})/k_\mathrm{B} \approx -3M_c^2/2N_c$ was used under the condition that $M_c \ll N_c$. However, for small N_c this condition may not hold. This is seen in figure 1, which shows spectral densities of fluctuations in the z-component of net alignment from simulations with $g = 1$, $D = 0$, $k_\mathrm{B}T/J \to \infty$, and $N_c = 4$ (blue), 9 (green), 16 (red), and 36 (black) spins per cluster. As predicted by equation (8), for cluster size $N_c = 36$ the spectrum is very nearly $1/f$ (indicated by the black dashed line). However, for smaller N_c, spectra deviate significantly from $1/f$ and the range over which $1/f$ type noise is observed shrinks progressively. This cluster size dependence is due to the breakdown of the condition $M_c \ll N_c$. Furthermore, the rollover to white noise is made more gradual by the breakdown of this condition. The reason for this is that the lowest frequency f_0 at which $1/f$ type noise will be observed corresponds to the inverse time it takes to flip a spin in a fully aligned cluster $f_0 \sim 1/\tau(M_c = N_c) \sim \mathrm{e}^{-3gN_c/2}$, and the condition $M_c \ll N_c$ of course breaks down before this point is reached. This is also seen in figure 1, where f_0 for $N_c = 4$ and 9 is marked by the diamond symbols. As is apparent from the $N_c = 9$ spectrum, the rollover to white noise begins before reaching f_0. For the similarly constrained Ising model [11] and the model of non-interacting spins with an explicit bath [49], the exact entropies are used in equation (4). As a consequence, this anomalous size dependence is not observed. For the Heisenberg model presenented here, the exact entropy is found by integrating the inverse Langevin function and the next largest term in the expansion is $\mathcal{O}(M^4)$ [47].

Having discussed the consequences of the constraint on the dynamics of our system, we now turn to its physical interpretation. The constraint allows us to relax two assumptions of Boltzmann's factor: (1) that the system is coupled to an effectively infinite thermal reservoir and (2) that the coupling is immediate; as a result, the thermal reservoir is unaltered by changes undergone by the system and does not depend upon the system state. At small enough length and time scales and in systems which are imperfectly coupled to the larger thermal environment, as is possible at low temperatures, these assumptions may not hold. Instead, during fluctuations, the heat provided

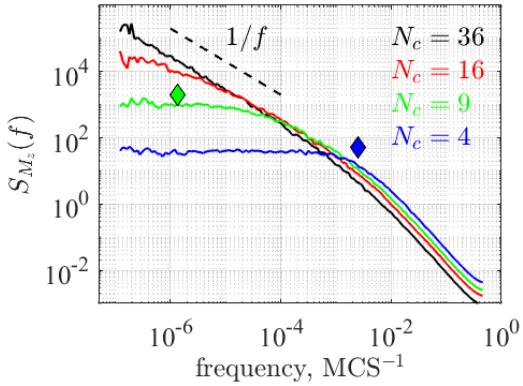

Figure 1. Spectral densities of fluctuations in the z-component of net alignment from simulations with $g = 1$, $D = 0$, $k_B T/J \to \infty$, and $N_c = 4$ (blue), 9 (green), 16 (red), and 36 (black) spins per cluster. In this high temperature limit, with $g = 1$ and $N_c = 36$, fluctuations approach an exact $1/f$ spectrum (indicated by the black dashed line). For smaller N_c, the assumption that $M_c \ll N_c$ no longer holds, so that the approximation $(S_c - S_c^{\max})/k_B \approx -3M_c^2/2N_c$ used in equations (5) and (8) is no longer justified. Diamond symbols mark frequencies $f_0 = e^{-3gN_c/2}$ for $N_c = 4$ (blue) and 9 green, roughly approximating where spectra are expected to roll over to white noise. Since these frequencies correspond to fully aligned clusters, the assumption $M_c \ll N_c$ does not hold and the rollover to white noise is gradual.

and/or dissipated by the bath to change the configurational entropy of the system must be mediated by the local environment. To recreate this imperfect coupling in our model, clusters of spins are taken to be coupled to their own finite, local entropy bath; the system + bath is then coupled to the larger thermal environment. On the time scale of single spin flips, entropy of the cluster plus its local bath is assumed to be maximized. In order to maintain maximum entropy, as the entropy of the cluster goes down, the entropy of its local bath must go up. As a result, when the cluster fluctuates into a low entropy state, changes in the state of the cluster are suppressed as newly available local bath states are explored and the local bath instead exchanges entropy with the larger thermal environment. This situation is illustrated in figure 2, where a constant amount of phase space is shared between a system and its local bath. Neglecting interactions (or letting $T \to \infty$) and setting $g = 1$, the shared phase space in this model truly becomes constant (that is, it is unchanged by interactions with the larger thermal environment). This is seen by considering that the constraint causes states to persist for an average lifetime of $\tau(M_c) = \Omega(0)/\Omega(M_c)$. So, the probability of finding a cluster with alignment M_c is constant and independent of M_c: $p(M_c) \propto \Omega(M_c) \times \tau(M_c) = \Omega(0)$ So, the time spent exploring states of the bath exactly balances the density of states in the system, as illustrated in figure 2.

So, the constraint causes the cluster to prefer low entropy states (thus slowing transtions) while the local bath is in a correspondingly high entropy state. In this way the constraint is analogous to Boltzmann's factor. In one method to derive Boltzmann's factor, the probability of a fluctuation of a local region is considered, $p \sim e^{\Delta S^*/k_B}$, where ΔS^* is the change in entropy of the bath. This probability is combined with the fundamental equation of thermodynamics for a system in contact with a bath at temperature

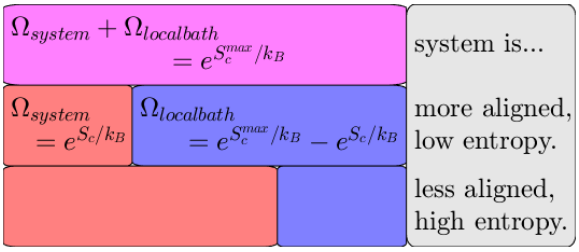

Figure 2. Illustration of a constant amount of phase space (pink) shared between a system (red) and its local bath (blue). When a cluster of spins is in a highly aligned, low-entropy state, spin-flips are suppressed by an amount proportional to the cluster's relative share of the total phase space, $\Omega_{\text{system}}/(\Omega_{\text{system}} + \Omega_{\text{local bath}}) = \mathrm{e}^{g(S_c - S_c^{\max})/k_{\mathrm{B}}} \sim \mathrm{e}^{-g(3M_c^2/2N_c)}$. Instead, transitions occur in the local bath's internal degrees of freedom, without altering the state of the system.

T, $\Delta S^* = \Delta E^*/T$. Conservation of energy is used to replace the change in the bath energy with the change in the system energy, $\Delta E^* = -\Delta E$. This yields Boltzmann's factor, equation (3), which determines the probability of changes in the internal energy. Boltzmann's factor states that the probability of a transition which lowers the system's internal energy is determined by the preference for the entropy of the bath to increase. The similarity between Boltzmann's factor and the nonlinear constraint is that the constraint favors low entropy states of the system due to a preference to raise the entropy of the local bath. The difference is that, in the case of our nonlinear constraint, transitions push the local bath out of equilibrium, whereas in Boltzmann's factor the bath returns to its original state after each transition. This difference manifests itself in the form of each constraint in two different ways.

One difference is that while Boltzmann's factor depends entirely upon the presence of internal energy due to spin-spin interactions, the nonlinear constraint depends solely upon the configurational entropy of the system, regardless of whether spin-spin interactions are present. However, fluctuations in the configurational entropy may still entail heat transfers. Heat/work exchange due to changes in the configurational entropy of a system, without a change in the system's internal energy, are seen in the work applied to stretch a freely-jointed chain against its entropic force [44] and the cooling caused by adiabatic demagnetization [45, 46]. Considering changes in configurational entropy of a cluster to be accompanied by heat exchanges with its local bath allows us to view the constraint in another way: as the cluster fluctuates into a low entropy state, the local bath is heated and spin flips are suppressed as the local bath equilibrates and exchanges heat with the larger thermal environment. With perfect coupling to an infinite bath, this equilibration occurs on a time scale much faster than that of changes in the state of the system, and the state of the system no appreciable impact on the thermal environment that the system sees and therefore no impact on the rate at which changes in the system's configuration are attempted. These considerations make apparent a second difference between Boltzmann's factor and our nonlinear constraint: a *change* in entropy appears in Boltzmann's factor, whereas an *offset* in entropy appears in our nonlinear constraint. Without time to equilibrate with the larger thermal environment, the state of the bath is determined by the *offset* in the entropy of the cluster. Considering the

offset in the cluster's entropy to be an accumulation of changes in entropy, it might be said that the local bath has a memory.

Generally, the nonlinear constraint causes low entropy states to persist by a factor of $\sim e^{g(3M_c^2/2N_c)}$ longer than without the constraint. Specifically, the effect of this constraint is to reduce the frequency of spin flips in more highly aligned clusters, effectively slowing their dynamics and leading to clusters with different relaxation times that evolve in time with the alignments of the clusters, even in an ostensibly uniform system. This can lead to $1/f$ noise in two ways: first, the distribution of cluster alignments results in a distribution of relaxation times, which leads to $1/f$ noise, as in models based on a fixed $1/\tau$ distribution of relaxation times [22]; second, the relaxation time of an individual cluster evolves in time with the cluster alignment so that the characteristic time is distributed in time, as in e.g. models based on power-law intermittency [50, 51]. These two effects are not mutually exclusive and both are expected to contribute to the observed spectrum of the entire sample. Note that no distribution of relaxation times among clusters and no time dependence of relaxation time for individual clusters are explicitly imposed. Instead, clusters naturally distribute themselves in such a way as to produce $1/f$ noise.

In this paper, we will compare the noise in the z-component of the net alignment of this model to SQUID flux noise. Specifically, the model produces spectra that, in the low-frequency regime, pivot about a common crossing frequency for different temperatures, similar to observations made by Anton *et al* [27] and Kempf *et al* [28].

2. Simulations and results

Monte Carlo simulations of the Heisenberg model presented here were performed using algorithms that were developed by the authors. The simulations are first initialized by setting all spin vectors to the positive z-direction and running for 10^6 Monte Carlo sweeps (MCS) without the additional nonlinear constraint and without anisotropy. The constraint and anisotropy (if applicable) are then applied and simulations are run for an additional $2^{17} \times 10^3$ MCS. Simulations are then run for $t_m = 2^{17} \times 10^3$ MCS for data collection. Over the course of data collection, four time series, each of length 2^{17} data, are recorded of the time-averaged z-component of the alignment $M_z(t)$, for averaging times of 10^0 to 10^3 MCS. From the time series of each averaging time, the spectral density of fluctuations is calculated $S_{M_z}(f) = \frac{1}{N}|\sum_{t=0}^{N-1} M_z(t)e^{2\pi i f t/t_m}|^2$. Spectra from five different simulations are averaged together. These averaged spectra are smoothed by dividing them into octaves and taking a linear least-squares fit to all data in that octave; the value of the spectral density is taken to be the value of this fit at the center frequency of each octave. Finally, the spectra for different averaging times are merged together. Since the spectra from each averaging time extend over ≈5 decades, but are separated by only a decade, there is significant overlap of spectra from different averaging times. These are merged using an average that is weighted more heavily at the center of each spectrum, where there is less noise in the spectrum. This overlap is also used to check for equilibration and stationarity by comparing the integrated spectra of each averaging time in the overlapping frequency range.

Using a value of $g = 1$ in the nonlinear constraint at $k_B T \to \infty$ produces an exact $1/f$ spectrum ($\alpha = 1$), while for finite temperatures $\alpha > 1$. Therefore, to reproduce the range $0.35 \lessapprox \alpha \lessapprox 1.40$ from spectra of SQUID flux noise, a value of $g < 1$ must be used. For the results presented in this section, a value of $g = 2/3$ was used. Figure 3(a) shows spectral densities from simulations with no anisotropy, $D = 0$. The spectral exponent α is frequency dependent, consisting of a tail at high frequency with an $\alpha \approx 1.8$, which is weakly dependent on temperature, crossing over to a much more strongly temperature-dependent low-frequency range. The high-frequency tail is on a short enough time scale that single spin flips determine the shape of the spectrum and our Monte Carlo simulations are not expected to realistically simulate dynamics, which cannot be considered stochastic on short enough time scales. For instance, the highest measurable frequency and the frequency of single spin flips are both on the order of 1 MCS^{-1} in our simulations. In experiments, this high frequency noise is invariably masked by another source of noise with a constant frequency dependence, $\alpha = 0$ (white noise) [27, 52, 53].

In the low-frequency range, α varies from $\approx$1.6 ($\approx$1.3 for anisotropic simulations, as discussed below) at the lowest temperatures to $\approx$0.4 at the highest temperatures, encompassing the range of values of α observed in SQUID flux noise as well as qualitatively reproducing its temperature dependence [16, 27, 28, 52, 53]. Least squares fits of the low-frequency portion (centered around $f = 10^{-6}$ MCS^{-1}) of the spectra to the function $S_{M_z,\mathrm{fit}}(f) = S_{M_z,0} \times (f/10^{-6}\,\mathrm{MCS}^{-1})^{-\alpha}$ were performed, where $S_{M_z,0} = S_{M_z,\mathrm{fit}}(f = 10^{-6}$ $\mathrm{MCS}^{-1})$ was chosen for clarity of presentation. The fits are presented in figure 3(b). For all fits the coefficient of determination was found to be $R^2 > 0.9$. The increase in alpha with decreasing temperature is clear here. Also clear is that the higher temperature spectra pivot about a common crossing frequency, $f_c = 5.36(+1.32/-1.06) \times 10^{-3}$ MCS^{-1}, similar to observations by Anton *et al* [27] and Kempf *et al* [28]. The crossing frequency (indicated by the dashed lines in figures 3(a) and (b)) and its uncertainty were calculated by taking the geometric mean and geometric standard deviation, respectively, of the crossing frequencies of all pairs of fits. Excluded from this calculation are the 6 lowest temperature spectra pictured. These low temperature spectra, for which $\alpha \gtrapprox 1$, begin to drop in amplitude, no longer passing through the crossing frequency shared by spectra with $\alpha \lessapprox 1$. This can be seen in the raw spectra and fits of figures 3(a) and (b), but is more clearly displayed in the inset of figure 3(b), where the value of the fit to the spectral density at the crossing frequency, $S_{M_z,\mathrm{fit}}(f_c)$, is plotted against α. The reason for this drop in amplitude is a dynamical freezing on the time scale of the simulation and will be discussed in more detail below.

Comparing the fits in figure 3(b) and the raw spectra in figure 3(a), the crossing in the raw spectra is obscured by the proximity of the crossing frequency to the frequency where all spectra change from the strongly temperature dependent low-frequency regime to the high-frequency tail. This gives the appearance that, rather than crossing each other, spectra converge in the high-frequency regime with approximately the same α and $S_{M_z,0}$. This suggests that the high-frequency ($f > f_c$) behavior, dominated by fast, single spin flips, remains relatively constant except at low temperatures, where $\alpha \gtrapprox 1$ and spin flips are strongly suppressed. Again, at these high frequencies, our Monte Carlo simulations are not expected to realistically simulate dynamics. Furthermore, in experiments, the high frequency behavior is always masked by some other source of white noise [27, 28, 52, 53]. The presence of white noise at high frequencies in

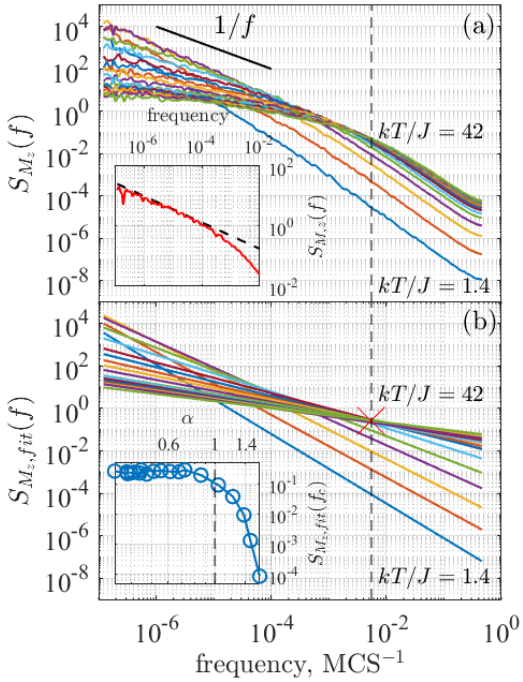

Figure 3. (a) Spectral densities of fluctuations in the z-component of net alignment. (Inset) Example of a fit (black dashed line) to the low-frequency portion of a spectrum ($kT/J = 21.2$). (b) Corresponding fits to the low-frequency portion (centered around $f = 10^{-6}$ MCS^{-1}) of the spectra. Simulations are isotropic ($D = 0$) and from temperatures $kT/J = 1.4$ to $kT/J = 42$. The crossing frequency $f_c = 5.36(+1.32/-1.06) \times 10^{-3}$ MCS^{-1} is indicated by the black dashed line in (a) and (b). Values of $f_c = 3.93(+1.16/-0.90) \times 10^{3}$ MCS^{-1} and $f_c = 6.60(+1.06/–0.91) \times 10^{-3}$ MCS^{-1} are found for $D = 2J$ and $4J$, respectively. The coefficient of determination $R^2 > 0.9$ for all fits. (Inset) The value of fits to the spectral density at f_c as a function of the spectral exponent α. The spectral density remains constant up to $\alpha \approx 1$ (indicated by black dashed line).

experiments gives the spectra positive curvature, which, instead of obscuring the presence of a crossing frequency, clarifies it. On the other hand, at low frequencies ($f < f_c$), where the slow, collective changes in the alignment of clusters dominates, the effect of the constraint is substantial and leads to the relationship between α and $S_{M_z,0}$ that produces a crossing frequency.

In figure 4(a), α is shown as a function of kT/J for different strengths of anisotropy $D = 0,\ 2J,\ 4J$. In figure 4(b) are the corresponding amplitudes of the spectral density $S_{M_z,0}$. The relationship between α and $S_{M_z,0}$ for $\alpha \lessapprox 1$ is clear from the similarity of the curves in these two figures. In the inset of figure 4(a), α and $S_{M_z,0}$ are plotted against each other. It can be seen here that, while they have different temperature dependencies, α and $S_{M_z,0}$ have approximately the same relationship for different strengths of anisotropy D, tying the relationship to the constraint. Similarly, experiments show that while α and $S_{M_z,0}$ of different SQUIDs may have quite different temperature

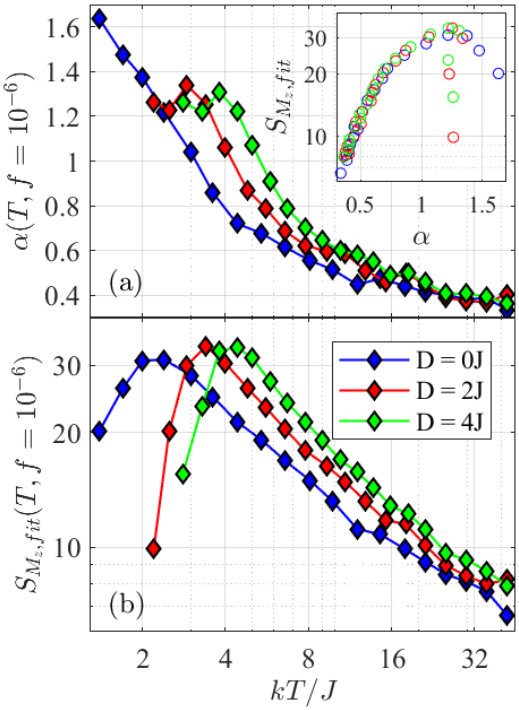

Figure 4. (a) Spectral exponent α (measured about $f = 10^{-6}$ MCS^{-1}) as a function of temperature for isotropic ($D = 0$) and anisotropic ($D = 2J$, $4J$) simulations. (b) Values of fits to the spectral density at $f = 10^{-6}$ MCS^{-1} as a function of temperature. (Inset) Values of fits to the spectral density at $f = 10^{-6}$ MCS^{-1} as a function of spectral exponent α (measured about $f = 10^{-6}$ MCS^{-1}). The relationship is independent of D.

dependencies, the correlation between α and $S_{M_z,0}$ is similar, independent of temperature [27, 28].

As discussed above, and as can be seen in figure 3, the correlation between α and $S_{M_z,0}$ begins to break down at low temperatures, where $\alpha \gtrapprox 1$. At lower temperatures, where $\alpha \approx 1.3$, the situation becomes even more severe and there is a peak in $S_{M_z,0}$ (figure 4(b)). Note that, since the slopes of the spectra are monotonically decreasing, the total noise power $\langle M_z^2 \rangle = \int S_{M_z}(f)\mathrm{d}f$ (not shown here) has a similar peak. This peak in noise power is similar to experimental observations of spin glasses [41, 54] as well as the Ising model with [38] and without [55] disorder, where maxima in noise power correspond to their respective spin glass and phase transitions, as suggested by the fluctuation–dissipation relation, which relates the noise power to the imaginary part of the susceptibility. While not indicative here of either a spin glass transition or a ferromagnetic phase transition (the classical $2D$ Heisenberg model does not undergo a ferromagnetic phase transition for $T > 0$ [56]), this peak does correspond to a dynamical freezing and a divergence in the time scales of cluster reorientation. This situation is illustrated in figure 5 by time series of the z-component of net alignment of a single cluster ($D = 2J$, $N_c = 36$) at temperatures $k_\mathrm{B}T/J = 7.8$ (a), 3.4 (b), and 2.5 (c). As the temperature is lowered, clusters undergo Ising-like switching ($k_\mathrm{B}T/J = 7.8$, 3.4) with

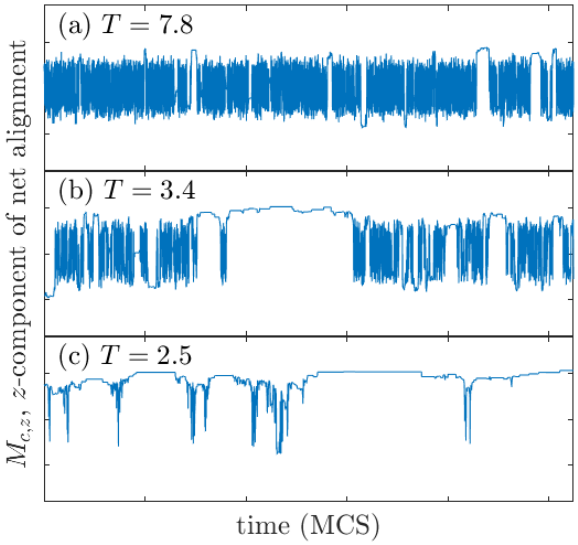

Figure 5. Time series of length $t = 2^{19}$ MCS of z-alignment of a cluster in a simulation with $D = 2J$, $N_c = 36$, $g = 2/3$ and temperatures $k_BT/J = 7.8$ (a), 3.4 (b), and 2.5 (c). The full extent of the vertical axis is fully aligned, $M_{c,z} = 36$. (a) At $k_BT/J = 7.8$ clusters undergo Ising like switching. (b) This behavior continues for $k_BT/J = 3.4$, but with more power in low frequency fluctuations (longer switching times τ). (c) At k_BT/J, clusters no longer undergo switching for the duration of the simulations. At these temperatures, clusters become strongly correlated and ergodicity is broken for time scales investigated.

progressively longer switching times until the switching time is on the order of the length of time simulated ($k_BT/J = 2.5$). At these temperatures, the time-averaged alignment is non-zero for all simulation times ($t_m = 2^{17} \times 10^3$ MCS), indicating that ergodicity has been broken on these time scales. It is also at this temperature that, for simulations with anisotropy (both $D = 2J$ and $4J$), α levels off at $\approx$1.3. For the Ising model with a similar constraint, simulations similarly freeze for $\alpha \approx 1.4$ [11]. It should be pointed out that the SQUID data presented by Anton *et al* [27] shows $0.35 \lessapprox \alpha \lessapprox 0.80$ for single SQUIDs and the data presented by Kempf *et al* [28] shows $0.50 \leqslant \alpha \leqslant 0.82$ for single SQUIDs and $0.34 \leqslant \alpha \leqslant 1.41$ for SQUID arrays. The experimental data are therefore within the range of values of α in our model for which no freezing occurs so that the relationship between α and $S_{M_z,0}$ holds. This suggests that at these temperatures, spins causing flux noise in SQUIDs may be proximal to a transition, as has been previously proposed [30, 39, 40].

To better understand this freezing, we note that the nonlinear constraint has the effect of extending the relaxation time of spins in clusters with higher net alignments. Therefore, as the temperature is reduced and clusters tend to fluctuate into higher alignments, the time scales of fluctuations begin to diverge rapidly, producing the observed slow dynamics and $1/f$ noise, and eventually the dynamical freezing and peak in noise power. From equation (5), we know that the constraint slows spin flips in clusters with net alignment M_c by a factor $\sim e^{g(3M_c^2/2N_c)}$. This allows us to establish some benchmarks regarding the range of frequencies over which we observe $1/f$ noise in our simulations

and for how long simulations must be run in order to be ergodic. Specifically, simulations are no longer ergodic when spin flips are slowed to times comparable to the simulation time t_m. For simulations presented here ($t_m = 2^{17} \times 10^3$), this is connected to the cluster alignment through the constraint, equation (5): spin flips are slowed by a factor of t_m when $M_c/N_c \sim \sqrt{\frac{2}{3gN_c} \ln(t_m)} \sim 0.72$. Indeed, our simulations showed a peak in noise power at temperatures where clusters had net alignments $M_c/N_c \approx 0.72$ and spin flips in such clusters were suppressed for the duration of measurement.

As another benchmark, the longest that the constraint can slow spin flips is for a fully aligned cluster, where spin flips are slowed by a factor $\sim e^{3gN_c/2}$. This roughly establishes a lowest frequency $f_0 \sim e^{-3gN_c/2}$ for which $1/f$ noise can be observed in this model and spectra become white [22]. This is illustrated in figure 1, where noise spectra from simulations of systems with $g = 1$ and $N = 4$ (blue), 9 (green), 16 (red), and 36 (black) spins per cluster are presented. As expected, increasing the size of clusters extends the range over which $1/f$ type noise is observed. For $N_c = 4$ and 9 spins per cluster, the frequencies $f_0 = e^{-3gN_c/2}$ are marked by the diamond symbols, showing approximately where spectra roll over to fully white noise. For the simulations with $N_c = 36$ and $g = 2/3$ presented in this section, $e^{3gN_c/2} \sim 4 \times 10^{15}$, which is 7 orders of magnitude longer than our longest simulation times, so that the frequency $f_0 \sim e^{-3gN_c/2} \sim 2 \times 10^{-16}$ MCS^{-1} is far outside of the measured range. Indeed, at the lowest measured frequency, a crossover to white noise was never observed in simulations with $N_c = 36$.

3. Conclusions

In summary, we have performed simulations of the classical $2D$ Heisenberg model with spin flips constrained according to the local configurational entropy of clusters containing the spins. Noise in the z-component of the net alignment of this model is of $1/f$ type over at least seven decades and qualitatively reproduces the temperature dependence of flux noise found in SQUIDs, including the existence of a crossing frequency. Interactions in the model are of uniform strength and chosen to be ferromagnetic, consistent with measurements indicating the breaking of time-reversal symmetry. The constraint produces $1/f$ noise naturally with no ad hoc distribution of time scales, cluster sizes, or interaction strengths. While producing $1/f$ noise and dynamical freezing similar to a spin glass, this model is fundamentally different in that interactions remain homogeneous and the heterogeneity is purely dynamic. Finally, constraints of this type are fungible, having been used to reproduce a number of other physical phenomena [8–12].

Acknowledgments

Most of the simulations utilized the A2C2 computing facility at Arizona State University.

References

[1] Böhmer R *et al* 1998 Nature of the non-exponential primary relaxation in structural glass-formers probed by dynamically selective experiments *J. Non.-Cryst. Solids* **235–7** 1–9

[2] Richert R 2002 Heterogeneous dynamics in liquids: fluctuations in space and time *J. Phys.: Condens. Matter* **14** 703–38

[3] Wang C-Y and Ediger M D 1999 Spatially heterogeneous dynamics in deeply supercooled liquids *AIP Conf. Proc.* **469** 339–49

[4] Hill T L 1963 Thermodynamics of Small Systems, part 1 (New York: W A Benjamin)

[5] Plyukhin A V and Schofield J 2001 Stochastic dynamics with a mesoscopic bath *Phys. Rev.* E **64** 041103

[6] Seifert U 2012 Stochastic thermodynamics, fluctuation theorems and molecular machines *Rep. Prog. Phys.* **75** 126001

[7] Sekimoto K 2009 Concept of heat on mesoscopic scales *Stochastic Energetics Lecture Notes in Physics* (Berlin: Springer)

[8] Chamberlin R V, Vermaas J V and Wolf G H 2009 Beyond the boltzmann factor for corrections to scaling in ferromagnetic materials and critical fluids *Eur. Phys. J.* B **71** 16

[9] Chamberlin R V 2012 Monte carlo simulations including energy from an entropic force *Physica* A **391** 5384–91

[10] Chamberlin R V and Davis B F 2013 Modified bose-einstein and fermi-dirac statistics if excitations are localized on an intermediate length scale: applications to non-debye specific heat *Phys. Rev.* E **88** 042108

[11] Chamberlin R V and Nasir D M 2014 $1/f$ noise from the laws of thermodynamics for finite-size fluctuations *Phys. Rev.* E **90** 012142

[12] Chamberlin R V 2017 Reducing low-frequency noise during reversible fluctuations *Eur. Phys. J. Spec. Top.* **226** 365–71

[13] Johnson J B 1925 The schottky effect in low frequency circuits *Phys. Rev.* **26** 7185

[14] Wellstood F C, Urbina C and Clarke J 1987 Low-frequency noise in dc superconducting quantum interference devices below 1 k *Appl. Phys. Lett.* **50** 772–4

[15] Weissman M B 1988 $1/f$ noise and other slow, nonexponential kinetics in condensed matter *Rev. Mod. Phys.* **60** 537–71

[16] Koch R, Clarke J, Martinis J, Goubau W, Pegrum C and Harlingen D 1983 Investigation of $1/f$ noise in tunnel junction dc squids *IEEE Trans. Magn.* **19** 449–52

[17] Yoshihara F, Harrabi K, Niskanen A O, Nakamura Y and Tsai J S 2006 Decoherence of flux qubits due to $1/f$ flux noise *Phys. Rev. Lett.* **97** 167001

[18] Kakuyanagi K, Meno T, Saito S, Nakano H, Semba K, Takayanagi H, Deppe F and Shnirman A 2007 Dephasing of a superconducting flux qubit *Phys. Rev. Lett.* **98** 047004

[19] Bialczak R C *et al* 2007 $1/f$ flux noise in Josephson phase qubits *Phys. Rev. Lett.* **99** 187006

[20] Rogers C T and Buhrman R A 1985 Nature of single-localized-electron states derived from tunneling measurements *Phys. Rev. Lett.* **55** 859–62

[21] Harlingen D J V, Robertson T L, Plourde B L T, Reichardt P A, Crane T A and Clarke J 2004 Decoherence in Josephson-junction qubits due to critical-current fluctuations *Phys. Rev.* B **70** 064517

[22] Kogan S 2009 *Electronic Noise and Fluctuations in Solids* (Cambridge: Cambridge University Press)

[23] Pottorf S, Patel V and Lukens J E 2009 Temperature dependence of critical current fluctuations in nb/alox/nb Josephson junctions *Appl. Phys. Lett.* **94** 043501

[24] Clarke J and Wilhelm F K 2008 Superconducting quantum bits *Nature* **453** 1031–42

[25] Sendelbach S, Hover D, Kittel A, Mck M, Martinis J M and Mcdermott R 2008 Magnetism in squids at millikelvin temperatures *Phys. Rev. Lett.* **100** 227006

[26] Sendelbach S, Hover D, Mck M and Mcdermott R 2009 Complex inductance, excess noise, and surface magnetism in dc squids *Phys. Rev. Lett.* **103** 117001

[27] Anton S M *et al* 2013 Magnetic flux noise in dc squids: temperature and geometry dependence *Phys. Rev. Lett.* **110** 147002

[28] Kempf S, Ferring A and Enss C 2016 Towards noise engineering: recent insights in low-frequency excess flux noise of superconducting quantum devices *Appl. Phys. Lett.* **109** 162601

[29] Laforest S and Sousa R D 2015 Flux-vector model of spin noise in superconducting circuits: electron versus nuclear spins and role of phase transition *Phys. Rev.* B **92** 054502

[30] Wang H, Shi C, Hu J, Han S, Yu C C and Wu R 2015 Candidate source of flux noise in squids: adsorbed oxygen molecules *Phys. Rev. Lett.* **115** 077002

[31] Kumar P *et al* 2016 Origin and reduction of $1/f$ magnetic flux noise in superconducting devices *Phys. Rev. Appl.* **6** 041001
[32] Choi S, Lee D-H, Louie S G and Clarke J 2009 Localization of metal-induced gap states at the metal-insulator interface: origin of flux noise in squids and superconducting qubits *Phys. Rev. Lett.* **103** 197001
[33] Sousa R D 2007 Dangling-bond spin relaxation and magnetic $1/f$ noise from the amorphous-semiconductor/oxide interface: theory *Phys. Rev.* B **76** 245306
[34] Faoro L and Ioffe L B 2008 Microscopic origin of low-frequency flux noise in Josephson circuits *Phys. Rev. Lett.* **100** 227005
[35] Atalaya J, Clarke J, Schn G and Shnirman A 2014 Flux $1/f^{\alpha}$ noise in two-dimensional Heisenberg spin glasses: effects of weak anisotropic interactions *Phys. Rev.* B **90** 014206
[36] Wu J and Yu C C 2012 Modeling flux noise in squids due to hyperfine interactions *Phys. Rev. Lett.* **108** 247001
[37] Agarwal K, Demler E and Martin I 2015 $1/f^{\alpha}$ noise and generalized diffusion in random heisenberg spin systems *Phys. Rev.* B **92** 184203
[38] Chen Z and Yu C C 2010 Comparison of ising spin glass noise to flux and inductance noise in squids *Phys. Rev. Lett.* **104** 247204
[39] De A 2014 Ising-glauber spin cluster model for temperature-dependent magnetization noise in squids *Phys. Rev. Lett.* **113** 217002
[40] Lanting T, Amin M H, Berkley A J, Rich C, Chen S-F, Laforest S and Sousa R D 2014 Evidence for temperature-dependent spin diffusion as a mechanism of intrinsic flux noise in squids *Phys. Rev.* B **89** 014503
[41] Weissman M B 1993 What is a spin glass? A glimpse via mesoscopic noise *Rev. Mod. Phys.* **65** 829–39
[42] Takeshi O and Sekimoto K 2005 Internal stress in a model elastoplastic fluid *Phys. Rev. Lett.* **95** 108301
[43] Miyamoto Y, Fukao K, Yamao H and Sekimoto K 2002 Memory effect on the glass transition in vulcanized rubber *Phys. Rev. Lett.* **88** 225504
[44] Feynman R P, Leighton R B and Sands M 1966 *The Feynmann Lectures on Physics* vol 1 (Reading, MA: Addison-Wesley)
[45] Kunzler J, Walker L and Galt J 1960 Adiabatic demagnetization and specific heat in ferrimagnets *Phys. Rev.* **119** 1106–10
[46] Kim T, Chamberlin R and Bird J 2013 Large magnetoresistance of nickel-silicide nanowires: non-equilibrium heating of magnetically-coupled dangling bonds *Nano Lett.* **13** 1106–10
[47] Hill T L 2007 *An Introduction to Statistical Thermodynamics* (New York: Dover)
[48] Halford D 1968 A general mechanical model for $|f|^{\alpha}$ spectral density random noise with special reference to flicker noise $1/|f|$ *Proc. IEEE* **56** 251–8
[49] Chamberlin R V, Abe S, Davis B F, Greenwood P E and Shevchuk A S 2016 Fluctuation theorems and $1/f$ noise from a simple matrix *Eur. Phys. J.* B **89** 185
[50] Niemann M, Kantz H and Barkai E 2013 Fluctuations of $1/f$ noise and the low-frequency cutoff paradox *Phys. Rev. Lett.* **110** 140603
[51] Rodrguez M A 2014 Complete spectral scaling of time series: towards a classification of $1/f$ noise *Phys. Rev.* E **90** 042122
[52] Drung D, Beyer J, Storm J-H, Peters M and Schurig T 2011 Investigation of low-frequency excess flux noise in dc squids at mk temperatures *IEEE Trans. Appl. Supercond.* **21** 340–4
[53] Schmelz M, Stolz R, Zakosarenko V, Anders S, Fritzsch L, Roth H and Meyer H-G 2012 Highly sensitive miniature squid magnetometer fabricated with cross-type Josephson tunnel junctions *Physica* C **476** 7780
[54] Refregier P, Ocio M and Bouchiat H 1987 Equilibrium magnetic fluctuations in spin glasses: temperature dependence and deviations from $1/f$ behaviour *Europhys. Lett.* **3** 503–10
[55] Chen Z and Yu C C 2007 Measurement-noise maximum as a signature of a phase transition *Phys. Rev. Lett.* **98** 057204
[56] Mermin N D and Wagner H 1966 Absence of ferromagnetism or antiferromagnetism in one- or two-dimensional isotropic Heisenberg models *Phys. Rev. Lett.* **17** 1307

B.2 Remarks

This work further developed the theory of multiplicity-dependent characteristic times from finite entropy baths. This model was useful in applying the results of the matrix model to more realistic systems. More realistic features include interactions between spins, interactions between the system + local bath and an infinite thermal reservoir, and continuous degrees of freedom.

This model may serve as a bridge between simple, discrete models of finite entropy baths and models using microscopically realistic simulation methods (*e.g.* molecular dynamics).